Investigating the molecular mechanisms underlying touch in mice

Dissertation

zur Erlangung des Grades eines
Doktors der Naturwissenschaften

der Mathematisch-Naturwissenschaftlichen Fakultät

und
der Medizinischen Fakultät
der Eberhard-Karls-Universität Tübingen

vorgelegt
von

Yanmei Qi
(祁艳梅)
aus Anhui, China

June, 2016

Tag der mündlichen Prüfung:	June 15, 2016
Dekan der Math.-Nat. Fakultät:	Prof. Dr. W. Rosenstiel
Dekan der Medizinischen Fakultät:	Prof. Dr. I. B. Autenrieth
1. Berichterstatter:	Prof. Dr. / PD Dr. Jing Hu
2. Berichterstatter:	Prof. Dr. / PD Dr. Robert Feil
Prüfungskommission:	Prof. Dr. / PD Dr. Jing Hu
	Prof. Dr. / PD Dr. Robert Feil
	Prof. Dr. / PD Dr. Simone Di Giovanni
	Prof. Dr. / PD Dr. Michela Deleidi

I hereby declare that I have produced the work entitled: “**Investigating the molecular mechanisms underlying touch in mice**”,

submitted for the award of a doctorate, on my own (without external help), have used only the sources and aids indicated and have marked passages included from other works, whether verbatim or in content, as such. I swear upon oath that these statements are true and that I have not concealed anything. I am aware that making a false declaration under oath is punishable by a term of imprisonment of up to three years or by a fine.

Tübingen, _____ _____

Date Signature

Description of personal contribution

1. The work presented in the first result section of this thesis (**STOML3 modulates mechanosensation via cholesterol enriched lipid rafts**) is partially adapted from the published manuscript:

Membrane stiffening by STOML3 facilitates mechanosensation in sensory neurons. Yanmei Qi, Flavia Frattini, Laura Andolfi, Marco Lazzarino, Jing Hu. Nat. Commun. 6:8512 doi: 10.1038/ncomms9512 (2015).

Own contribution: All electrophysiological and molecular biological experiments, data acquisition, analysis of data and preparation of the figures presented in Chapter 4.1 of this thesis.

2. The work presented in the first result section of this thesis (**The role of cholesterol-rich lipid rafts in the regulation of ASICs activity by STOML3**) is partially adapted from the manuscript:

The regulation acid-sensing ion channels by STOML3 requires cholesterol-rich lipid rafts", Yanmei Qi, Jing Hu.

Own contribution: Experimental work, data acquisition, analysis of data and preparation of the figures presented in Chapter 4.2 of this thesis.

Contents

Common Abbreviations

AFM	Atomic force microscopy
AP	Action potential
ASICs	Acid-sensing ion channels
αTAT1	α-tubulin K40 acetyltransferase
CCI	Chronic constriction injury
CHO	Chinese hamster ovarian
CNS	Central nervous system
DEG/ENaC	Degenerins/epithelial Na channel
DRG	Dorsal root ganglia
DRM	Detergent-resistant membrane
ECM	Extracellular matrix
EGF	Epidermal growth factor
GFP	Green fluorescent protein
GPI	Glycosylphosphatidylinositol
HDAC6	Histone deacetylase 6
HEK293	Human embryonic kidney 293
HRP	Horseradish peroxidase
HTM	High-threshold receptors
IA	Intermediate adapting
I-V	Current–voltage
LPC	Lysophosphatidylcholine

LTM	Low-threshold mechanorecptors
MβCD	Methyl-β-cyclodextrin
MRC	Mechanoreceptor current
MscL	Mechanosensitive channel with a large conductance
MscS	Mechanosensitive channel with a small conductance
PNS	Peripheral sensory neurons
PVDF	Polyvinylidene difluoride
RA	Rapidly adapting
RMP	Rest membrane potential
SA	Slowing adapting
SIRT2	Sirtuin type 2
STOML3	Stomatin like protein 3
TEM	Transmission electron microscope
TG	Trigeminal ganglia
TRP	Transient receptor potential
TRPV1	Vanilloid receptor subtype 1
TTX	Tetrodotoxin
UTLD	Upper tip-link density
YFP	Yellow fluorescent protein

Lists of figures and tables

1. Summary

Although mechanosensation might be the most ancient one among our five senses, the mechanotransduction mechanism underlying the sense of touch remains to be least understood. A Stomatin like protein-3 (STOML3) has been shown to be essential for touch sensation in mouse. However, the molecular mechanisms by which STOML3 contribute to mechanotransduction remain elusive.

In the first chapter of the thesis, we suggest a novel mechanism by which STOML3 modulates sensory mechanostransduction. STOML3, via binding cholesterol, controls membrane mechanics, thus facilitates the force transfer and tunes the sensitivity of the mechanically gated channels, including Piezo channels. Several lines of evidence support this conclusion. First, STOML3 is detected in cholesterol enriched lipid raft. Depletion of cholesterol and deficiency of STOML3 in sensory neurons similarly and interdependently affect membrane mechanics and attenuate mechanosensitivity. Second, we demonstrate that an intact STOML3 is essential for maintaining membrane mechanics to sensitize mechanically gated Piezo1 and Piezo2 channels in heterologous systems. Such a stiffened membrane can be softened by either depleting cholesterol or genetic disruption of cholesterol binding of STOML3. Third, mutation of residue involved in cholesterol binding (STOML-P40S) fails to modulate the sensitivity of Piezo channels or restore the mechanosensitivity of *STOML3*$^{-/-}$ sensory neurons. Finally, using a behavioral test, we show that cholesterol depletion could attenuate tactile allodynia and this effect involves STOML3. Factoring all these together, we propose that the stiffened membrane by STOML3 is essential for sensory mechanotransdution *in vitro* and the tactile sensitivity *in vivo*.

STOML3 has been previously shown to interact with and inhibit the activity of Acid-sensing ion channels (ASICs). However, little is known about how this works. In the second chapter of the thesis, we examined whether STOML3 requires cholesterol-rich lipid rafts for regulating the activities of its associated ASIC channels. We show disrupting cholesterol-rich lipid rafts with Methyl-β-cyclodextrin robustly increases the proton-gated ASICs-like current in sensory neurons from C57BL/6N but not *STOML3*$^{-/-}$ mice, suggesting that the regulation of acid-sensing ion channels by lipid rafts involves STOML3 in sensory neurons. In heterologous expression cells, cholesterol depletion

increases proton-gated ASICs-mediated currents and abolishes the inhibition of STOML3 on ASIC channel activity. Collectively, we suggest the regulation of ASIC channel by STOML3 requires the involvement of cholesterol-rich lipid rafts in mouse sensory neurons.

In summary, with the above mentioned work, we would like to propose that binding cholesterol might be a general mechanism for STOML3 to regulate its associated ion channels including Piezos and ASICs. ~~Furthermore,~~ Touch evoked pain is the most common symptom of chronic pain and the effective treatment is absent. Our work~~s~~ on STOML3 would ~~potentially facilitate the study of STOML3's role on regulating channel activity and~~ provide therapeutic opportunity for treating chronic pain.

2. Introduction

All living organisms have mechanical sensing. Bacteria sense osmotic pressure, plants respond to gravity, and we humans depend on touch and hearing for most of our everyday activities. The sensing of mechanical forces is vital for animals to survive in surrounding environments, and might be the most ancient one of Aristotle's five senses. Mechanotransduction is the process that converts mechanical signal into electrical and biochemical signal, which constitutes the basis of the fundamental physiological function of animals.

2.1 Mechanotransduction in mammalian sensory neurons

2.1.1 Diversity of mechanosensitive sensory neurons

In mammalian somatosensory system, detection of mechanical force is performed by specialized primary sensory neurons. The cell body of these neurons localizes in the dorsal root ganglia (DRG) or trigeminal ganglia (TG), and their nerve endings are distributed in skin different layers and deep body structures. Cutaneous mechanoreceptors are imbedded in specialized structures such as Merkel disk, Pacinian corpuscles and Meissner corpuscles, wrapped around the hair follicles or free in epidermis layer of skin. The transduction of mechanical stimuli is suggested to occur at the peripheral ending of cutaneous sensory neuron, where mechanical forces open mechanosensitive ion channels and thus depolarize and excite neurons [1]. However, recent studies point out epidermal Merkel cells are considered not merely a supportive tissue for the function of nerve ending, but also are inherently mechanosensitive. Merkel cells can encode static stimuli such as pressure into Ca^{2+}-action potential and drive the Aβ-sensory afferents to fire slowly adapting inpulse [2-4].

Cutaneous sensory neurons are remarkably diverse[5]. According to the electrophysiological properties of sensory afferent, they are classified into three broad groups by the speed of action potential propagation which is set by myelin thickness: thickly myelinated Aβ, thinly myelinated Aδ and non-myelinated C-fibres (Figure 1). Receptor in fibre endings can be further classified as low-threshold mechanorecptors

(LTM) preferentially responding to innocuous mechanical forces such as gentle brush, and high-threshold receptors (HTM) excited by noxious mechanical forces such as pinching. Most thickly myelinated Aβ afferents, such as those that innervate merkel disk or around hair shaft, have low mechanical threshold and likely to be light-touch mechanoreceptor. Thinly myelinated Aδ-fibres that terminate in the dermis and most of unmyelinated C-fibres that terminate in the epidermal layers have high mechanical threshold and thus thought to be mechanociceptor [5-7].

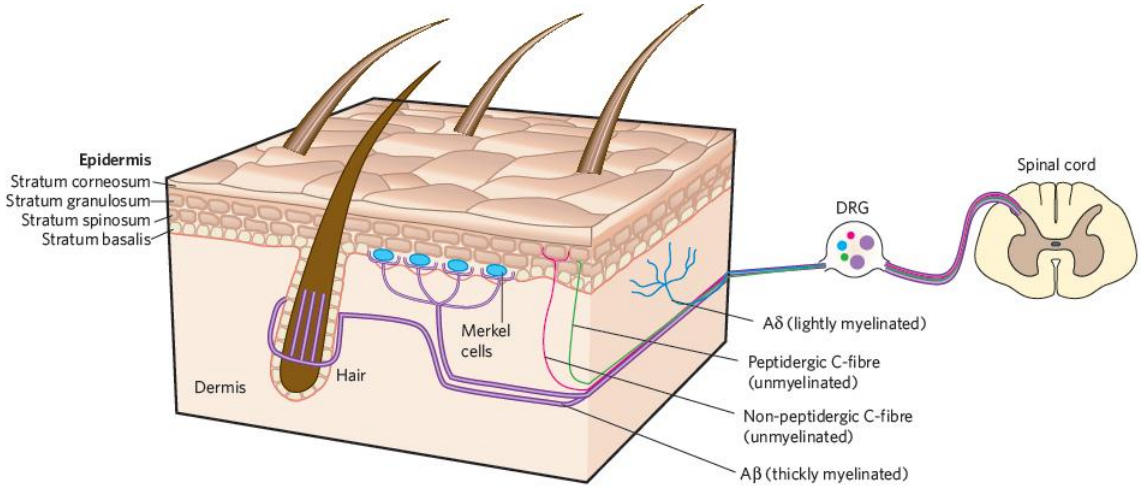

Figure 1. Diversity of somatosensenory neurons in the skin. The skin is innervated by somatosensory neurons that project to the spinal cord [5].

2.1.2 Electrophysiological and pharmacological properties of mechanosensitive currents

Electrophysiological and pharmacological properties of mechanosensitive currents have been characterized from studies of mechanosensitive ion channels in cultured sensory neurons. In sensory neuron, three distinct types of mechanically gated currents are cataloged base on different inactivation kinetics [8,9], including rapidly adapting (RA) with very fast decay, intermediate adapting (IA) and slowing adapting response (SA, no adaptation) (Figure 2). The latency and activation kinetics of recorded mechanosensitive currents are within submillisecond range, strongly supporting that mechanosensitive

channel in membrane is directly gated by mechanical force without any intervening enzymatic step. Most of cultured DRG neurons harbor either RA or SA conductance, and only small proportion of cells (around 10%) have IA conductance. RA currents are present in mechanoreceptors that are supposed to detect light touch, while IA and SA currents are found mainly in nociceptors that are supposed to encode nocuous mechanical stimuli [9]. The heterogeneity of mechanically gated currents implies the existence of distinct ion channels or gating mechanisms underlying these currents.

The transducer for detection of force is thought to be either cation-nonselective or sodium selective [8-10]. Studies in mice sensory neuron show RA and SA currents have apparently different reverse potential, around +80mV and +7mV respectively, and RA currents are almost completely blocked when extracellular sodium is replaced by impermeant cation $NMDG^+$. These results indicate RA currents are largely selectively for sodium ions whereas SA currents are cation non-selective [9]. The ion selectivity reported in mice is controversial to those in rat, wherein both RA and SA currents are cation non-selective [10]. This discrepancy may be due to species difference or different velocity of mechanical stimulus used by different labs.

From previous pharmacological studies of mechanosensitive ion channels, Gadolinium and styryl dye FM1-43 can block both RA and SA mechanically activated conductances [9-11]. Rruthenium red, an TRP (transient receptor potential) channel inhibitor, is effective in SA currents but not RA current [9]. Drew and colleagues develop a conopeptide analogue termed NMB-1 which selectively inhibits SA mechanically activated current in sensory neurons [12]. Hitherto, specific drug to block RA currents is still under discovery.

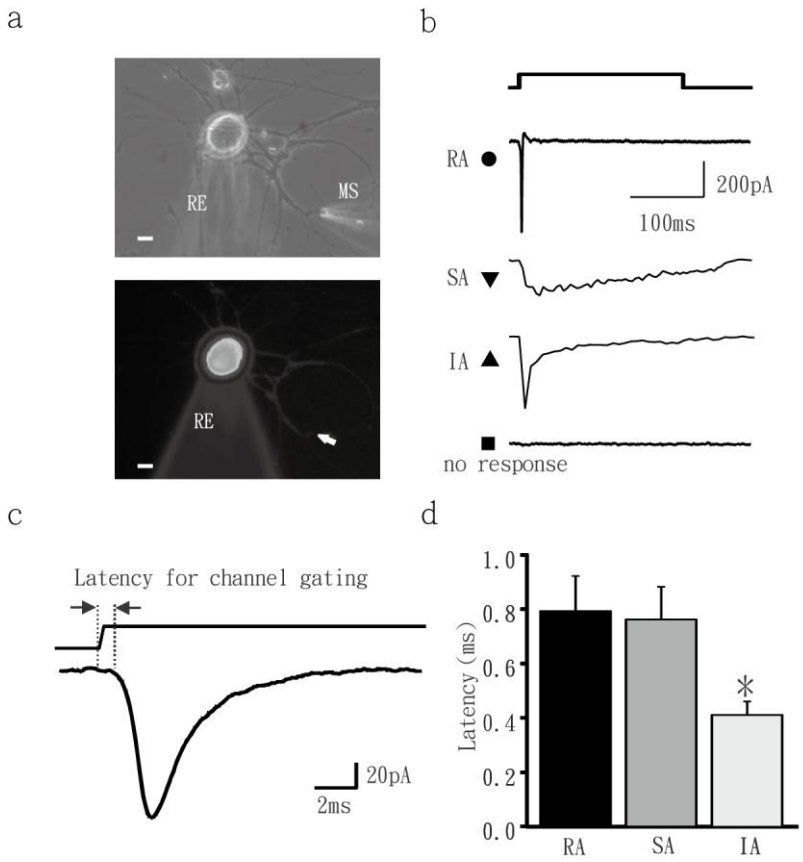

Figure 2. Mechanosensitivity of DRG neurons cultured on poly-L-lysine–laminin substrate. (a), images of single DRG neurone in the whole-cell recording configuration with the mechanical stimulator (MS) poised to stimulate one of the neurites. Phase-contrast image (top) and fluorescent image (bottom). The cell and neurites were loaded with Lucifer Yellow dye via the recording electrode (RE). The arrow shows the site of stimulation with the MS. Scale, 10 μm. (b), sample traces of the different types of mechanically gated currents obtained. RA, rapidly adapting; SA, slowly adapting; IA, intermediate adapting. (c), example of an RA current drawn on an expanded scale showing how mechanical latency was measured. (d), the mean mechanical latency for RA, IA and SA currents are shown [9].

2.2 Potential gating mechanism for mechanotransduction

Two models of gating have been proposed for sensory mechanosensitive channels [13,14], the first one is stretch-activated gating model, in which forces changes in the lipid bilayer, such as stretch of membrane or changes in osmolarity, directly gate the channel without need of other proteins (Figure 3a). The second one is called tether gating model,

in which the gating forces are transmitted to transduction channel through a tether (Figure 3b and 3c).

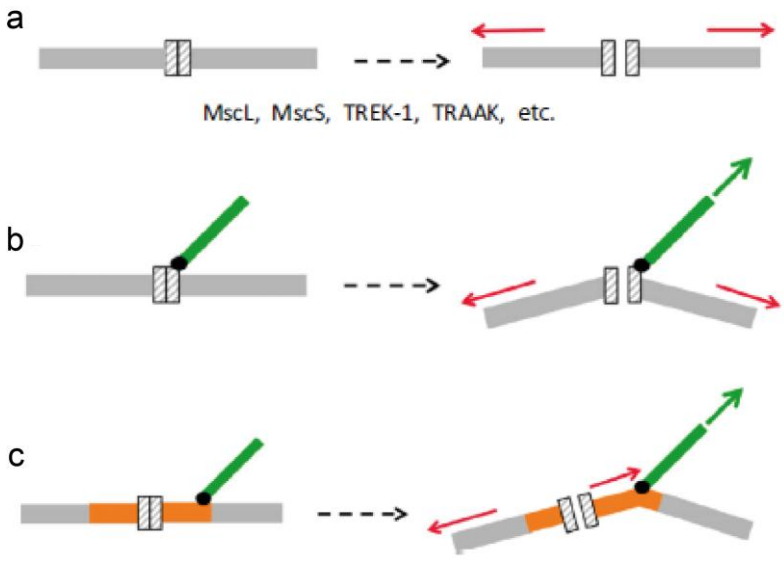

Figure 3. Gating models of mechanotransduction channels. (a) Diagram of a stretch of the bilayer opens purified channels reconstituted in lipid bilayer, including the bacterial MscL, MscS, the veterbrate TREK-1, TRAAK and others. (b, c) Two possible models of how a tether gates an MS channel. The tether either pulls on the channel protein directly (b) or on the surrounding lipids (c) [13].

2.2.1 Stretch-activated gating model

The stretch-activated gating model has been proven in bacteria mechanosensitive channels [15]. During a severe osmotic down-shock, bacteria release cytoplasmic solutes to reduce turgor pressure by opening mechanosensitive channels that acts as an 'emergency valves' [16]. Bacteria mechanosensitive channels are the first bona fide mechanotransducer to be identified. The observation that stretching membrane of an E. coli giant spheroplast can activate channel leads to the discovery of a bacteria mechanosensitive channel with a large conductance (~3 nS, MscL) and one with a small conductance (~1 nS, MscS) [17]. Bacteria mechanosensitive channel is suggested to be gated by only the force from lipid bilayer, because MscL channel can be activated by pressure if reconstituted in a cell-free lipid system [17,18]. Here there are only lipids themselves and no other components in this system, thus the stretch force that activates the MscL channel must be transmitted from

the lipid bilayers. Since bacteria mechanosensitive channel is gated by force from lipid, the bilayer mechanical properties would be expected to play important role for mechanosensitive channel gating. Indeed, changing the bilayer intrinsic curvature by adding charged amphipaths or lysophosphatidylcholine (LPC) in bilayer expressing bacteria mechanosensitive channel are sufficient to modulate channel gating [18,19]. These studies from prokaryotic mechanosensitive channels support the model that force from lipid gates mechanosensitive channel.

Besides bacteria mechanosensitive channels, this model is also applied for mammalian mechanosensitive ion channels such as two pore K+ channels (K2p) TREK-1 and TRAAK, several types of TRP (transient receptor potential) channels including TRPC1, TRPC6, TRPV1 and TRPV4 [20], and a recently identified new mechanosensitive channel family piezos [21]. These studies suggest a general principle that force form lipid bilayer opens mechanosensitive channels.

2.2.2 Tether gating model

The tether gating model is well supported in vertebrate inner hair cells [1,14]. Hair cells in the vertebrate inner ear are specialized mechanoreceptor cells that convert mechanical stimuli generated from sound and head movement into neural signal. The mechanosensitive organelle, the hair bundle composed of tens to hundreds of F-actin-riched stereocilia in mature mammalian cochlear hair, is organized in precise rows of increasing heights. This mechanotransduction process is initiated by opening of cation channel near the tips of stereocilia, deflection toward the tallest stereocilia (positive deflections) induce transduction channel to open, whereas deflections toward the shortest stereocilia close the channel [22]. Tip links are thought to transmit the force onto the hair cell's mechanosensitive channel [23]. Disrupting tip links by mutating genes that constitute tip links or by treatment with protein elastase affects mechanotransduction [23,24]. In this tether gating model, the transduction channel, an unknown molecular localized at the tip of each stereocilia, is directly or indirectly tethered to both the extracellular tip links that connect the stereocilia and the internal the actin filaments [1,14].

Tip links are fine extracellular filament that connects the tips of one stereocilium to the side of an adjacent taller stereocilium. Two members of the cadherin superfamily, cadherin 23 and protocadherin 15, interact to form tip links, where each tip link is an asymmetric protein complex containing cadherin 23 at the upper part and protocadherin 15 at the lower part [25]. Besides tip-link cadherin, the tip-link complex also includes scaffolding proteins and myosin motor. For example, in upper tip-link density (UTLD), harmonin b, a scaffolding and actin-bundling protein, is present in stereocilia of hair cells and interacts with both F-actin and cadherin 23 [26,27]. Motor protein myosin VIIa binds to harmonin b and transport it to the tip region of stereocilium along the actin core of the developing stereocilia [27], in addition, myosin VIIa also binds to cadherin 23, suggesting the three proteins form a molecular complex that anchors the tip link to the actin filament of stereocilia. There is little doubt that the transducer receives force from the tether [20]. However, the tip-link is unlikely to be the gate spring which is thought to gate mechanotransducer in hair cells, because the estimated stiffness of tip-link is ~40-60 mN/m which is far larger than the value of gate spring ~1 mN/m. The higher rigidity of tip-link with estimated stiffness ~40-60 mN/m makes it unlikely to be the gate spring with stiffness around 1 mN/m, which is thought to gate mechanotransducer. The tip-link thereby might transmit the force to lipid bilayer, thus altering the tension in the lipid bilayer around the transduction channel after the positive deflection of sterocilia, which would trigger the opening of channel [14,28]. No doubt, in this tether-gating model, we could not negate the effect of force transfer to mechano-gated channels on channel gating [20].

2.3 Molecular complex for mechanotransduction in nematodes and mammals

2.3.1 Molecular model of gentle touch sensing in *Caenorhabditis elegans*

Most of our knowledge about cellular and molecular mechanism of mechanical sensing benefit from the genetic screen of touch-insensitive mutants in model organism such as *Caenorhabditis elegans*. *C. elegans*, a tiny soil nematode, show avoid behavior to touch. Touching the anterior part of worm causes the animals to move backward, while stimulating the tail causes worm to speed up. *C. elegans* has six touch receptor neurons,

which run longitudinally along the body of the worm. These touch neurons are initially known as microtubules cells because their process are filled with special 15-protofilament microtubules [29]. Chalfie and colleagues mutagenized worms and screened for mutations that selectively caused mechanosensory abnormal (*mec*). Using this screening method, seventeen genes (named *MEC*) have been discovered to be important for touch sensation.

In *Caenorhabditis elegans*, it is considered that the mechanoreceptor channel complex, extracellular matrix (ECM) and intracellular 15-protofilament microtubules synergistically contribute to nematode mechanotransduction (Figure 1). In this model, the mechanoreceptor channel complex includes proteins encoded by *mec-4*, *mec-10*, *mec-6* and *mec-2*, and this complex localizes as a regular puncta along the process of touch receptor neuron. MEC-4 and MEC-10, two degenerins/epithelial Na channel (DEG/ENaC) proteins, are pore-forming subunits of mechanosensory complex [30,31]. Mechanical stimulation of the worm body wall evokes a rapidly adapting mechanoreceptor current (MRC) which is carried by MEC-4/MEC-10 transduction channel complex [30]. MEC-2 (a Stomatin-like protein) and MEC-6 (a Paraoxonase-like membrane protein) are essential accessory proteins of pore-forming subunits MEC-4/MEC-10 [32-35], *mec-2* and *mec-6* single null mutant are touch insensitive and mechanoreceptor currents are also abolished [30]. *In vitro*, MEC-2/MEC-6 physically interact with MEC-4/10 channel complex and probably synergistically enhance channel activity by increasing more channel in an active state [32,33,35]. *In vivo*, MEC-2/MEC-6 co-localize with MEC-4 channel along touch-neuron process in discrete puncta [32,33]. MEC-6 is required for the punctate distribution of MEC-4 channel, disruption of MEC-6 but not MEC-2 affects MEC-4 puncta [32,34], implying MEC-6 is a part of mechanosensory channel complex in touch receptor neuron.

The extracellular matrix is composed of MEC-1, MEC-9 and MEC-5 [36,37]. Both MEC-1 and MEC-9 are extracellular proteins with epidermal growth factor (EGF)-like and kunitz (EGF/kunitz) domain. MEC-5 is similar to mammal collagen which is secreted by the epidermal cells that surround the touch receptor neuron. Loss of function mutation of MEC-1, MEC-5 or MEC-9 causes touch insensitivity, suggesting ECM components are required for nematode touch sensation [36,37]. ECM components colocalize with the

mechanosensory channel complex in puncta and are required for the correct localization of MEC-4 mechanosensory channel complex [34,37], It is therefore proposed that ECM is tethered to the mechanosensory ion channel complex, and ECM tethering is required for channel gating in nematode touch receptor neuron,

In *Caenorhabditis elegans*, internal microtubules are also required for touch sensation, disruption of microtubules by loss of MEC-12 (α-tubulin) or MEC-7 (β-tubulin) causes touch insensitivity [38]. The large-diameter microtubules server multiple and specific roles in touch sensory neuron, such as altering distribution of mechanosensory channel subunits in the touch receptor neuron process and slowing transduction channel adaptation. But it is proposed that microtubules do not tether the mechanosensory channel complex and are not essential for channel gating, because microtubules do not organize the localization of MEC-4 mechanosensory channel complex and elimination of microtubules in touch neuron only reduces but not abrogate mechanoreceptor currents [30,38]. Microtubules probably attach to plasma membrane and accelerate the full activation of mechanosensory transduction channel. Additionally, recent studies show MEC-17, an α-tubulin acetyltransferase, also contributes to touch sensation [39,40]. However, the underlying mechanisms for MEC-17's function in touch sensation remains elusive.

The molecular model in *Caenorhabditis elegans* well support the tether-gating model, in which the ion channel complex is tethered to extracellular ECM and cytoskeleton, and movement of this rigid structure leads to the opening of channel [14,37,41].

2.3.2 Similarity of molecular model for mechanotransduction between *C. elegans* and mammals

A similar molecular architecture is proposed in mouse mechano-sensory system [9,42,43]. As shown in Figure 4, molecular machinery of transduction in mouse sensory system is composed of three components as in *C. elegans*: extracellular tether proteins, transduction channel complex in membrane and intracellular cytoskeleton.

In mouse sensory neurons, a novel link proteins tethering neuritis to extracellular matrix has been observed using transmission electron microscope [16], and cleavage of these tether with a protease abolishes the RA conductance of mechanoreceptor [42,43]. These evidences

suggest that the tether exists although its molecular entity is unknown, and is probably required for efficient gating of sensory mechanosensitive channels as nematode extracellular matrix proteins.

Intracelluar cytoskeletal elements are also important for mechanotransduction in mammalian sensory neuron [8,10]. Disrupting cytoskeletal by microtubule depolymerizing or actin depolymerizing reagent, reduces the activity of mechanosensitive channels in sensory neurons [8,10]. α-tubulin K40 acetyltransferase (αTAT1), an mammalian orthologue of nematode MEC-17, has been identified to be a major a-tubulin acetyltransferase in mice [44]. But, it is still unknown whether aTAT1 is important for mechanosensation in mouse.

With regards to the transduction channel complex in mammal, mammalian MEC-4/MEC-10 orthologues acid sensitive ion channels (ASICs) are not true transducer in sensory mechanotransduction, and probably function as a component or modulator of the mechanosensory transduction apparatus [4]. Piezos, a new family of mechanically activated channels, have been identified as potential candidates for sensory mechanotransduction [21,45]. Recently, Patapoutian A group show piezo2 is a major mechanotransducer for touch sensation in mice [46]. Importantly, like MEC-2 in *C. elegans*, mammalian MEC-2 orthologue STOML3 (stomatin like protein 3) is the first identified protein demonstrated to be essential for mechanotransduction in mouse [47]. Additionally, STOML3 not only physically interacts with ASICs and piezos, but also regulate ASICs-mediated proton gated currents and piezos-mediated mechanosensitive currents [48,49]. However, the molecular mechanism for STOML3 to regulate the mechanotransduction and its associated ion channels remains elusive. Here in this thesis, we determine to investigate this question.

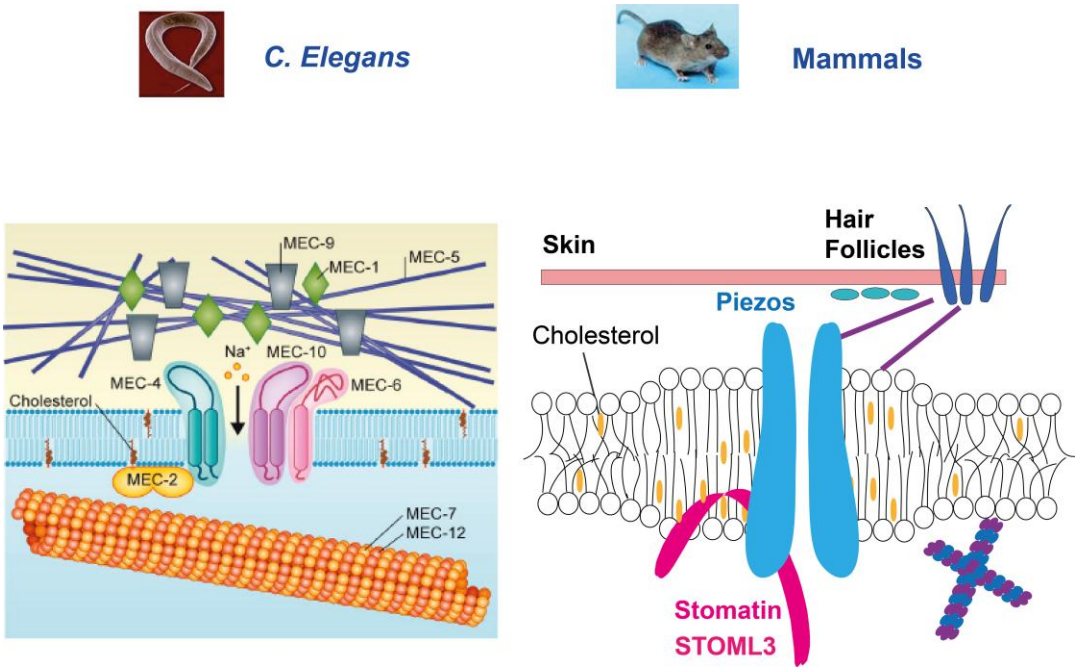

Figure 4. A molecular model of touch in *Caenorhabditis elegans* and mouse.
Left panel for *C. Elegans*: MEC-4 and MEC-10 are DEG/ENaC channels that serve as pore-forming subunit. Functional channels likely contain MEC-2 and MEC-6 are essential accessory subunits that enable channel activity The extracellular matrix, consisting of MEC-5, a collagen isoform, and MEC-1 and MEC-9, both with multiple EGF repeats are also required for mechanotransduction. MEC-7 and MEC-12 are tubulin monomers that form 15-protofilament microtubules required for touch sensitivity [3].
Right panel for mouse: Piezos proteins are a potential candidate for mechanotransduction channels [45,46]. STOML3, a mammalian orthologue of MEC-2, is a necessary accessory protein for mechanotransduction [47,48]. The extracellular tether protein with unknown identity is also required for RA (rapidly adapting) conductance [42], and the intracellular cytoskeleton composing of actin and microtubule are important for mechanotransduction [10].

2.4 Stomatin domain-containing proteins in mechanotransduction and acid sensing

2.4.1 Structure features of stomatin domain-containing proteins

The defining feature of stomatin domain-containing protein family is the stomatin domain itself, and the mammalian members of this family include stomatin, stomain-like proteins (STOMLs) and podocin. The typical stomatin-domain protein is an integral membrane protein with a short hydrophobic region followed by the core stomatin domain (Figure 5a). The N-terminal hydrophobic region enters the inner leaflet of the bilayer and

contributes to the hairpin-like topology of stomatin-domain protein with both the N- and C-terminal tail facing the cytoplasm [50].

Stomatin domain-containing proteins have a tendency to form oligomer. Stomatin have been found to exist as oligomers of some 9–12 monomers in the plasma membrane of epithelial cells [51]. A small C-terminal region of stomatin that is largely hydrophobic is suggested to be involved in oligomerization [52]. The crystal structures of stomatin-domain dimer of mouse stomatin have been resolved. The stomatin-domain dimer assemble into a banana-shape which is formed by an intermolecular β-sheet at the C-terminus of the stomatin domain (Figure 5b), and the banana-shaped dimer is suggested to be the basic functional building block of stomatin [53].

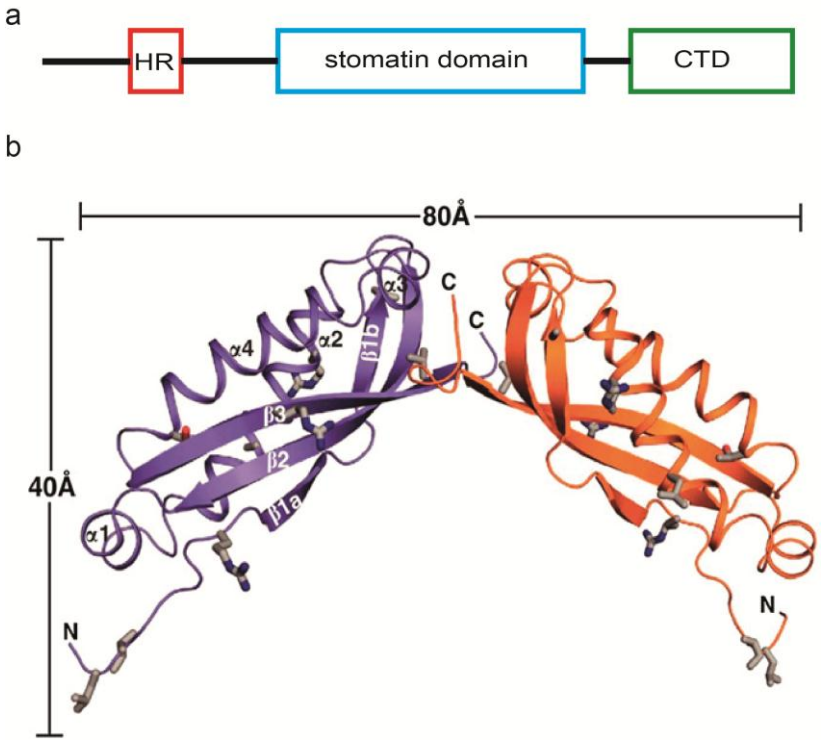

Figure 5. Structure of the mouse stomatin domain. (a) Structure-based domain architecture of stomatin domain-containing protein family. HR, hydrophobic region; CTD, C-terminal domain. (b) Crystal-structure diagram of the mouse stomatin dimer, with the N- and C-termini indicated [53].

2.4.2 Role of stomatin domain-containing proteins in mechanotransduction

2.4.2.1 The role of stomatin in sensory mechanotransduction

Stomatin, a ubiquitous integral membrane protein, was originally isolated from normal human erythrocytes [54]. Human red blood cells that are deficient in stomatin show extremely high membrane permeability to the univalent cations Na^+ and K^+, stomatin is thus presumed to regulate channel or transport in erythrocytes [54,55]. In sensory system, stomatin plays minor role in mechanotransduction, only one subtype of cutaneous mechanoreceptors, D-type receptor, displays impaired sensitivity to mechanical stimuli in the absence of stomatin [56].

2.4.2.2 STOML3 is required for sensory mechanosensation in mouse

STOML3 (stomatin-like protein), an orthologue of nematode MEC-2, was first identified in olfactory sensory neurons with unknown function [57]. Mouse STOML3 is predicted to encode a polypeptide of 287 amino acids and shares 82% sequence similarity with the murine stomatin, 78% with nematode MEC-2. Unlike stomatin, STOML3 is specifically expressed in sensory neuron [58]. STOML3 has been shown to be required for mechanosensation [47]. Earlier electrophysiological studies revealed that roughly thirty-six percent of sensory neurons from *STOML3*$^{-/-}$ mice had no response to mechanical stimuli including slowly adapting mechanoreceptors (SAMs) and rapidly adapting mechanoreceptors upon mechanical stimulation with neurite-indentation, and subpopulation of Aβ fibres and Aδ fibres in *STOML3*$^{-/-}$ mice also lost mechanosensitivity using ex *in vivo* skin-nerve recording [47]. Moreover, touch-driven behavior analysis revealed that STOML3 mutant showed a reduction in tactile discrimination capability [47]. Recent study from *STOML3*$^{-/-}$ sensory neurons further show that loss of STOML3 function causes to the dramatic increase of displacement threshold, which probably account for the earlier observed mechano-insensitivity [48]. Moreover, Poole and colleagues observed a longer latency for mechanosensitive currents including RA, IA and SA in *STOML3*$^{-/-}$ sensory neurons [48]. They suggest STOML3 might facilitate the transfer of force to mechanically gated channels. Taken together, STOML3 is considered to be in an essential subunit for mouse mechanosensation.

2.4.2.3 STOML3 modulates mechanosensitive channel Piezos

2.4.2.3.1 Piezos proteins are bona-fide mechanosensitive channels

Piezos proteins have been identified as true mechanosensitive channel implicated in mammalian sensory mechanotransduction and in fly nociception [21,45,59]. Mammalian piezos including piezo1 and piezo2 can induce mechanically activated currents when expressed in heterologous systems [45]. Of the two members of mammalian piezos, piezo2 is largely expressed in sensory neurons, and knockdown of *piezo2* with RNAi selectively affects rapidly-adapting mechanosensitive currents in cultured sensory neuron, indicating piezo2 probably is a core component of mechanically activated ion channel complex [45]. Moreover, a recent study show piezo2 is a principle mechanotransduction channel in mouse, depletion of *piezo2* in sensory neurons by genetic ablation specifically abolishes RA-mechanosensitive conductance, and causes mice insensitive to innocuous touch sensation [46]. Collectively, these findings suggest piezos are bona-fide mechanotransducer and indeed have physiological function in mammalian mechanosensation.

2.4.2.3.2 STOML3 modulates piezos-mediated mechanosensitive currents

STOML3 functionally interacts with piezos proteins including piezo1 and piezo2, it not only increases the mechanically activated current mediated by piezos, but also potentiates the sensitivity of piezos to be able to detect molecular-scale deflection (~10nm) [48]. Structure-function experiments show the stomatin-domain in STOML3 is responsible for its modulation on piezos [48]. STOML3 is thus considered to be a potent modulator of piezos channels, and the presence of STOML3 in sensory neuron is suggested to fine-tune mechanoreceptor sensitivity. The remaining question is how STOML3 fine regulates piezos-medicated mechanosensitive currents.

2.4.2.4 MEC-2 requires cholesterol to modulate touch sensation in *C.elegans*

MEC-2 physically binds to cholesterol *in vitro*, and the cholesterol-binding activity is required for MEC-2 to regulate the activity of its associated mechanosensitive channel MEC-4/MEC-10 and animal touch sensation [35,60]. Disrupting cholesterol binding activity by mutating the conserved proline residue greatly attenuates MEC-2's action on channel activity and animal touch sensation [60]. Moreover, sensation of touch requires cholesterol in *C. elegans*, animals grown in low cholesterol or cholesterol free medium for several generations have severe defect in touch sensitivity compared with normal animals [60]. Recruiting cholesterol by MEC-2 appears to contribute to touch sensation.

2.4.2.5 Podocin requires cholesterol to regulate its associated mechanosensitive ion channel

Podocytes are visceral epithelial cells supporting the permeability properties of the glomerular filtration barrier. The foot processes of interdigitating podocytes enwrap the glomerular capillaries, and they are connected by a highly specialized membrane-like structure called slit diaphragm, which is considered to monitor glomerular pressure of filtration rate channels [61]. The slit diaphragm is composed of a dynamic multiprotein complex that includes receptors, cytoskeletal and adaptor molecules and ion channels [61]. Several important molecular have been identified in slit diaphragm protein complex such as transmembrane proteins nephrin, podocin, TRPC6 and cytoplasmic adaptor protein CD2AP [62-64]. It is the podocin-TRPC6 channel complex in slit diaphragm that might detect the mechanical tension [60,65]. TRPC6, a member of cation-selective transient receptor potential (TRP) channel family, is a stretch activated channel in podocyte and can be activated by pressure and indention of plasma membrane [66,67]. Podocin co-localizes with TRPC6 in slit diaphragm and regulates TRPC6 activity [60,63,65,67]. Like MEC-2, cholesterol-binding is also required for podocin to regulate TRPC6 channel activity [60,65]. Thus, stomatin family proteins are likely to regulate the activity of associated channels via cholesterol-rich lipid rafts.

2.4.3 Stomatin-domain proteins modulate acid-sensing ion channels

2.4.3.1 Characterization of the acid-sensing ion channels

Acid-sensing ion channels (ASICs), mammalian orthologues of nematode MEC-4/MEC-10, belong to the DEG/ENaC (degenerin /epithelial amiloride-sensitive sodium channel) ion channel family, which is characterized in structure with two hydrophobic transmembrane regions flanking a large extracellular domain. ASICs are voltage-independent Na+ channel which are activated by extracellular acidosis [68]. Seven subunits of ASICs encoded by four genes have been identified in mammals, including ASIC1a/1b/1b2[69-71], ASIC2a/2b[72,73], ASIC3 [74] and ASIC4[75]. Except for ASIC2b and ASIC4, other subunits could form functional homomeric channels [76], whereas specific subunit combinations of ASICs form functional homomeric channels and heteromeric channel complexes with a variety of kinetics properties, pH sensitivity and tissue distribution [77-79].

ASICs are mainly expressed in central nervous system (CNS) and in peripheral sensory neurons (PNS). In central neurons, the acid-sensing ion channels (ASICs) are composed primarily of a combination of ASIC1a homomers and ASIC1a/2 heteromeric channels [80], and are suggested to play an important role in synaptic plasticity, pain processing and multiples neurological diseases such as brain ischemia, some neurodegenerative disease, and multiple sclerosis [81-83]. In peripheral sensory neurons, the channel, consisting of ASIC1/2/3 heteromers [78,84], is distributed on cell body and sensory nerve ending, where they are suggested to involve in mechanosensation and pain perception [85-88].

2.4.3.2 Acid-sensing ion channels regulate mammalian cutaneous mechanosensation

Several lines of evidences suggest the involvement of ASICs in cutaneous mechanosensation. ASIC2a and ASIC3 are localized in cutaneous mechanoreceptors including specialized sensory structures such as meissner corpuscles, merkel cell-neurite complex, and palisades of lanceolate nerve endings of hairy skin [85,86]. Distributions of ASICs in nerve ending imply its potential role in mechanosensation. Single fibre recording from *in vitro* skin-nerve preparation shows certain classes of fibres display aberrant mechanical response properties in ASICs single, double or triple mutants. The

absence of *ASIC2* leads to a decrease of mechanosensitivity in rapidly adapting-Aβ mechanoreceptor, suggesting ASIC2 might play a potential role on the normal detection of light touch [85]. In *ASIC3* null mutant, mechanosensitivity is attenuated in Aδ- and C-mechanociceptor, but is enhanced in rapidly adapting Aβ-mechanoreceptor [86,89]. The later phenotype is probably due to the reduced adaption during ramp stimuli, ASIC3 channel in rapidly adapting-Aβ mechanoreceptor is thus suggested to modulate receptor adaptation [89]. Additionally, simultaneous disruption of mouse *ASIC1a, 2* and *3 genes* (*triple-knockout*) leads to an increase of A-mechanociceptor [90]. Consistent with what they observed in single fibre recording, behavioral study with Von Frey filament show the triple-knockout displays an increase of mechanosensitivity [90]. However, whole-cell recording of mechanically activated current from ASICs double and triple mutants suggests ASICs do not contribute to mechanically activated current [91]. These studies suggest ASICs could not directly transduce mechanical stimuli, and are likely to function as a component of the mechanosensory transduction apparatus to regulate mechanosensation.

2.4.3.3 Stomatin-domain proteins modulate the activity of the acid-sensing ion channels

In *Caenorhabditis elegans*, MEC-2 functionally interact with DEG/ENaC channels [14]. Likewise, mammalian MEC-2 orthologues such as stomatin and STOML3 bind to ASICs and modulate channel activity [49,92]. Price and colleagues show stomatin accelerates the rate of ASIC2 desensitization, and potently decreases the acid-activated current of ASIC3 without altering its surface expression and channel kinetics in heterologous expression cells [92]. Further structure-function analysis reveals that the stomatin-domain of stomatin assembles into a banana-shaped dimer, and the dimerization is crucial for the inhibition of ASIC3 current [53].

Similar to stomatin, STOML3 also physically interacts with ASICs including ASIC1a, ASIC2a and ASIC3, and inhibits acid sensitive ion channels in both heterologous expression cells and sensory neurons [47,49]. In *STOML3*$^{-/-}$ sensory neurons, the proton-gated currents are elevated. In heterologous expression systems, STOML3 inhibits

proton-gated ASICs-mediated currents without altering ASICs surface protein expression [47,49]. However, little is known about how this works. STOML3 might require cholesterol-rich lipid rafts to regulate the activity of ASICs.

2.5 Cholesterol-enriched lipid rafts

2.5.1 Lipid rafts and detergent-resistant membrane (DRM)

Lipid rafts are a highly dynamic and liquid-ordered membrane microdomain enriched with cholesterol, sphingolipid and some proteins [93]. The term "rafts" is originally defined by the procedures used to separate a population of cell membranes. Rafts are biochemically extracted due to resistance to non-ionic detergent at low degree, and thus considered as a collection of detergent-resistant membrane (DRM) fractions featured by insolubility in non-ionic detergents and light buoyant density on sucrose gradient [94]. Moreover, DRMs fractions isolated from cells are also rich in cholesterol and sphingolipid and are in the liquid-ordered phase using electron spin resonance [95]. Isolation of DRMs is thus considered to be one of the most widely used methods to study the components of lipid rafts [93].

2.5.2 Physical properties of cholesterol enriched rafts membrane

Compared with non-rafts bilayer, lipid rafts are suggested to harbor different physical properties in membrane thickness, elasticity, rigidity, dynamics, and lateral pressure profile [96-98]. Presences of cholesterol and sphingolipid in rafts-like membrane increase thickness and rigidity of bilayers by enhancing the lateral packing and suppressing the lateral diffusion of lipids and ordering of acyl chain, and change the lateral force profile of bilayers [96,99]. Lipid rafts might influence the activity of mechanosensitive ion channel due to its different physical properties compared with non-raft bilayer. Indeed, it has been proposed that the particular physical properties due to the presence of cholesterol and sphingolipid in rafts facilitate the opening of mechanosensitive ion channel, such as bacteria stretch activated channel MscL [96,99].

2.5.2 Functional diversity of lipid rafts on cellular process

The ordered rafts microdomain is considered to be involved in various cellular process such as membrane trafficking, protein transporting, membrane polarization, signaling transduction [100-103]. Lipid rafts probably provide an environment to assemble and concentrate proteins within the plane of the bilayer [100], some proteins preferentially partition into lipid rafts-like microdomain, typical examples includes glycosylphosphatidylinositol (GPI)-anchored proteins, palmitoylated proteins, cholesterol binding proteins, sphingolipid binding proteins, phospholipid binding proteins. In nervous system, lipid rafts are proposed to function in controlling neurotransmitter and ionotropic receptors transports, neural signaling, neuronal cell adhesion, and axon guidance [104]. Growing evidence also reveal its participation in the regulation of various types of ion channels [105].

2.6 Objectives

Of animal's five senses, the molecular basis of sight, smell and taste are well known, which are initiated by the binding of a ligand to its specific G-protein coupled receptor. However, the molecular basis of mechanosensation remains to be least understood. In mammal, STOML3 is identified to be an essential subunit of mammalian mechanotransducer [47]. However, the molecular mechanism for STOML3 to regulate the mechanotransduction remains elusive. As mentioned earlier in this Chapter, lipid rafts, known as a dynamic nanoscale microdomain enriched in cholesterol and sphingolipid in biological membrane, modify the physical properties of its neighboring membrane such as thickness, stiffness and pressure profile, which would ultimately regulate the activity of mechanosensitive ion channels [96,99]. Moreover, previous studies have suggested recruiting cholesterol by MEC-2 regulates the activity of its associated MEC-4 channel complex and contributes to touch sensation in *C. elegans* [35,60]. Furthermore, several other members of stomatin like protein family have been detected in cholesterol-enriched membrane fraction derived from plasma membrane such as stomatin and STOML-1 [106-

[108]. Thus here the objective in this thesis is to test whether STOML3, as a member of stomatin like protein family, regulates the activity of mechanosensitive channels in mammalian sensory neurons and its associated ASICs channel through associating with cholesterol enriched lipid rafts.

3. Materials and methods

3.1 Animals

Experiments were carried out in adult C57BL/6 and *STOML3*$^{-/-}$ mice (male, aged 8-10 weeks, 20-25g in weight). Mice were housed 3 to 5 per cage, and maintained in a temperature and humidity-controlled room on a 12/12h light/dark cycle with access to rodent chow and water ad libitum. All experiments were conducted according to the guidelines of German Animal Protection Law.

3.2 Cell culture

3.2.1 Cell culture and transient transfection

Chinese hamster ovarian (CHO) cells, human embryonic kidney (HEK) 293 cells and mouse neuroblastoma N2a cells were cultured at 37°C, 5% CO2 in DMEM nutrient medium (GIBCO) supplemented with 10% fetal bovine serum and 1% penicillin-streptomycin. Cells were transfected with cDNA using lipofectamine 2000 transfection reagent (Invitrogen) according to the manufacturer's recommendations. For electrophysiological studies in CHO cells, cells were plated at a roughly 50% confluence onto 12-mm round glass coverslips in 24-well plates, ASIC3 (1μg) was cotransfected with pEGFP as control, green fluorescent protein (eGFP)-tagged STOML3 or STOML3 mutants at a 8:1 ratio into CHO cells. Around 90% of green cells have an acid response current. Whole cell patch clamp was performed 18-30h after transfection.

N2a cells used for electrophysiological recording were plated at a roughly 50% confluence onto 12-mm round glass coverslips in 24-well plates and transfected with green fluorescent protein (EGFP)-tagged STOML3 or STOML3-P40S. Whole cell patch clamp recording was performed 18-30h after transfection in green cells. Whole cell patch clamp recording was performed 18-30h after transfection. For stiffness measurement, *Piezo1*-IRES-GFP (a kind gift from Ardem Patapoutian Group) was co-transfected with

Myc-STOML3, Myc-STOML3-P40S or empty pcDNA3.1(+) vector at a 1:8 ratio in HEK293 cells and were used 48 hour later.

3.2.2 DRG neurons culture and transfection

DRG neurones from mice were prepared as previously described [9]. Briefly, mice were killed by placement in a CO2-filled chamber followed by cervical dislocation, DRG from all spinal levels were removed. Animal housing and care, as well as protocols for killing, are registered with and approved by the appropriate German federal authorities. The DRG neurons were incubated with 1mg/ml collagenase IV (Sigma,) and 0.05% trypsin (Sigma) for 30 min each at 37◦C. DRG neurons were mechanically dissociated into a suspension of single cells in DMEM/Hams-F12 medium containing 10% heat-inactivated horse serum, 20mm glutamine, 0.8% glucose, 100 U penicillin and 100 mg ml−1 streptomycin, and were then spot-plated on poly-l-lysine (500µg/ml)–laminin (20µg/ml)-coated coverslips, and maintained at 37◦C in 5% CO_2 . The median time in culture was 24 h (range, 16–48 h), and no nerve growth factor or other neurotrophin was added to the medium.

DRG neurons were transfected using the Nucleofector system (Lonza AG) according to the manufacturer's instructions. In brief, neurons were suspended in 20 µl of Mouse Neuron Nucleofector solution (SCN nucleofector kit) and a total 4-5µg of plasmid DNA at room temperature. The mixture was transferred to a cuvette and electroporated with the preinstalled program SCN Basic Neuro program 6. After electroporation, neurons were allowed to recover in RPMI medium supplemented with 10% horse serum for 10 min at 37°C, and then plated on pre-coated coverslips. RPMI medium was replaced with fresh growth medium (supplemented with 100 ng/ml nerve growth factor (NGF), 50 ng/ml BDNF) 3-4 h later, and neurons were grown for 18-24 hours.

3.3 Molecular biology and biochemistry analysis

3.3.1 Molecular cloning and cDNA construct

RNA was isolated from adult mice dorsal root ganglia(DRG) using RNA extraction kit (Qiagen). The resulting 1μg of poly(A)- RNA from DRG was reverse transcribed using SuperScript II reverse transcriptase (Invitrogen), followed by polymerase chain reaction (PCR) with below listed primers: for ASIC1a (Gen-Bank accession number NM_009597), 5'ATGGAACTGAAGACCGAGGAGG3' (forward) and 5'CTTAGCAGGTAAAGTCCTCAAACG 3'(reverse); for ASIC2a(Gen-Bank accession number NM_001034013), 5'GCCTCGGGCTGAATGAATG 3'(forward) and 5'GTTAGTTCTTGGACAGTTC 3'(reverse); for ASIC3(Gen-Bank accession number NM_183000), 5' TCCCTGCTCCAGCCATGAAAC 3'(forward) and 5'CTAGAGCCTTGTCACGAGGTAA 3'(reverse); for STOML3(Gen-Bank accession number NM_153156), 5' AGGCACCTCAAGAATGAGATGG 3' (forward) and 5' CAGGCTGTTACGTGGAAGACC 3' (reverse);

Mouse *ASIC1*, *ASIC2a*, *ASIC3* and *STOML3* cDNA were then subcloned into pcDNA3.1(+) expression vector (provided by), Flag(D Y K D D D D K) and Myc (E Q K L I S E E D L) sequences were tagged at C-terminus of ASICs and STOML3 respectively. Mouse *STOML3* cDNA was also subcloned into pEGFP-N1 expression vector. Proline was mutated to serine (TCC) at position 40, and Cysteine was mutated to Alanine (TGC to GCC) at positions 46 and 80 of STOML3 amino acid sequences by recombinant PCR.

3.3.2 Isolation of lipid rafts with detergent-resistant method

Lipid rafts from transfected CHO would be obtained by methods similar to those described previously [109]. Briefly, transiently transfected cells or isolated DRG neurons would be homogenized in 0.5-1% Triton X-100 containing lysis buffer (20 mM HEPES, 5 mM EDTA, 150 mM NaCl, pH 7.4) with Complete protease inhibitors. The solution was then lysated by ultrasonication, and 500 μl of lysate would be mixed with 500 μl of 80% sucrose solution (final concentration, 40%) and applied in the bottom of a centrifugation tube. A discontinuous sucrose gradient was prepared by layering 2ml 35% sucrose and 1ml 5% sucrose. Gradients are centrifuged at 50,000rpm for 22 h in a Thermo TH-660 rotor at 4°C in a WX80 Ultracentrifuge. After centrifugation, eight

fractions (500 μl) from the top would be collected, and equal volumes of each fraction were analyzed by western blotting. The endogenous raft-specific protein Flotillin2 was used to check the effectivity of this method, which is supposed to be expressed in buoyant, low-density fractions.

3.3.3 Immunoblotting

Samples were separated by 10% SDS-PAGE gel and transferred to a Polyvinylidene difluoride (PVDF) membrane (Roche). The membrane was blocked in 5% bovine serum albumin in TBST (10mM Tris, 150mM NaCl and 0.1% Tween 20, pH 8.0) and then incubated with primary antibody: anti-c-Myc(1:3000; Sigma), anti-Flotilin-2(1:2000; Santa Cruz). Membranes were subsequently incubated with Horseradish peroxidase (HRP) conjugated anti-rabbit IgG (1:5000: sigma) and developed with an enhanced chemiluminiscence kit (Roche). Quantification analysis was performed with ImageJ software.

3.3.4 Cholesterol depletion

Cholesterol depletion would be performed as described previously [110]. Briefly, raft-like microdomains were chemically disrupted by depleting cholesterol with methyl-β-cyclodextrin (MβCD; Sigma). In all cases, cells were washed twice with PBS and then incubated with MβCD. For electrophysiological experiments, cells were preincubated at 37°C for 1h in 5mM MβCD; For filipin staining, control and MβCD-treated DRG neurons were fixed in 4% paraformaldehyde in PBS for 10min at room temperature (RT), followed by three rinses in PBS. Filipin (50μg/ml in PBS, 2 hours at RT, sigma), a cholesterol-binding fluorescent agent, was used to visualize cholesterol.

3.4 Electrophysiology

3.4.1 Electrophysiology

Patch-clamp experiments were performed in standard whole-cell recordings using fire-polished glass electrodes with a resistance of 3–5MΩ. Extracellular solution for DRG contained (mM): NaCl 140, MgCl2 1, CaCl2 2, KCl 4, glucose 4 and Hepes 10 (pH 7.4 adjusted with NaOH), and electrodes were filled with solution containing (mM): KCl 110, Na+ 10, MgCl2 1, EGTA 1 and Hepes 10 (pH 7.3 adjusted with KOH). External solution for CHO contained (mM): NaCl 140, KCl 4, MgCl2 1, CaCl2 1.8, glucose 4 and HEPES 10 (pH7.4 adjusted with NaOH), and internal solution for CHO contained (mM): KCl 140, Na+ 5, MgCl2 1.6, EGTA 5 and Hepes 10 (pH 7.3 adjusted with KOH).

Cells were perfused with drug-containing solutions by moving an array of outlets in front of the patched cells (WAS02; Ditel, Prague), and observed with Observer A1 inverted microscope (Zeiss, Germany) equipped with a CCD camera and the imaging software AxioVision. The measurement of DRG soma size was made using digital photographs of each recorded cell, and diameter of each soma was calculated from the mean of the longest and shortest diameters. Membrane current and voltage were amplified and acquired using an EPC-10 amplifier sampled at 40 kHz; signals were analyzed using Pulse and PulseFit software (HEKA). Pipette and membrane capacitance were compensated with the auto function of Pulse, the membrane voltage was held at −60 mV with the voltage-clamp circuit. After establishing whole-cell configuration in DRG neurons, voltage-gated currents were measured using a standard series of testing potential. Briefly, the cells were prepulsed to −120 mV for 150 ms and depolarized from −65 to +55 mV in 5mV increments (40 ms test pulse duration). Next action potentials were evoked by current injection in current-clamp mode (pulses varied from 0.02 to 10 nA for 80 ms). For most of recording in DRG cells, to minimize the voltage error, 70% of the series resistance was compensated. All experiments were performed at room temperature.

For patch clamp experiments examining proton-gated currents in CHO cells, low pH solutions (buffered with 10mM MES) were applied by moving an array of outlets in front of the patched cells [47]. Peak inward currents were measured in voltage clamp at a holding potential of –60 mV during super perfusion of low pH solutions

3.4.2 Mechanical stimulation

Mechanical stimuli were applied using a heat-polished glass pipette (tip diameter 1–4 μm), driven by a MM3A Micromanipulator system (Kleindiek), positioned at an angle of 45 degrees to the surface of the dish. The nanometer is a piezo-based motor equipped with coarse and fine modes of operation. In the coarse mode, the motor moves a slider very rapidly in single steps. Calibration of single-step size in the coarse mode can be done by instructing the motor to move a large number of steps and measuring the moved distance. The velocity of the motor is set by changing frequency which controls how rapidly the piezo crystal is activated. The maximum velocity of movement for 1μm is 10μm/ms. The voltage signal sent to the nanomotor was simultaneously fed into EPC9 amplifier so that the timing of the nanomotor movement related to mechanically activated current can be accurately measured. In the fine mode of nanomotor, the accuracy and speed of displacement stimuli was tested by measuring actual movement of the tip was a laser interferometre. The maximum movement of motor is 1000 fine steps which correspond approximately to 1000nm, and the speed of movement in the fine mode is set to 10μm/ms.

The probe was positioned near the neurite or cell body, moved forward in steps of 200–600nm for 500ms and then withdrawn in fine mode. If there was no response, the probe was moved forward by one step coarse mode; the same procedure was repeated until a mechanically activated inward current was recorded. For the data analysis, mean amplitude of the mechanically gated currents and the measured kinetic parameters of the currents were obtained using the 512nm step. For analysis of the kinetic properties of mechanically activated current, traces were fit with single exponential functions using the Fitmaster software (HEKA). Data are presented as mean±s.e.m.

3.5 Atomic force microscopy (AFM) measurements

3.5.1 Force-spectroscopy measurements

Force spectroscopy measurements were performed by using a NanoWizard **atomic** AFM (JPK Instruments, Berlin, Germany) equipped with a fluid chamber (Biocell; JPK) for live cell analysis and an inverted optical microscope (Axiovert 200; Zeiss) for sample

observation. DRG neurons or HEK cells were inserted into the fluid chamber immersed in culture medium and measurements were carried out at room temperature. The status of cells was constantly monitored by optical microscope. Indenters for probing cell elasticity were prepared by mounting silica microspheres of 4.5μm nominal diameter to silicon AFM tipless cantilevers of nominal spring constant k = 0.04 N/m (Nanoworld Arrow TL1Au with Ti/Au back tip coating) by using UV sensitive glue. Silica beads were picked under microscopy control. Before measurements the spring constant of the cantilevers was calibrated by using the thermal noise method [111]. Nano-indentation measurements were performed to evaluate cell elasticity. By using optical microscope the bead-mounted cantilever was brought over the soma of single DRG and pressed down to indent the cell. The motion of the z-piezo and the force were recorded. On each cell eight-about ten force-displacement (F-D) curves were acquired with a force load of 0.5 nN and at a rate of 5μm/sec in closed loop feed-back mode. For evaluation of cell viscosity, the force needed to pull a plasma membrane tether (i.e. tether force) at a constant speed is measured and then the dependence of tether force on speed is analyzed. In these measurements the bead-mounted cantilever was pressed against the cell soma with a contact force of 500 pN for contact time of 10-30 sec to allow the cell establishing adhesion points with the silica-bead. Afterward the cantilever was retracted with different pulling speed (2, 5, 8, 12 18 μm/sec). After each force measurement, the cell was allowed to recover for a time period comparable to the contact time, before performing further pulling measurements. The resulting F-D retraction curves present a long plateau with steps like features whose height provides a direct measure of tether force.

3.5.2 Evaluation of cell elasticity

Cell elastic properties can be assessed by determining the Young's modulus. The Hertz model describes the relation between the applied force (F), indentation (δ) and Young's modulus (E). To evaluate E from the force-indentation curves, a Sneddon's modification of the Hertz model for the elastic indentation of a flat, soft sample by a stiff sphere can be used [112].

$$F = \frac{4}{3}\frac{E}{(1-\nu^2)}\sqrt{R}\,\delta^{3/2}$$

However, a cell comprises of different structures starting from the external plasma membrane, cortical actin, cytoskeleton, cytoplasmic organelles and nucleus, which make it a complicated mechanical system. The deformations of different cell structures could determine different regimes which will appear convoluted into a single force-indentation curve. The total indentation in this case would comprise of two (or even more) contributions: the first from the compression of the superficial layer of the cell, while the other corresponding to the rest of cell structures (i.e. cytoskeleton, nuclei, etc.). In order to take into account the presence of such different contributions we used a variation of this model. We consider the cell as a set of elastic components where firstly it is indented the external layer and then the second internal one. If we assume that the each single part deforms elastically, the fitting curve can be written as follow:

$F(\delta) = F_0 + A1(\delta-\delta_1)^{3/2} + A2\,(\delta-\delta_2)^{3/2}$

$$A1 = \frac{4}{3}\frac{E1}{(1-\nu^2)}\sqrt{R}$$

$$A2 = \frac{4}{3}\frac{E2}{(1-\nu^2)}\sqrt{R}$$

where F_0 is the force at zero deformation, R is the radius of the spherical indenter, ν is the sample's Poisson ratio (set to 0.5 for cell). $E1$ and $E2$ are the Young's modulus as obtained for the first and second elastic component of the curve, while δ is the indentation. δ_1 and δ_2 represent the first and the second contact point. The first contact point, defined as the point where the cantilever deflection starts to rise and the second point where the curve changes regime. Hence, the second contact point, as revealed by the fitting procedure, can be used to identify the regime variation in the curve.

Data fitting was performed on the approach part of the recorded F-D curves. JPK DP software was used to convert the curve into force-indentation curve by subtracting the cantilever bending from the signal height to calculate indentation. The total number of

curves for WT and *STOML3*$^{-/-}$ sensory neuron was then fitted by a MatLab routine. Resulting *E*1 and *E*2 values were plotted as bar graph and statistically analyzed.

In those cases in which significant changes in regime were not observed and the fit provided a second contact point outside the experimental data range, only the *E*1 value is provided for the whole cell.

According to this fitting procedure we could identify a second contact point at 360 ± 10 nm for WT and 330 ± 10 nm for *STOML3*$^{-/-}$. In total 31% of the curves for WT DRG and 41% for *STOML3*$^{-/-}$ displayed two different regimes in the fitting range of force-indentation curve (-1 and +1 μm). This suggests that in some cases the superficial layer of the cell has significantly different elastic properties from the rest of the cell, while in other cases the cell behaves as a homogenous elastic material and the fit can be performed with a classical Hertz model for a homogeneous material.

In the case of HEK293 cells transfected with empty vector, the second contact point was found at 420 ± 20 nm, consistent with all the other transfected groups analyzed

3.5.3 Evaluation of membrane viscosity and tension

For evaluating cell membrane viscosity, the mean tether force per cell was obtained and then the average on more than 20 cells was plotted as function of the pulling velocity. The effective viscosity η_{eff} and threshold pulling force F_0 were then obtained by a linear fit of the force-velocity curve [113]

$F=F_0+2\pi\eta_{eff}V_t$

The F_0 threshold force for extracting a tether is given by

$F_0= 2\pi\sqrt{2B\ (T+\gamma)}$

where *B* is the membrane-bending stiffness, *T* in-plane membrane tension and γ is membrane-cytoskeleton adhesion energy. The sum (T+ γ) provides the apparent surface tension (T_{app}). Hence by using the formula : $T_{app}= F_0^2/(8\ \pi B)$ we evaluated the apparent surface tension considering a *B* value of 2.7 x 10^{-19} N.m [113]. Percentage of error has been evaluated according to propagation of error.

3.6 Induction of neuropathic pain by chronic constriction injury and nociceptive behavior tests

CCI (chronic constriction injury) model was induced as described [47]. In brief, in deeply anaesthetized mice (isoflurane) four loose silk ligatures (4/0) were placed (with about 0.5 mm spacing) around the sciatic nerve at the level of the right mid-thigh. Ligatures were tied until they elicited a brief twitch in the respective hind limb. Mechanical allodynia was measured using von Frey filament [114]. Intraplantar injection of MβCD (Sigma, 2mg/kg) dissolved in sterile saline was performed 2 days after CCI. The withdrawal threshold was measured for each mouse before and at various times after injection. All experiments were performed blind to both the genotype of the mice and the injected drug.

3.7 Statistics

Fitmaster and Graphpad Prism 4 software suites were used to perform linear and nonlinear fitting of data. The time course of current activation and inactivation τ were fitted to first order exponential. Current-stimulus curves were fitted using the following Boltzman function: $I(\chi) = I_{max}[1+\exp(\chi_{1/2}-\chi)/s]^{-1}$, where I is the peak amplitude at holding potential -60mV, χ is the displacement (in nanometer) of the mechano-probe, I_{max} is the maximum current, $\chi_{1/2}$ is the displacement value producing 50% of I_{max} and s is the slope sensitivity indicating the change in channel active state probability for a given change in force. All statistical comparisons were two-sided and were performed with Prism. For all in vitro experiment, recordings were pooled from at least three mice. The sample size was justified by significance testing, taking into account available number of neurons per in vitro experiment or mice from same litters. Unpaired two-tailed t-tests were used for two-group comparison. One-way repeated measures ANOVA analysis with post hoc Dunnett's Multiple Comparision Test was used to judge MβCD effect over time. Two-way repeated measures ANOVA analysis was performed to compare the MβCD effect on C57BL/6N and *STOML3*$^{-/-}$ mice over time. $P<0.05$ was considered to be statistically. All means are expressed as mean ± standard error of the mean. All replicates were biological and all experiments were performed blind to the genotype of the mice.

4. Results

4.1 STOML3 modulates mechanosensation via cholesterol enriched lipid rafts

The following chapter (4.1.1-4.1.4) are taken from "Membrane stiffening by STOML3 facilitates mechanosensation in sensory neurons", Yanmei Qi, Flavia Frattini, Laura Andolfi, Marco Lazzarino, Jing Hu. Nat. Commun. 6:8512 doi: 10.1038/ncomms9512 (2015).

4.1.1 Effects of cholesterol depletion on mechanotransduction in sensory neurons

4.1.1.1 Methyl-β-cyclodextrin is effective on depleting cholesterol in sensory neurons

Methyl-β-cyclodextrin (MβCD), a water-soluble cyclic oligosaccharide, is commonly utilized as an efficient agent to remove membrane cholesterol and disrupt lipid raft integrity [115,116], and the importance of lipid rafts can be inferred from cholesterol depletion [93]. To test whether cholesterol enriched lipid rafts play a role in mechanotransduction, cultured DRG sensory neurons were treated with or without MβCD. We labeled the membrane cholesterol in DRG neurons using filipin staining, a fluorescent cholesterol-binding molecular. Treatment with 5mM MβCD for 1h resulted in a strong decrease of cholesterol in sensory neuron plasma membrane without change of cell morphology (Figure 6), indicating the efficacy of MβCD under our treatment condition (5mM, 1h) in DRG sensory neuron.

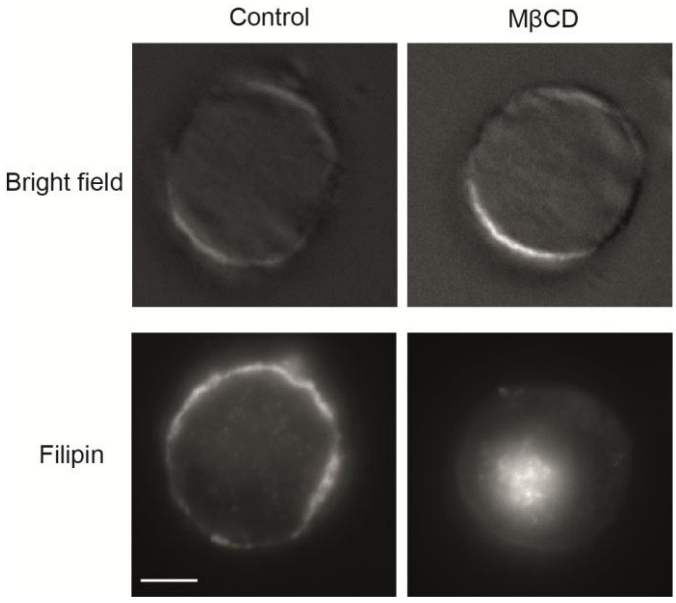

Figure 6. Bright field and fluorescence (bottom) image of filipin labeled neurons treated without (left) or with Methyl-β-cyclodextrin (MβCD). A marked reduction of membrane cholesterol was observed in neurons treated with MβCD (5mM, 1h). Scale bar: 10μm

4.1.1.2 Cholesterol depletion abolishes the mechanosensitivity of slowly adapting mechanosensitive channel in sensory neurons

To determine the effects of cholesterol depletion on mechanotransduction, whole-cell patch clamp recording was performed immediately after MβCD (5mM, 1h) treatment to record mechanosensitive currents while small mechanical stimulus was given to the neurite (~500nm displacement). We found cholesterol depletion with MβCD elevated significantly the proportion of neurons that have no mechanical response (Figure 7), with around 28% (17 of 60 cells) sensory neurons in cholesterol depleted DRG neuron in contrast to 10% (6 of 58 cells) in control group (Fisher's exact test, $^{**}p<0.01$). According to the adaptation property of mechanically activated current, responsive cells can be further grouped into rapidly adapting (RA, inactivation in <5ms), intermediately adapting (IA, inactivation in <50ms) or slowly adapting (SA, no adaptation during 230ms stimulus) [9]. Remarkably, the proportion of sensory neurons with a SA-mechanosensitive current was significantly reduced from 22% (13/58 cells) in the control

to just 5% (3/60 cells) in MβCD-treated cultures (Fisher's exact test, $^{**}p<0.01$), while the incidence of RA- or IA-mechanosensitive currents was not affected (Figure 4). Mechanosensitivity of neurons that have a SA-mechanosensitive current was obviously suppressed by cholesterol depletion. While cholesterol depletion did not alter the latency, activation time constant and current amplitude of the remaining SA-mechanosensitive currents (Table 1). These data suggest disrupting cholesterol enriched lipid rafts, thus changing the local membrane environment, has a dramatic influence on SA-mechanosensitive conductance.

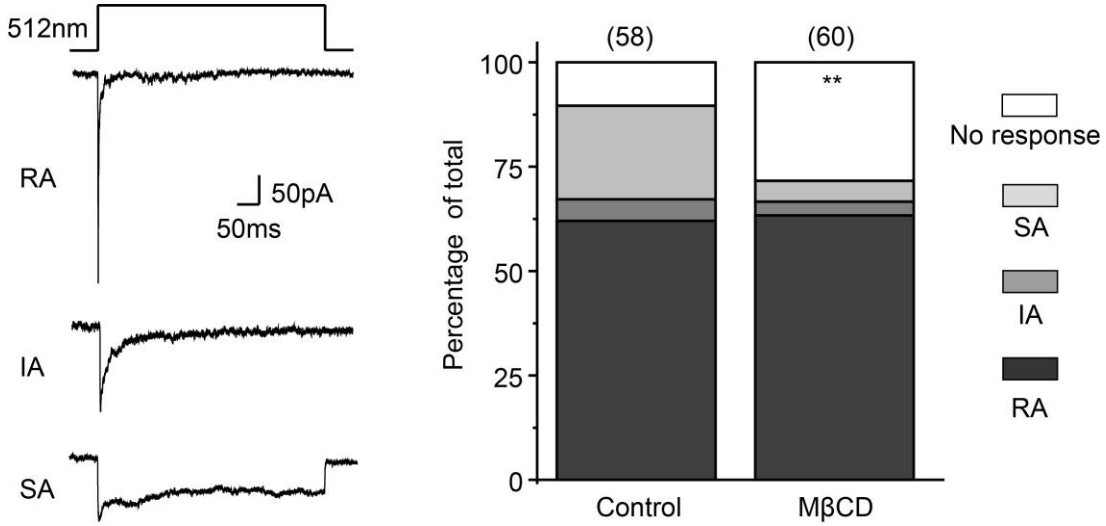

Figure 7. Cholesterol depletion abolishes slowly adapting mechanosensitive conductance. Left: representative traces of rapidly adapting (RA), intermediately adapting (IA) and slowly adapting(SA) mechanosensitive currents evoked by stimulating sensory neuron neurites. Right: Stacked histograms show the proportion of the three types of mechanosensitive current observed in control and MβCD-treated neurons. Note the marked loss of SA-mechanosensitive current in MβCD treated group (The number of recorded neurons is noted at the top of each histogram, data are analysed using Fisher's exact test, $^{**}p<0.01$).

4.1.1.3 Effects of cholesterol depletion on membrane electrophysiological properties of sensory neurons

Cholesterol is well known as one important molecular in cell plasma membrane and is emerging to regulate the functions of many types of ion channels [105], we would like to

examine the effects of MβCD treatment (5mM, 1h at 37◦C) on membrane electrophysiological properties of DRG neurons. It has been suggested that mechanoreceptors are likely to have narrow action potential (AP) and nociceptors potentially possess broad action potential [9], we thus grouped neurons into mechanoreceptor (half AP duration <1ms) and nociceptor (half AP duration ≥1ms), and compared the membrane properties of mechanoreceptor or nociceptor between control and MβCD treated groups. MβCD treatment did not alter the membrane capacitance and input resistance in both mechanoreceptor and nociceptor (Figure 8a and 8b, unpaired t-test, $p>0.05$). While the rest membrane potential (RMP) recorded under current clamp mode was slightly but significantly depolarized in mechanoreceptor after MβCD treatment (Figure 8c, unpaired t-test, ** $p<0.01$). Cholesterol depletion did not significantly affect the action potential threshold (injected current to initiate AP) in both mechanoreceptor and nociceptor (Figure 8e), but significantly reduced the AP amplitude in mechanoreceptor (Figure 8d, unpaired t-test, ** $p<0.01$). Plots of current–voltage (I-V) curve for voltage gated inward and outward currents revealed that cholesterol depletion reduced the voltage gated inward current density in nociceptors but not in mechanoreceptors (Figure 9), which is consistent with previous report showing the association of tetrodotoxin (TTX)-resistant voltage gated sodium channels with lipid rafts in nociceptors [117]. All together, these data suggest cholesterol depletion with MβCD modulates the membrane electrophysiological properties in sensory neuron.

Table 1. Physiological properties of the mechanosensitive current

	WT Control n=58	WT MßCD n=60
RA cells	n=36	n=38
mean soma size(µm)	23.5±0.6 (17-35µm)	24.5±0.6 (19-32µm)
mean current amplitude(pA)	106.8±17.2	57.1±7.74**
latency(ms)	1.11±0.13	1.03±0.07
activation τ1 (ms)	0.51±0.06	0.38±0.05
inactivation τ2 (ms)	0.9±0.11	0.9±0.13
RMP(mV)	-64.18±0.77	-62.5±0.61
SA cells	n=13	n=3
mean soma size(µm)	22.1±1.02 (13-26µm)	25.0±1.4 (22-27µm)
mean current amplitude(pA)	107.2±20.7	141.0±104
latency(ms)	1.06±0.24	1.24±0.42
activation τ1 (ms)	0.52±0.08	0.55±0.26
RMP(mV)	-66.7±1.01	-63.3±2.6
IA cells	n=3	n=2
mean soma size(µm)	23.8±0.9 (22-26µm)	20.7±3.9 (16-25µm)
mean current amplitude(pA)	128.3±42	59.1±33.7
latency(ms)	0.88±0.1	0.26±0.82
activation τ1 (ms)	0.28±0.08	1.25±0.13
inactivation τ2 (ms)	14.05±3.63	13.52±7.28
RMP(mV)	-66.3±2.3	-66.5±3.5
No response	n=6	n=17
mean soma size(µm)	20.44±1.39 (18-27µm)	20.8±0.93 (16-28µm)
RMP(mV)	-60.67±2.1	-61.88±0.62

unpaired t test, one asterisk, $p<0.05$

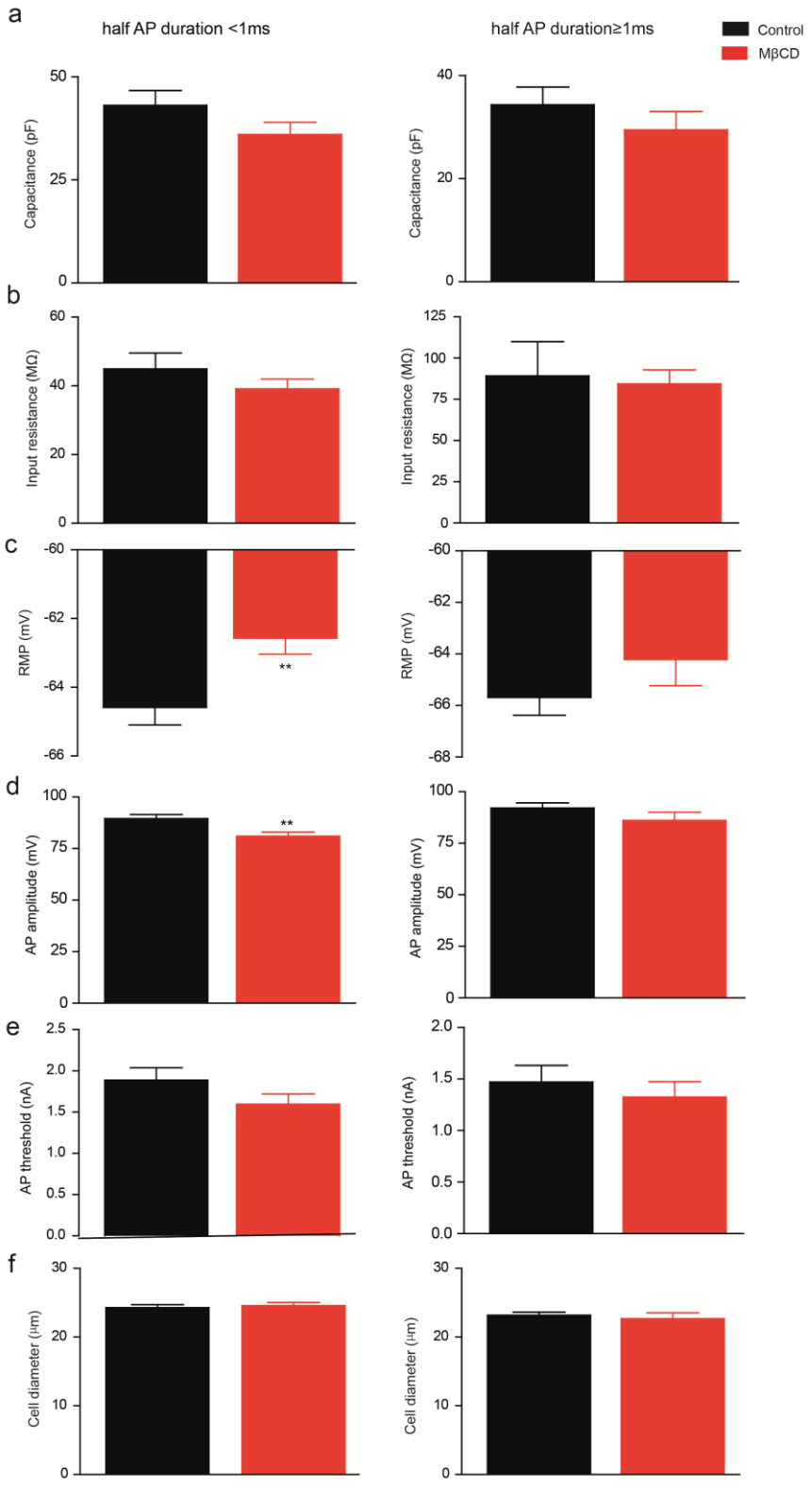

Figure 8. Effects of cholesterol depletion on membrane properties of wild-type sensory neurons. Neurons are grouped into mechanoreceptor (left; 1/2 AP duration

<1ms) and nociceptor (right; 1/2 AP duration ≥ 1ms). (a, b) Summary of membrane capacitance (a) and input resistance (b) for control and MβCD-treated cells. No significant differences were observed as compared with controls in both mechanoreceptor (n=44-49, unpaired t-Test $p>0.05$) and nociceptor (n=23-33, unpaired t-Test p>0.05). (c) Quantitative comparison of rest membrane potential (RMP) in control and MβCD-treated neurons. MβCD slightly depolarized RMP in mechanoreceptor (n=44-49, unpaired t-Test **$p<0.01$) but not in nociceptor (n=23-32, unpaired t-Test $p>0.05$). (d) Mean AP amplitude at current-clamp mode for control and MβCD-treated cells. Note the significant reduction of AP amplitude in mechanoreceptor after MβCD treatment (n=44-49, unpaired t-Test **$p<0.01$). MβCD did not alter the AP amplitude in nociceptor (n=23-33, unpaired t-Test $p>0.05$). (e) Threshold current for AP initiation measured at current-clamp mode for control and MβCD-treated cells). No significant differences were observed as compared with controls in both mechanoreceptor (n=44-49, unpaired t-Test $p>0.05$) and nociceptor (n=23-33, unpaired t-Test $p>0.05$). (f) Mean cell diameter of recorded sensory neurons from control and MβCD-treated groups. No significant differences were observed as compared with controls in both mechanoreceptor (n=44-49, unpaired t-Test $p>0.05$) and nociceptor (n=23-33, unpaired t-Test $p>0.05$). Error bar indicates s.e.m.

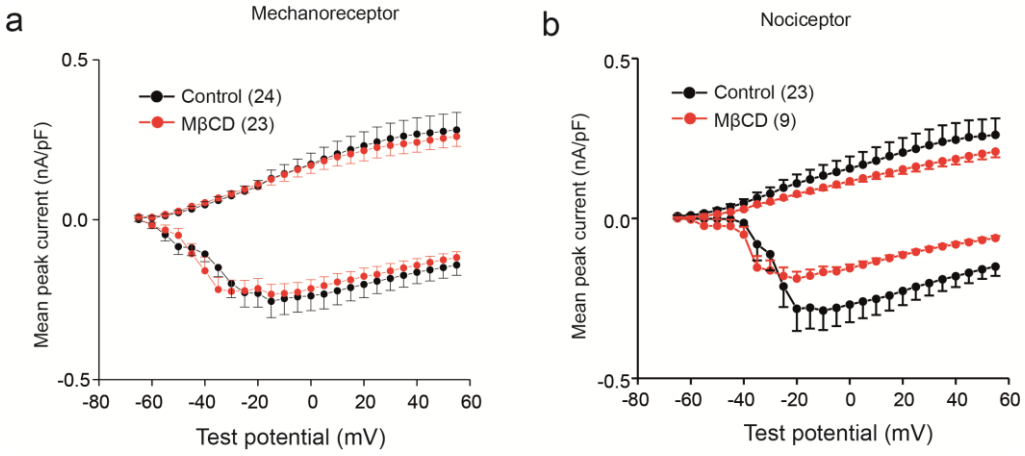

Figure 9. Effects of MβCD treatment on voltage gated currents in cultured sensory neurons. Mean whole-cell inward and outward currents measured at different test potentials for control and MβCD-treated cells. Neurons are grouped into mechanoreceptor (a) (1/2 AP duration <1ms) and nociceptor. (b) (1/2 AP duration ≥ 1ms). Cells were first prepulsed to -120mV and then depolarized from -65mV to 55mV in 5-mV increment. No significant change was seen in the peak amplitude of voltage gated inward and outward current between control and MβCD-treated cells at each test potential for mechanoreceptor or nociceptor (Two-way analysis of variance (ANOVA) followed by Bonferroni *post hoc* test, $p>0.05$). The number of cells is noted. Data are expressed as mean±s.e.m.

4.1.1.4 Effects of depleting cholesterol on rapidly adapting mechanosensitive currents in sensory neuron

4.1.1.4.1 Depleting cholesterol reduces rapidly adapting mechanosensitive currents in sensory neuron

In our recording, cells that have rapidly adapting (RA) mechanosensitive currents accounted for roughly 60% of total DRG neurons in both control and MβCD-treated groups (Figure 7). To explore the effects of depleting cholesterol on RA channel sensitivity, we went on to analyse the peak amplitude, latency and inactivation time constant of RA- mechanosensitive currents. We show cholesterol depletion with MβCD suppressed RA-mechanosensitive ion channel activity. The peak amplitude of RA mechanically currents was significantly reduced in MβCD treated cells compared to control (Figure 10a and 10b; from 106.8 ±17.3 pA at -60mV, n=36 to 57±7.7 pA at -60mV, n=38; unpaired t-test $p<0.01$). Additionally, the kinetics properties of RA currents including latency and inactivation time constant were not affected by MβCD pretreatment (Figure 10c), indicating the gating properties of RA channels are intact. The reduction of RA currents after MβCD treatment is probably due to the change of channel number in an active state.

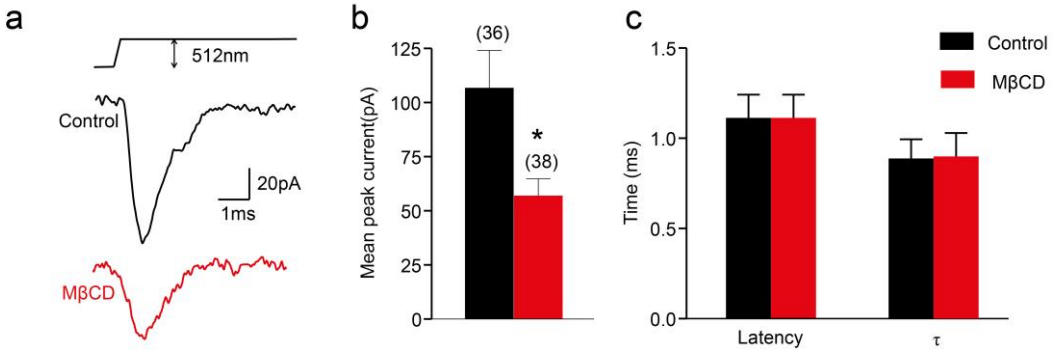

Figure 10. Cholesterol depletion reduces rapidly adapting mechaosensitive currents in sensory neurons. (a) Representative traces of RA-mechanosensitve currents recorded from control or MβCD-treated neurons. (b) Quantitative comparison of the peak amplitude of RA mechanosensitive currents recorded in control and MβCD treated neurons. Data are represented as mean ± s.e.m, the number of recorded neurons is noted

above each column. Note that the amplitude of RA-mechanosensitive current in MβCD treated group was significantly smaller than control (*p<0.05, unpaired t-Test). (c) Mean latency and inactivation time constant (τ) of RA-mechanosensitive current in control and MβCD-treated neurons. No significant differences were observed as compared with controls (n=36-38, P>0.05 student's Test).

4.1.1.4.2 Effects of cholesterol depletion on coding properties of RA currents

To further investigate the effects of cholesterol depletion on the coding properties of RA mechanosensitive currents, we recorded mechanically activated current in whole-cell patch clamp mode for control and MβCD treated-neurons when different magnitude of displacement ranging from 125nm to 512nm were given at the constant velocity. The amplitude of RA currents recorded in both control and MβCD treated neurons increased in proportion with applied displacement at the constant velocity (Figure 11a). However, comparison of current-displacement curves (fit to Boltzmann distribution) revealed a 45% decrease in the slope sensitivity s (Figure 11a; from 55.37±17.37 pA/nm, n=10 to 30.31±10.37 pA/nm, n=6; unpaired t-test p<0.05). The slope sensitivity s is proportional to the change in channel active state probability for a given change in force [118], and the observed reduction suggested that depleting cholesterol affected RA channel activity. The maximum current amplitude was also reduced by 43% in the MβCD treated group (from 85.6±18.0 pA, n=10 to 48.4±6.0 pA, n=6; unpaired t-test p<0.05). In contrast, the activation stimulus midpoint $\chi_{1/2}$ was comparable between control and MβCD treated group (435.8±28.0 nm, n=10 and 423.8±11.68 pA, n=6, respectively; unpaired t-test p>0.05), suggesting the force sensed by RA channel is not affected by cholesterol depletion. Additionally, the kinetics of RA-mechanosensitive currents including the latency and inactivation time constant were identical for both groups and remained constant regardless of the amplitude of the stimulus (Figure 11b and 11c).

It has been shown that RA currents are able to encode the dynamic parameters of the mechanical stimulus [119,120]. To investigate whether cholesterol depletion with MβCD can alter the dynamic coding properties of RA currents, mechanically activated currents were recorded for control and MβCD treated-neurons when different velocities ranging from 341 to 4654μm/s were applied. A plot of current amplitude as a function of the velocity revealed that MβCD did not affect the ability of RA currents to code the dynamic

properties of stimulus. The amplitude of RA currents recorded in both control and MβCD treated neurons also increased in proportion with applied displacement at the constant displacement, although it is in general smaller in MβCD treated neurons (Figure 12a). The latency and inactivation time constant of RA currents were also plotted against increasing mechanical speed. There were also no difference between control and MβCD treated groups on kinetics of RA currents. The latency of RA currents in both control and MβCD treated neurons slightly shortened with increasing stimulus velocity (Figure 12b), and the inactivation time constant in both control and MβCD treated neurons remained constant regardless of the velocity of the stimulus (Figure 12c).

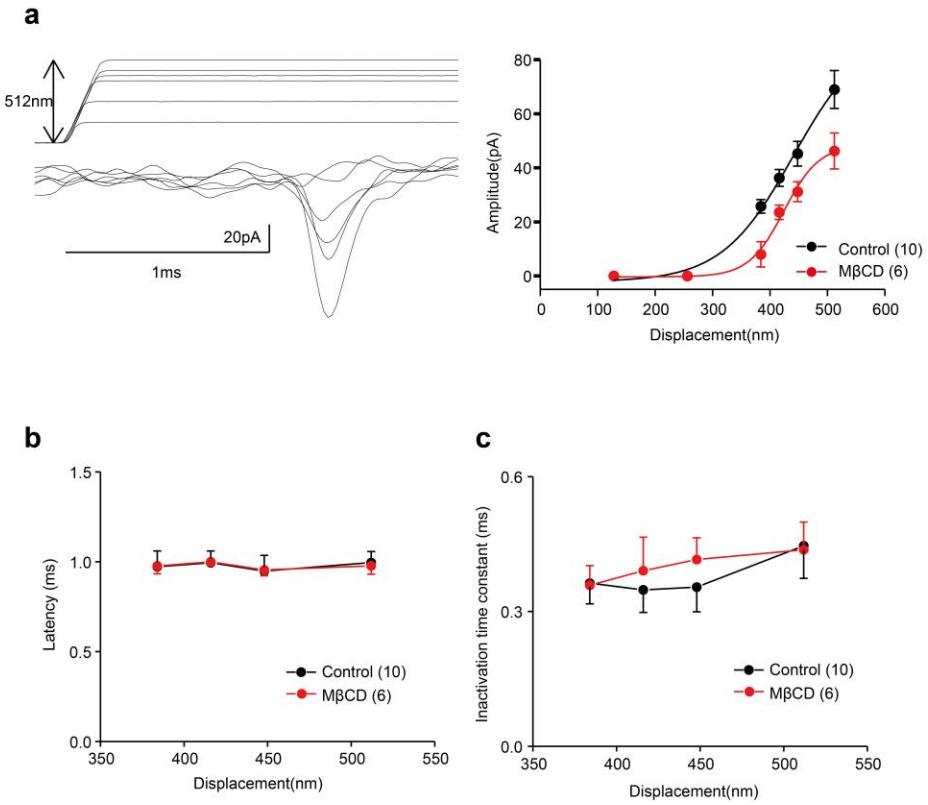

Figure 11. Effects of cholesterol depletion on displacement-response function for RA-mechanosensitive currents in sensory neuron. (a) Left: a sample trace of RA currents in response to mechanical stimulus of varying displacement (128, 256, 384, 416, 448 and 512nm) from control group. Right: The mean peak amplitude of mechanically evoked currents as a function of displacement at constant-ramp velocity is plotted for control and MβCD-treated neurons. Current activation curve fitted to a Boltzmann function with activation stimulus midpoint. Data are expressed as mean±s.e.m, the number of recorded neurons is indicated in parentheses in each panel. (b, c) The latency (b) and inactivation time constant (c) of mechanically activated RA currents plotted

against the mechanical stimulus intensity at constant velocity (3011μm/s) for control and MβCD treated neurons. No significant difference was observed in the latency and inactivation time constant of RA currents between control and MβCD-treated cells at each stimulus strength (Two-way repeated ANOVA followed by Bonferroni *post hoc* test, $p>0.05$).The number of cells is noted. Error bar indicates s.e.m.

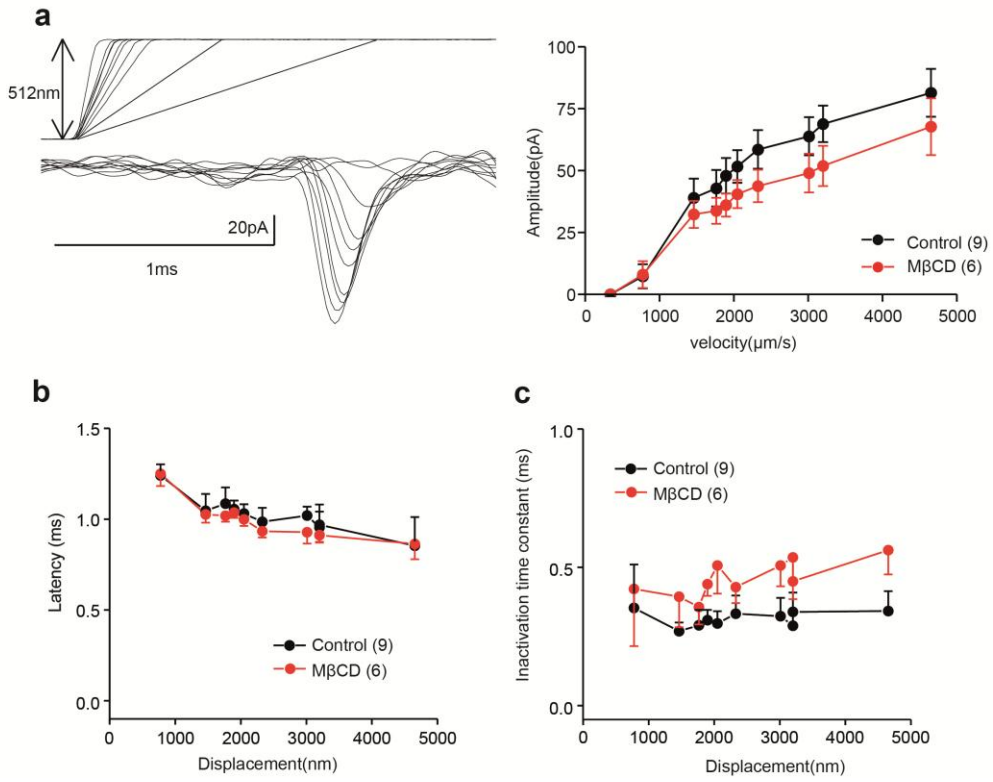

Figure 12. Effects of cholesterol depletion on the encoding of speed for RA-mechanosensitive currents. (a) Left: a sample trace of RA mechanosensitive currents evoked by different probe velocity ranging from 341 to 4654 μm/s. Right: The amplitude of mechanically evoked RA currents as a function of velocity at constant displacement (512nm) was plotted for control and MβCD-treated neurons. Data are expressed as mean ± s.e.m, the number of recorded neurons is noted. (b, c) The latency (b) and inactivation time constant (c) of RA-mechanosensitive currents plotted against the stimulus velocity at 512nm mechanical stimuli for control and MβCD-treated groups. No significant difference was observed in the latency and inactivation time constant of RA currents between control and MβCD-treated cells at each stimulus velocity (Two-way repeated ANOVA followed by Bonferroni *post hoc* test, $p>0.05$).

4.1.1.4.3 Cholesterol depletion does not alter ion selectivity and the ability of RA channel to respond to repetitive stimulus

We also tested if cholesterol depletion with MβCD affects the ion selectivity of RA-mechanosensitive channel. Replacement of sodium ion in the extracellular buffer with the non-permeant cation NMDG largely abolished the RA current in both control and MβCD-treated groups (Figure 13), suggesting cholesterol depletion does not alter the sodium selectivity of RA-mechanosensitive channel.

Previous study has shown that RA channel adapts fast and does not desensitize when the mechanical stimuli was repetitively given with long interval [121]. We would like to examine if cholesterol depletion affects the ability of RA-mechanosensitive channel to response to repetitive stimulus. Successive mechanical stimulation of DRG neurons with 5ms stimulus interval did not decrease the amplitude of the mechanically activated currents in either control or MβCD-treated neurons (Figure 14), suggesting cholesterol depletion does not alter the ability of RA channel to respond to repetitive stimulus.

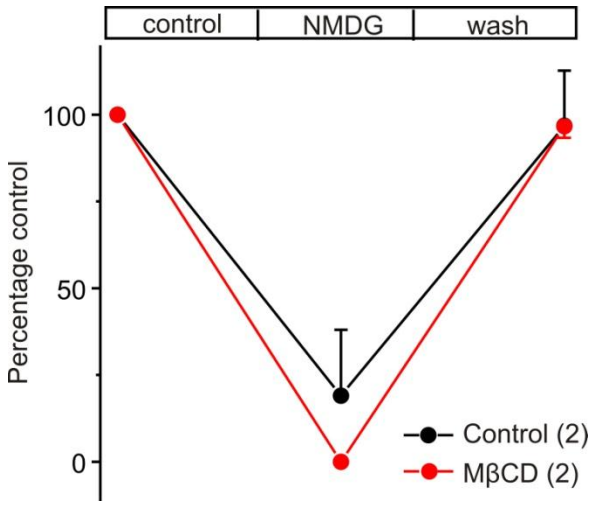

Figure 13. MβCD does not influence the ion selectivity of RA currents. The RA currents amplitude was almost inhibited by the replacement of sodium ion in the extracellular buffer with the non-permeant cation $NMDG^+$ in both control (n=2) and MβCD (n=2) groups.

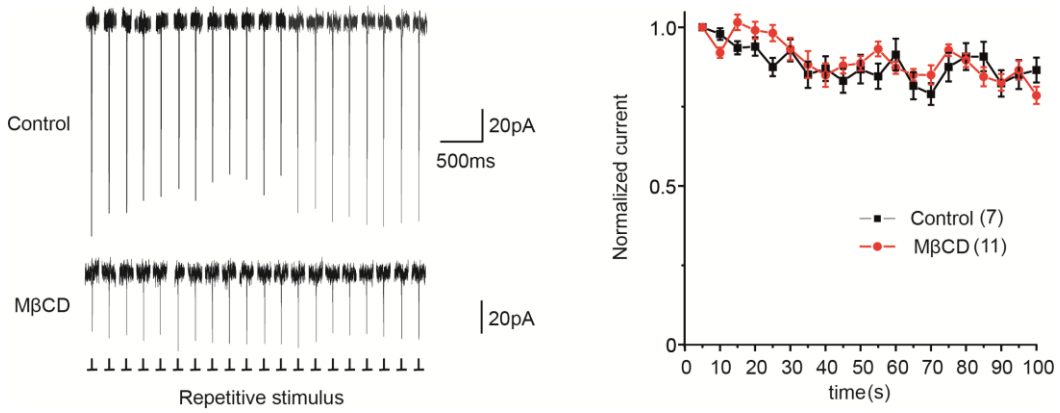

Figure 14. Mechanosensitive RA-type currents do not desensitize with repeated mechanical stimuli in either control or MβCD treated neurons. Left: Two example traces of a RA-current activation in control and MβCD treated neurons are shown. Right: Successive mechanical stimulation of DRG neurons do not decrease the amplitude of the mechanically activated current in either control or MβCD treated neurons (time effect: one-way ANOVA, control p>0.05, MβCD *p*>0.05; control versus MβCD, two-way ANOVA, *p*>0.05). The number of cells is indicated in parentheses in each panel. Error bar indicates s.e.m.

4.1.2 STOML3 regulates sensory mechanotransduction *in vitro* via cholesterol enriched lipid rafts

4.1.2.1 STOML3 distributes in both lipid rafts and non-rafts membrane fractions

We have suggested the involvement of cholesterol enriched lipid rafts in mechanosensation. Next we set out to determine whether STOML3 regulates the mechanosensitivity through cholesterol enriched lipid rafts. We first examined if STOML3 localizes in lipid rafts. Many members of stomatin domain-containing protein family including stomatin, SLP-1, MEC-2 and podocin, have been found to associate with lipid rafts [50]. However, to date there is no direct evidence showing that STOML3 is associated with cholesterol-enriched lipid rafts. To examine this, we expressed STOML3 tagged with myc epitope at the N-terminal in CHO cells, and performed sucrose-density-gradient centrifugation of cell lysate to isolate the detergent resistant membranes (DRMs) which is considered to be one of the most widely used methods to separate lipid rafts fractions [93]. Western blot analysis revealed that STOML3 was enriched in both the

fractions toward the top of the gradient and some fractions at the bottom of the gradient, corresponding to the lipid rafts fractions and the non-rafts membrane fractions, respectively, while the lipid-raft marker flotilin-2 was only detected in rafts fractions (Figure 15).

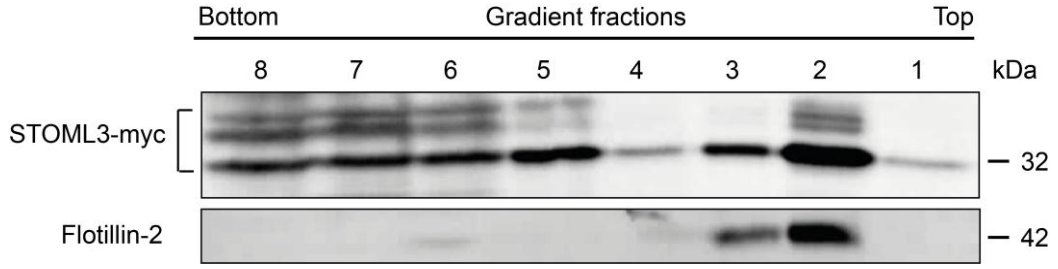

Figure 15. Distribution of STOML3 in sucrose-density-gradient fractions. CHO cells expressing Myc epitope-tagged wild-type STOML3 and P40S mutant were lysated and submitted to sucrose-density-gradient centrifugation, totally eight fractions were collected from the top of the gradient. Equal volumes of each fraction were separated by SDS-PAGE, and detected by anti-Myc for STOML3, STOML3-P40S and specific antibody for the raft marker flotillin-2. The representative blots are shown from four to five independent experiments. Flolilin-2 was specifically detected in rafts fractions (top 1 to 3), STOML3 was abundantly detected in both raft-associated fractions (top 1 to 3) and non-rafts fractions (5 to 8). STOML3 appeared as a triplet near the predicted molecular weight (~32kDa). Note that the molecular mass in kDa for STOML3 (~32kDa) and flolilin-2 (~42kDa) on the right-hand side of the blots.

4.1.2.2 Cholesterol-rich lipid rafts regulates mechanosensitivity involves STOML3

Previously, it has been shown that about 36% mechanosensitive channels in sensory neurons do not function without STOML3 regardless of the type of mechanosensitive channels [47]. Considering the similarity of cholesterol depletion to *STOML3* deficiency, both affected the sensitivity of RA and SA currents, we proposed that STOML3 and lipid rafts might regulate the activity of mechanosensitive channels through the same pathway. To test this idea, we performed cholesterol depletion with MβCD (5mM, 1h) in *STOML3*$^{-/-}$ sensory neurons, and mechanically gated response was recorded and analysed under the given mechanical stimulus (~ 512nm displacement) to neurite as we did in wide type DRG neurons. Intriguingly, cholesterol depletion did not further reduce the

mechanosensitivity of *STOML3*$^{-/-}$ neurons. Different from wild type sensory neurons, neither the proportion of no response neurons (Figure 16a; 10 out of 21cells in control versus 11 out of 19 cells in MβCD-treated *STOML3*$^{-/-}$ neurons, Fisher's exact test, p>0.05) nor the peak amplitude of RA current (Figure 16b; 113±24.9pA in control vs 110±37.8pA in MβCD-treated *STOML3-/-* neurons, unpaired t-test, p>0.05) was altered after MβCD treatment. Obviously, STOML3 and lipid rafts could not be in two parallel and distinct pathways, they are probably involved in the same regulation pathway in mechanosensation. Taken together, lack of an addition effect of MβCD on mechanosensitive currents in *STOML3*$^{-/-}$ sensory neurons suggests that the regulation of mechanosensitivity by cholesterol enriched lipid rafts involves STOML3.

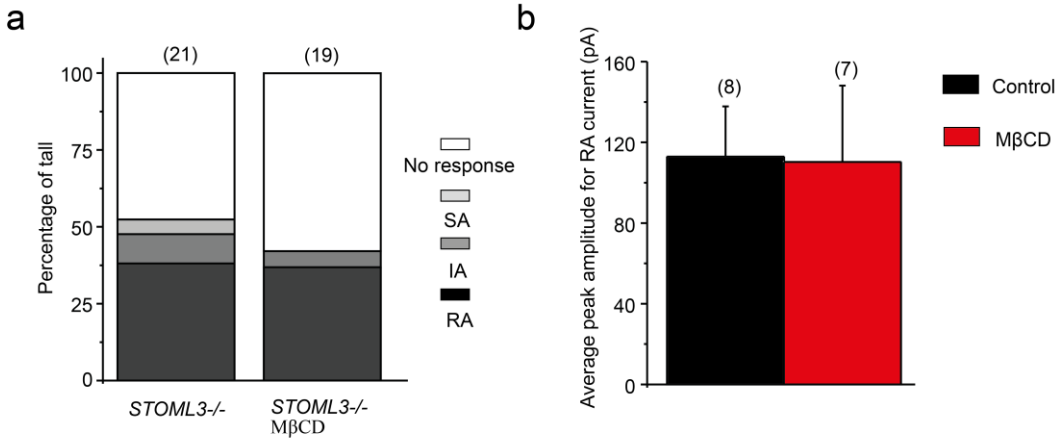

Figure 16. Cholesterol depletion does not alter the mechanosensitivity of *STOML3*$^{-/-}$ neurons. (a) Stacked histograms reveal MβCD treatment did not further significantly reduce mechanosensitivity in *STOML3*$^{-/-}$ sensory neuron. No significant difference of the proportion of no response neuron between control (10/21) and MβCD-treated (11/19) groups (χ^2 test, p>0.05). The number of recorded cells is noted on the top of each histogram. (b) MβCD did not alter the RA mechanosensitive current amplitude evoked by mechanical stimuli to neurite in *STOML3*$^{-/-}$ DRG neurons. All data are expressed as mean ± s.e.m, n=7-8, p>0.05, unpaired t-Test).

4.1.2.3 Effects of cholesterol depletion on membrane electrophysiological properties of *STOML3*$^{-/-}$ sensory neurons

Additionally, we examined the effects of MβCD on membrane electrophysiological properties of *STOML3*$^{-/-}$ sensory neurons. MβCD did not significantly alter rest

membrane potential and action potential amplitude in both mechanoreceptor and nociceptor (Figure 17a and 17b). However, MβCD significantly reduced the action potential threshold (injected current to initiate AP) in both mechanoreceptor (unpaired t-test, $^{**}p<0.01$) and nociceptor (unpaired t-test, $^{*}p<0.05$) (Figure 17c), suggesting cholesterol depletion potentially enhances neuron excitability. Plots of current–voltage (I-V) curve for voltage gated inward and outward currents in *STOML3*$^{-/-}$ sensory neurons revealed that cholesterol depletion reduced the voltage gated inward current density in nociceptors (Figure 18). As what we observed in wild-type sensory neurons, cholesterol depletion also modulates the membrane electrophysiological properties in *STOML3*$^{-/-}$ sensory neurons.

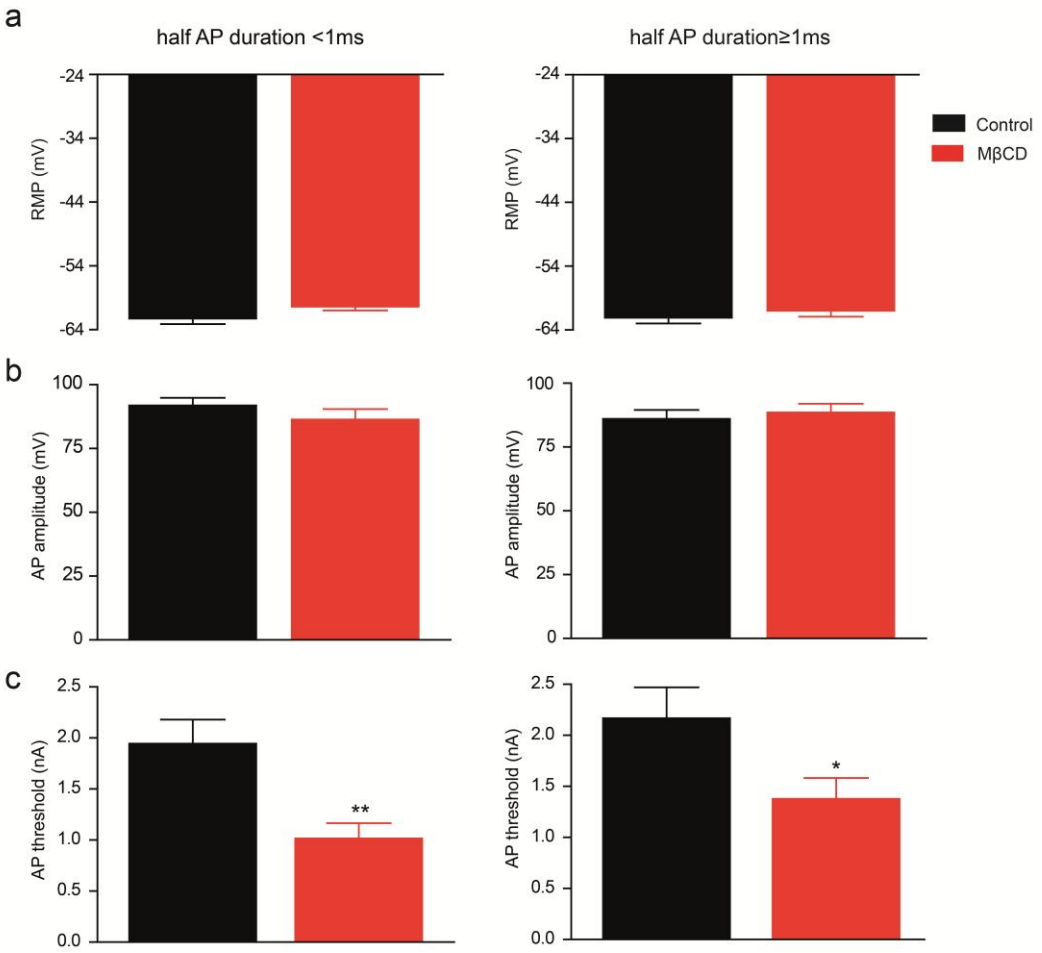

Figure 17. Effects of cholesterol depletion on membrane properties in *STOML3*$^{-/-}$ sensory neurons. Neurons are grouped into mechanoreceptor (left; 1/2 AP duration <1ms) and nociceptor (right; 1/2 AP duration ≥ 1ms). (a) Quantitative comparison of rest membrane potential (RMP) in control and MβCD-treated neurons. No significant

differences were observed as compared with controls in both mechanoreceptor (n=21-23, unpaired t-Test $p>0.05$) and nociceptor (n=13-18, unpaired t-Test $p>0.05$). (b) Mean AP amplitude at current-clamp mode for control and MβCD-treated cells. No significant differences were observed as compared with controls in both mechanoreceptor (n=21-23, unpaired t-Test $p>0.05$) and nociceptor (n=13-18, unpaired t-Test $p>0.05$). (c) Threshold current for AP initiation measured at current-clamp mode for control and MβCD-treated cells. MβCD significantly reduced the action potential threshold in both mechanoreceptor (n=21-23, unpaired t-test, **p<0.01) and nociceptor (n=13-18, unpaired t-test, *$p<0.05$).

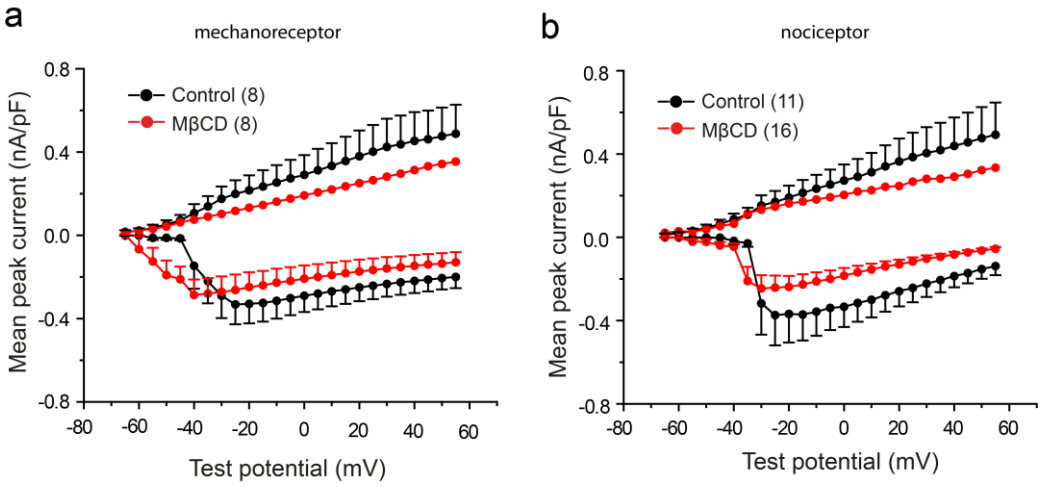

Figure 18. Effects of MβCD treatment on voltage gated currents in *STOML3*$^{-/-}$ sensory neurons. Mean whole-cell inward and outward currents measured at different test potentials for control (positive triangle) and MβCD-treated *STOML3*$^{-/-}$ sensory neurons (empty circle). Neurons are grouped into mechanoreceptor (a) (1/2 AP duration <1ms) and nociceptor (b) (1/2 AP duration ≥ 1ms). Cells were first prepulsed to -120mV and then depolarized from -65mV to 55mV in 5-mV increment. No significant change was seen in the peak amplitude of voltage gated inward and outward current between control and MβCD-treated cells at each test potential for mechanoreceptor or nociceptor (Two-way analysis of variance (ANOVA) followed by Bonferroni *post hoc* test, $p>0.05$). The number of cells is noted. Data are expressed as mean±s.e.m.

4.1.2.4 STOML3 mutant deficient in cholesterol binding fails to restore the mechanosensitivity of *STOML3*$^{-/-}$ sensory neurons

However, the question remains that whether lipid rafts are required for STOML3 to regulate the activity of mechanosensitive channels. To answer this, we sought to specifically disrupt the ability of STOML3 associating with cholesterol. Previous study has demonstrated that one proline residue (P134) in hydrophobic region is critical for

MEC-2 to bind cholesterol and regulate touch sensitivity in *C. elegans* [60]. Moreover, the proline residue is highly conserved among MEC-2, SLP-1, STOML3, stomatin and podocin (Figure 19a), indicating a conserved function of this residue for the stomatin protein family. We thereby would like to study the role of this conserved proline residue (P40) in the rafts-distribution of STOML3. To end this, we substituted proline 40 in STOML3 by a serine residue and expressed myc epitope tagged STOML3^{P40S} mutant in CHO cells. Western blot analysis show that STOML3^{P40S} mutant was mostly detected in the non-rafts fractions, mutation of proline residue (P40S) disrupted the association of STOML3 with cholesterol enriched lipid rafts (Figure 19b and 19c). These data suggest proline residue (P40) is required for STOML3 to associate with cholesterol enriched lipid rafts.

Next we sought to determine the importance of proline residue for STOML3 to function on mechanosensation. We transfected wide type STOML3 or STOML3^{P40S} mutant into *STOML3*$^{-/-}$ sensory neurons, and mechanically activated currents were recorded when a small displacement (~500nm) was given to neurite. To visualize transfected neurons, we expressed STOML3 or STOML3^{P40S} mutant fused with GFP at its Carbon-terminal. Consistent with previous report [47], fluorescently labeled wild-type STOML3 was observed in a punctuate pattern in neurites (Figure 20a), and expression of wide type STOML3 could rescue the deficiency of mechanosensitivity in *STOML3*$^{-/-}$ sensory neurons (Figure 20b; 15 out of 16 labeled cells exhibited mechanosensitive currents).

In contrary, the STOML3^{P40S} mutant was more uniformly distributed along the sensory neurite (Figure 20a), suggesting mutation of proline residue substantially altered STOML3 distribution. Intriguingly, STOML3^{P40S} mutant had no effect on the incidence of mechanosensitive currents (Figure 20b; 8 out of 17 labeled cells had no mechanosensitive current). Thus the STOML3^{P40S} mutant failed to rescue the loss of mechanosensitivity in *STOML3*$^{-/-}$ neurons as wild-type does and this deficiency probably resulted from the disruption of STOML3-lipid-rafts supercomplex. These data suggest that STOML3 binding cholesterol is essential for its function in the formation of high-order structure on plasma membrane and regulating mechanotransduction.

a

```
mstomatin       -----MSDKR----------------------QSSHVQS---------------------- 12
mec-2           -MSATMSSARNSVVSLSSNGSVKVETRLVSNERSSSIQQEGAMLPSSSSKDDDLLSTSSD 59
mslp3           -----MDSPE---------------------------------------------------- 5
mpodocin        MDSRARSSSREAHGRSS--------------RSSSRDDKKAKAGRGSRGRARPDAGAER 45
                     .. .

mstomatin       ----------QRIPES------------------------------FRENSKTELGACGW 32
mec-2           EVENMATRTLQQLEESTSIISANSDDDSVKKEKQAEKDVEKGNGKEEKANIQNEFGVCGW 119
mslp3           -----------KLEKNN---------------------------LVGTNKSRLGVCGW 25
mpodocin        QSTGRTATRGEPRAPAATATVVDVDEVRGPGEEGTEVVALLESERPEEGIKPSGLGACEW 105
                                                              . :*.* *

mstomatin       ILVAASFFFVIITFPISIWICIKIVKEYERVIIFRLGRILQGGAKGPGLFFILPCTDSLI 92
mec-2           ILTILSYLLIFFTLPISAQMCIKVVQEYERAVIFRLGRLMPGGAKGPGIFFIVPCIDTYR 179
mslp3           ILFFLSFLLMLVTFPISVWMCLKIIKEYERAVVFRLGRIQADKAKGPGLILVLPCIDVFV 85
mpodocin        LLVLASLIFIIMTFPFSIWFCIKVVQEYERVIIFRLGHLLPGRAKGPGLFFFLPCLDTYH 165
                :*   * :::::*:*:*  :*:*:::**** .::****::  .  *****::::** *
                                              PHB domain
mstomatin       KVDMRTISFDIPPQEVLTKDSVTISVDGVVYYRVQNATLAVANITNADSATRLLAQTTLR 152
mec-2           KVDLRVLSFEVPPQEILSKDSVTVAVDAVVYFRISNATISVTNVEDAARSTKLLAQTTLR 239
mslp3           KVDLRTVTCNIPPQEILTRDSVTTQVDGVVYYRIYSAVSAVANVNDVHQATFLLAQTTLR 145
mpodocin        KVDLRLQTLEIPEHFVVTKDMEIMFIDAVCYYRMFNASLLLSSLAHVSKAIQFLVQTTMK 225
                ***:*  : ::* :*::::* .   :*.* *:*: .*   ::.: ..  :  :*.***::

mstomatin       NALGTKNLSQILSDREEIAHHMQSTLDDATDDWGIKVERVEIKDVKLPVQLQRAMAAEAE 212
mec-2           NILGTKTLAEMLSDREAISHQMQTTLDEATEPWGVKVERVEVKDVRLPVQLQRAMAAEAE 299
mslp3           NVLGTQTLSQILSGREEIAHSIQTLLDDATELWGIRVARVEIKDVRIPVQLQRSMAAEAE 205
mpodocin        RLLAHRSLTETLLERKSIAQDVKVALDAVTCIWGIKVERTEIKDVRLPAGLQHSLAVEAE 285
                . *. :.*:::*  *: *:: ::  ** .*  **::* *.*:***::*. **:::*.***

mstomatin       AAREARAKVIAAEGEMNASRALKEASMVITESPAALQLRYLQTLTTIAAEKNSTIVFPLP 272
mec-2           AAREARAKVIVAEGEQKASRALKEAAEVIAESPSALQLRYLQTLNSISAEKNSTIIFPFP 359
mslp3           ATREARAKVLAAEGEMNASKSLKSASMVLAESPVALQLRYLQTLTTVATEKNSTIVFPLP 265
mpodocin        AQRQAKVRVIAAEGEKAASESLRMAAEILSGTPAAVQLRYLHTLQSLSTEKPATVVLPLP 345
                * *:*:.:*:.****  **.:*: *: ::: :* *:*****:** ::::** :*:::*:*

mstomatin       VDMLQGIMG------------SNH----------------- 284
mec-2           IDLLSAFLQRTPPKVDNNFAFPTHKAGGIPSSS-------- 392
mslp3           MNILEGIGG---------ISYGNNKK--VTAKA-------- 287
mpodocin        FDMLSLLSS-PGNRAQGSINYPSSSKPVEPLNPKKKDSPML 385
```

b

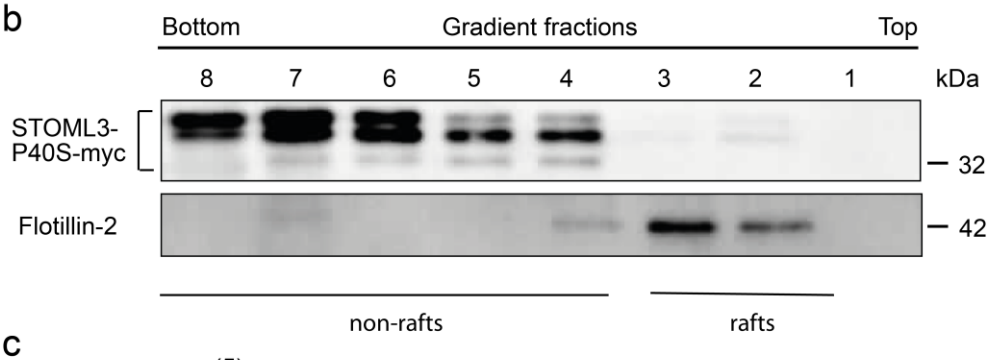

c

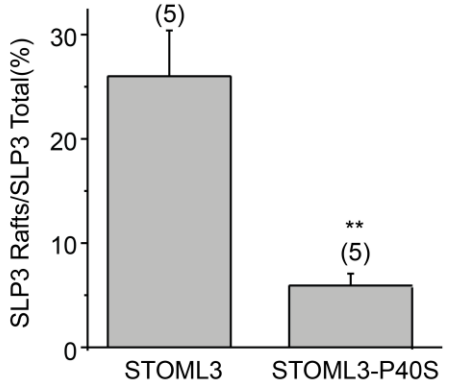

Figure 19. Mutation of proline residue (P40S) disrupts the association of STOML3 with lipid rafts. (**a**) Alignment of the amino acid sequences of stomatin family proteins including mouse STOML3, mouse stomatin, mouse podocin and nematode MEC-2. *'represents conserved amino acids, ':'represents high similarity, '.' represents low similarity. The deduced hydrophobic regions are underlined. The putative hydrophobic domain is underlined, and the conserved proline and cysteine residues are indicted with solid circles. The putative PHB domain is boxed, (**b**) Representative blots showing that P40S mutation abolishes the distribution of STOML3 in lipid rafts. CHO cells expressing Myc epitope-tagged P40S mutant were lysated and submitted to sucrose-density-gradient centrifugation, totally eight fractions were collected from the top of the gradient. Equal volumes of each fraction were separated by SDS-PAGE, and detected by anti-Myc for STOML3-P40S and specific antibody for the raft marker flotilin-2. The representative blots are shown from four to five independent experiments. STOML3 appeared as a triplet near the predicted molecular weight (~32kDa). The P40S mutation altered the relative intensity of the three bands. Note that the molecular mass in kDa for STOML3 (~32kDa) and flolilin-2 (~42kDa) on the right-hand side of the blots. (**c**) Quantitative comparison of percentage of rafts-associated proteins (fractions 1 to 3) relative to total amount of STOML3 or STOML3-P40S mutant protein. Data are shown as percentage of total± s.e.m, n=5, **p<0.01 student's unpaired Test.

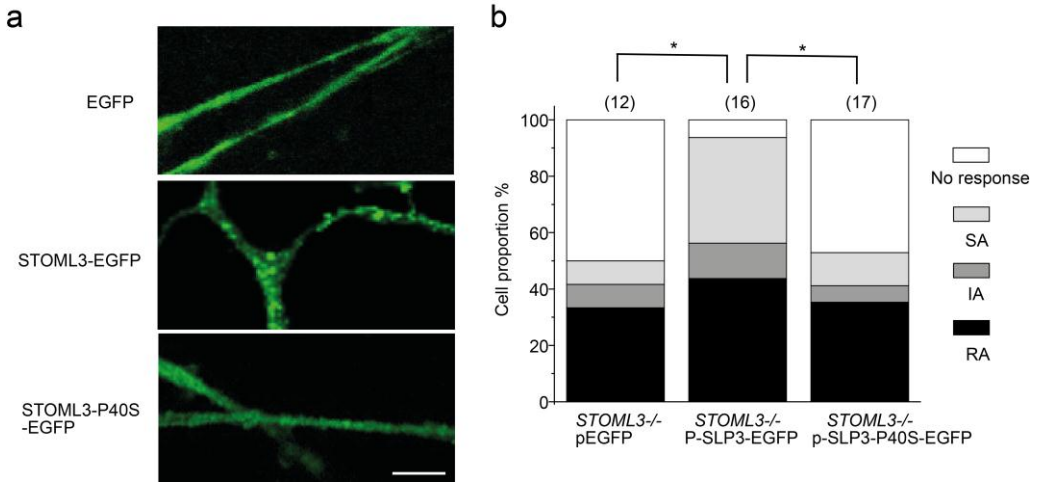

Figure 20. Mutation of proline residue (P40S) fails to rescue mechanosensitivity of *STOML3*$^{-/-}$ neurons. (a) Representative images of empty EGFP, wild-type STOML3-EGFP and STOML3-P40S-EGFP mutant in transfected *STOML3*$^{-/-}$ sensory neuron. Punctata distribution of wild-type STOML3 along neuritis was not observed in proline mutant (P40S) by confocal scanning microscope. Scale bar: 10μm. (b) Stacked histograms of the proportions of sensory neurons with the different mechanosensitive currents from *STOML3*$^{-/-}$ neurons transfected with empty EGFP, EGFP-tagged STOML3 or STOML3-P40S mutant. Expression of STOML3^{P40S} mutant in STOML3 deficiency neurons did not restore the loss of mechanosensitive currents as wild-type did. Note the significant increase in the proportion of neurons having a mechanosensitive current in wild-type STOML3-transefected group (15 response out of 16 cells) compared with

group transfected with either empty EGFP (6 response out of 12 cells) or STOML3^{P40S} mutant (9 out of 17 cells). The number of recorded cells is indicated on the top of each histogram, data are analysed using Fisher's exact test, *p<0.05.

4.1.2.6 STOML3 modulates Piezo channel activity through cholesterol-rich lipid rafts

Our electrophysiological findings demonstrate that cholesterol depletion altered both RA and SA mechanosensitive currents in sensory neurons. While at the moment the cation channels which account for SA currents in nociceptors remain unknown, Piezo channels have been recently discovered as true mechanosensitive channel [45,46]. And Piezo2 channel mediates RA mechanosensitive currents in sensory neurons. STOML3 interacts with piezo channels and sensitizes piezo1-mediated currents in N2a neuroblastoma cells [48]. However, whether STOML3 modulates peizo channels activity through cholesterol-rich lipid rafts remain unknown. We therefore first tested whether STOML3 modulates Piezo1 channel activity through cholesterol-rich lipid rafts. To test this, MβCD treatment (5mM, 1h) was performed in N2a cells, which express low levels endogenous STOML3. After MβCD treatment, we have observed an almost complete loss of mechanically gated currents within our stimulus range (0-4.2μm) (Figure 21a and 21b). Next N2a cells transfected with either eGFP-tagged wild-type STOML3 or STOML3^{P40S} mutant were treated with or without MβCD. As previously reported [48], overexpression of STOML3 robustly potentiated the mechanosensitive currents in N2a cells (Figure 21c and 21d). However, this effect was substantially attenuated by depleting cholesterol with MβCD (Figure 21c and 21d; two-way ANOVA followed by Bonferroni *post hoc* test, **p<0.01). Our RT-PCR results show *peizo1* but not *piezo2* was mainly expressed in N2a cells (Figure 22), which accords well with previous report showing peizo1 is responsible for the mechanosensitive currents recorded in N2a cells [45,48]. These data indicate STOML3 modulates Piezo1-mediated currents via cholesterol-rich lipid rafts.

We next determined whether STOML3 associating with cholesterol is important for its function in sensitization of Piezo1 channel activity. Expression of STOML3^{P40S} deficient in associating with cholesterol failed to potentiate pizeo1 currents in N2a cells, while

depletion of cholesterol did not show any further effect (Figure and 21f). Thus, STOML3 modulates Piezo1 cehnnel activity via associating with cholesterol.

We next coexpressed Piezo2 channel with STOML3 in HEK293 cells. Similar to the results with Piezo1, MβCD treatment also attenuated the potentiation effect of STOML3 on Piezo2 mediated mechanosensitive currents, while expression of STOML3-P40S mutant failed to potentiate Piezo2 currents (Figure 21g and 21h). Thus, STOML3 modulates both Piezo1 and Piezo2 channels activity via association with cholesterol. As reported in previous study [122], we also observed that Piezo2 channel is much more difficult to express than Piezo1 channel, possibly due to the cellular toxicity of heterologous overexpression of Piezo2. Since we observed that STOML3 exhibited similar effect on Piezo1 and Piezo2 mediated mechanosensitive currents, we used Piezo1 for heterologous expression in the following experiments.

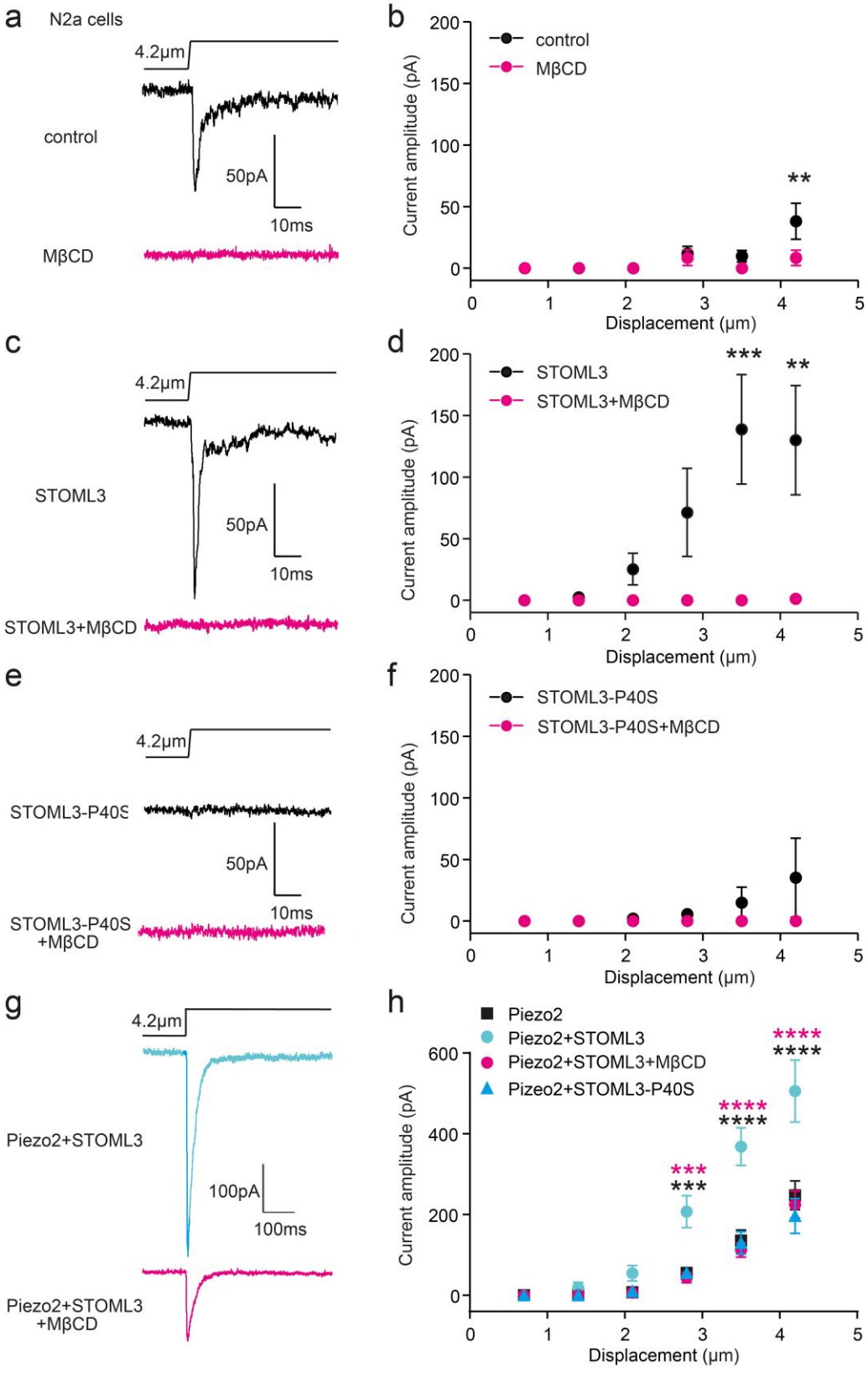
a
N2a cells
4.2μm
control
50pA
10ms
MβCD
b
control
MβCD
Current amplitude (pA)
Displacement (μm)
**
c
4.2μm
STOML3
50pA
10ms
STOML3+MβCD
d
STOML3
STOML3+MβCD
***
**
Current amplitude (pA)
Displacement (μm)
e
4.2μm
STOML3-P40S
50pA
10ms
STOML3-P40S
+MβCD
f
STOML3-P40S
STOML3-P40S+MβCD
Current amplitude (pA)
Displacement (μm)
g
4.2μm
Piezo2+STOML3
100pA
100ms
Piezo2+STOML3
+MβCD
h
Piezo2
Piezo2+STOML3
Piezo2+STOML3+MβCD
Pizeo2+STOML3-P40S
***
***
****
****
****
****
Current amplitude (pA)
Displacement (μm)

Figure 21. STOML3 modulates Piezo1 and Piezo2 channels activity though associating with cholesterol. (a, c, e) Example traces of mechanically gated currents in N2a cells (a) or N2a cells expressing STOML3 (c) or N2a cells expressing STOML3-P40S mutant (e) treated with or without MβCD at the given indentation (4.2μm). (b) Current-displacement curves in N2a cells treated with or without MβCD. When N2a cells were treated with MβCD (n=33), mechanosensitivity was significantly reduced at 4.2μm displacement compared with cells without MβCD (n=27) (two-way ANOVA $P>0.05$, with *post-hoc* Bonferroni's test **-$P<0.01$) (d) Current-displacement curves for N2a cells expressing STOML3 wild-type treated with or without MβCD. MβCD significantly reduced the mechanosensitive currents in N2a cells expressing STOML3 (STOML3: n=11, STOML3+MβCD : n=8; two-way ANOVA, p<0.0001, with *post-hoc* Bonferroni's test ** P<0.01, ***p<0.001) (f) Current-displacement curves for N2a cells expressing STOML3-P40S mutant treated with or without MβCD. MβCD did not alter the mechanosensitive currents in N2a cells expressing MβCD (STOML3-P40S: n=6, STOML3-P40S+MβCD: n=7; two-way ANOVA P>0.05, with *post-hoc* Bonferroni's test). Data are shown as mean±s.e.m. (g) Representative traces of mechanically gated currents in HEK293 cells expressing Piezo2 and STOML3 treated with or without MβCD at the given indentation (4.2μm). (h) MβCD treatment significantly reduced the potentiation effect of STOML3 on Piezo2 mediated mechanosensitive currents in HEK293 cells, while STOML3-P40S mutant failed to potentiate Piezo2 currents (two-way ANOVA with *post-hoc* Bonferroni's test; STOML3 effect: Piezo2 versus Piezo2 + STOML3, P<0.0001, black *; MβCD effect: Piezo2 + STOML3 versus Piezo2 + STOML3 + MβCD, $P<0.0001$, pink *; STOML3-P40S effect: Piezo2 versus Piezo2+STOML3-P40S, p>0.05; Piezo2: n=9, Piezo2+STOML3: n=7, Piezo2 + STOML3 + MβCD: n=5, Piezo2+STOML3-P40S: n=7). ** $P<0.01$, *** $P<0.001$, **** P<0.0001. Error bars indicate s.e.m.

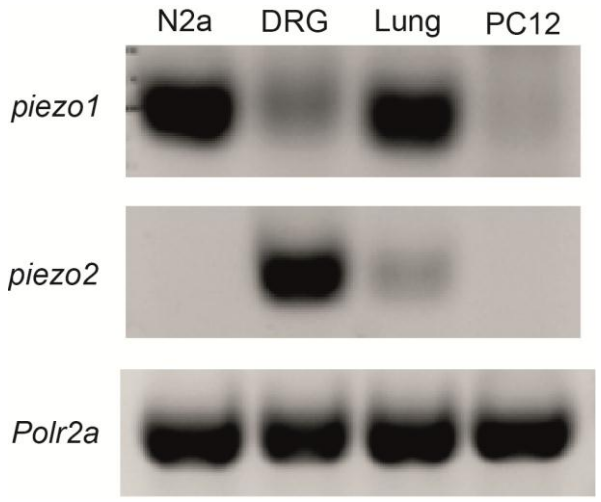

Figure 22. *Pizeo1* mRNA but not *piezo2* mRNA is mainly expressed in N2a neuroblastoma cells. RT-PCR was used to detect the expression of *pizeo1* and *piezo2* mRNA in different cells and mice tissues, including N2a neuroblastoma cells (N2a), mice DRG tissue (DRG), mice lung (lung) and PC12 cells. DNA-dependent RNA polymerase *Polr2a* mRNA was used as housekeep gene.

4.1.3 STOML3 modulates membrane mechanical properties via association with cholesterol

4.1.3.1 Altered membrane mechanical properties in STOML3 deficient sensory neurons

Previously, removing membrane cholesterol with cyclodextrin has been shown to result in the reduction of the membrane stiffness in DRG neurons using atomic force microcopy (AFM) [123]. In view of our data showing that STOML3 modified the activity of mechanosensitive ion channels via cholesterol enriched lipid rafts, we further explored the possibility that knocking out STOML3 would also influence the membrane stiffness of sensory neurons. The AFS technique was thus employed to determine the elasticity modulus *E* (i.e., stiffness) of sensory neurons from WT and *STOML3*$^{-/-}$ mice. Individual sensory neurons were localized using optical phase contrast microscopy (Figure 23a and 23b). We found that the force required to produce same indentation on the cell was significantly lower in *STOML3*$^{-/-}$ neurons as compared to WT neurons (Figure 23c).

Living cells can be considered mechanically as a multilayered structure: an external layer including a plasma membrane/cortical actin layer and an internal cytoplasm organization [124]. The stiffness of the external 'layer' of the sensory neurons was analyzed by fitting the force-indentation curves with a variation of Hertz model that considers the presence of multiple elastic contributions (Figure 23c). By using this procedure we observed that *STOML3*$^{-/-}$ are significantly softer than WT neurons regarding the first elastic component $E1$ (Figure 23d; two-way ANOVA with post-hoc Bonferroni's Multiple Comparison Test, $P<0.05$), which is mainly related to the mechanics of the plasma membrane and the actin immediately underneath, while for the second elastic component $E2$ (internal cell organization) statistically significant difference was not observed. Such results suggest that STOML3 acts to selectively increase the stiffness of the external layer of sensory neurons, including plasma membrane and cortical actin.

To further determine whether this decrement in E values at small indentation depth is correlated with membrane mechanical properties, we evaluated membrane viscosity and tension. The force required to pull membrane tethers from neurons at a constant velocity V_t was measured and then the dependence of force on velocity was analyzed. This procedure allowed us to evaluate the static tether force at zero velocity F_0 and to assess changes in the membrane surface viscosity η_{eff} (Figure 23e and 23f; Table 2). An increase in membrane viscosity in *STOML3*$^{-/-}$ neurons was observed, confirming an alteration of plasma membrane organization by STOML3. The apparent membrane tension, T_{app}, which is a sum of the membrane-cytoskeleton adhesion energy (γ) and in-plane membrane tension (T_m) [125], was computed from F_0. We found T_{app} was lower in *STOML3*$^{-/-}$ than WT sensory neurons (Table 2), suggesting that an intact STOML3 is needed in sensory neuron to generate a proper membrane tension.

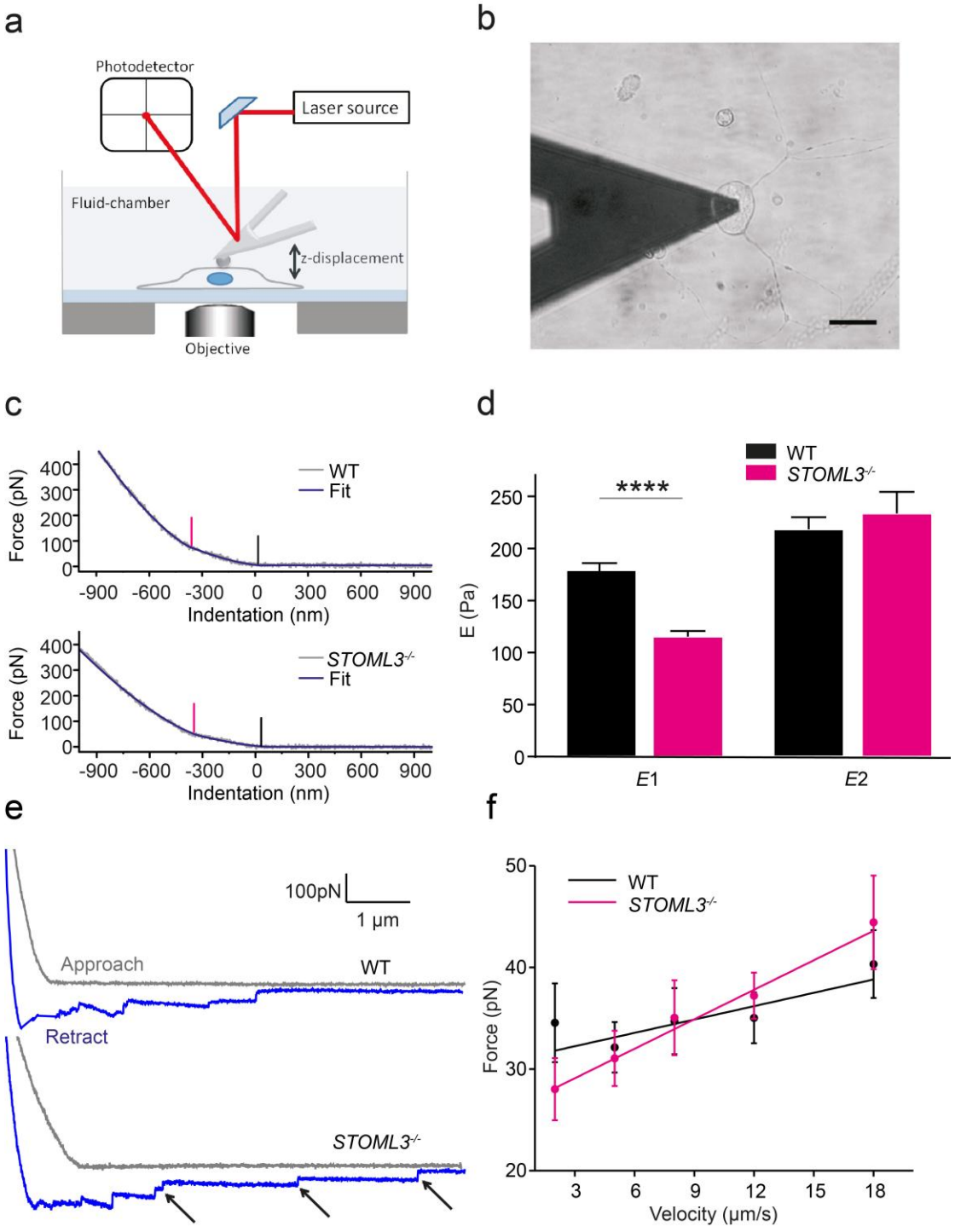

Figure 23. Altered membrane mechanical properties in STOML3 deficient sensory neurons. (a) Sketch of AFM set-up used for indentation measurements including a bead (4.5µm diameter) glued at the end of a tipless cantilever. The cantilever is moved up and down by a piezo-system. The bending of the cantilever is measured by a laser beam detected by a photodetector. And the AFM cantilever bending is linearly proportional to the force applied on the cell. (b) Differential interference contrast optical image of the

bead-cantilever pushed onto a cultured DRG neuron (scale bar 20 μm). (c**)** Examples of Force-indentation curves for WT and *STOML3*$^{-/-}$ sensory neurons as fitted for double contributions: in the curve two regimes with different elastic properties can be identified (*black marker* first point for first elastic component *E*1 and *pink marker* second point for second elastic component *E*2) (Methods, Supplementary Fig.2 and 3). (d) Quantitative comparison of elasticity modulus *E*1 and *E*2 values obtained by fitting procedure (WT: *n*=110 neurons from 4 cultures, 4 animals; *STOML3*$^{-/-}$: *n*=120 neurons from 4 cultures, 4 animals; two-way ANOVA with *post-hoc* Bonferroni's test, $P<0.05$). See also Supplementary Fig. 4. (e) Representative force-distance curves (approach in gray, retraction in blue) acquired at 5μm s^{-1}. On the retraction curve, after first detachment force several step-like structures are clearly discernible (indicated by arrows), corresponding to the sequential detachment of membrane tethers from the cantilever. (f) Tether force as function of pulling velocity in WT and *STOML3*$^{-/-}$ sensory neurons (WT: *n*=20 neurons from 2 cultures, 2 animals; *STOML3*$^{-/-}$: *n*=19 neurons from 2 cultures, 2 animals). Solid lines are the linear fit of force-velocity curves used to estimate the static tether force at zero F_0 and the effective viscosity η_{eff} (Methods, Supplementary Table 2) (R value is 0.6 for WT and 0.97 for *STOML3*$^{-/-}$). **** $P<0.0001$; Error bars indicate s.e.m.

Table 2.Values of the static tether force at zero F0, the effective viscosity ηeff and the apparent surface tension Tapp analyzed from the liner fit of tether force as function of pulling velocity.

	WT n=10	*STOML3*$^{-/-}$ n=6
$2\pi\eta_{eff}$ (pNsec/μm)	0.44±0.16	0.97±0.07
F_0 (pN)	30.9±1.6	26.2±0.7
T_{app} (pN/μm)	42.3±0.1	31.74±0.02

4.1.3.2 STOML3 modulates membrane mechanical properties via association with cholesterol in heterologous expression cells

However, it remains elusive whether the MβCD treatment displays similar effect on HEK293 cell membrane. We therefore performed AFS measurements on HEK293 cells treated with or without MβCD. A significant reduction in cell stiffness after MβCD treatment was observed (Figure 24a), suggesting that modifying membrane cholesterol level affects cell mechanics in HEK293 cells. We next ask whether the mechanical properties of membrane in which Piezo channels are embedded are controlled by STOML3 via associating with cholesterol. To address this question, HEK293 cells

expressing STOML3 wild-type (STOML3-EGFP) or STOML3-P40S mutant (STOML3-P40S-EGFP) were subjected to AFS measurements. Analysis of force-indentation curves demonstrated that cells expressing STOML3-P40S mutant were significantly softer than cells with STOML3 wild-type (Figure 24b). Interestingly, the reduction effect of STOML3-P40S mutant on the cell stiffness was comparable with the effect of cholesterol depletion, implying that the difference of cell stiffness between STOML3 wild-type and STOML3-P40S mutant transfected HEK293 cells are mainly due to the ability of STOML3 associating with cholesterol.

Next we expressed Piezo1 channel together with STOML3 wild-type or STOML3-P40S mutant in HEK293 cells. Similarly as the result obtained from STOML3-P40S mutant alone expression, the cell stiffness was significantly reduced in cells co-expressed Piezo1 and STOML3-P40S mutant when compared with cells co-expressed Piezo1 and STOML3 wild-type (Figure 4c). This data suggests that STOML3 associates with cholesterol and modulates cell stiffness regardless the presence of Piezo1 channel. Thus, in heterologous expression system, the interaction between STOML3 and cholesterol appears to be necessary for maintaining the membrane stiffness to enable efficient force transfer to Piezo channels.

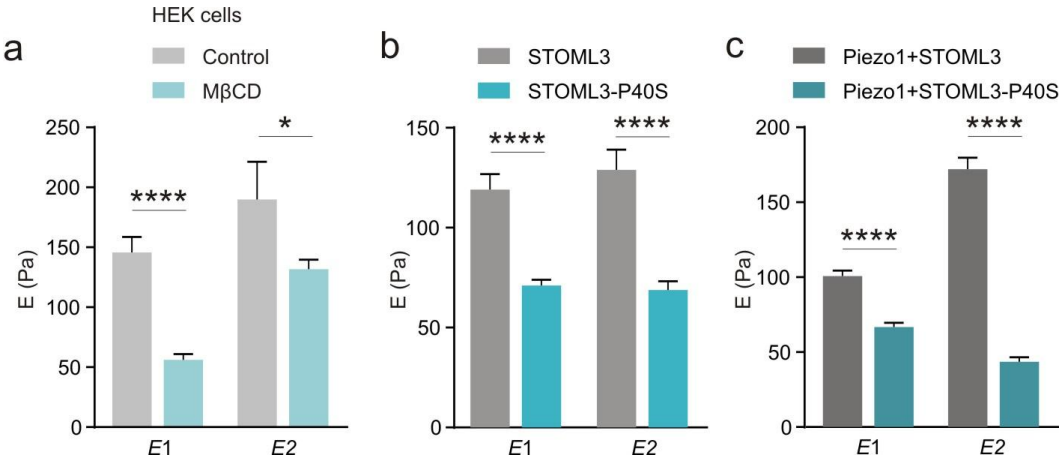

Figure 24. STOML3 modulates membrane mechanics via association with cholesterol. (a) Quantitative comparison of elasticity modulus *E*1 and *E*2 values obtained by fitting procedure in HEK293 cells treated with or without MβCD (control: *n*=16; MβCD: *n*=17; two-way ANOVA with *post-hoc* Bonferroni's test, *P*<0.0001). (b)

Quantitative comparison of elasticity modulus *E*1 and *E*2 values obtained by fitting procedure in HEK293 cells expressing STOML3 or STOML3-P40 (STOML3: *n*=25; STOML3-P40: *n*=23; two-way ANOVA with *post-hoc* Bonferroni's test, *P*<0.0001). (c) Quantitative comparison of elasticity modulus *E*1 and *E*2 values obtained by fitting procedure in HEK293 cells expressing STOML3 or STOML3-P40 in the presence of Piezo1 channel (Piezo1+STOML3: *n*=59; Piezo1+STOML3-P40: *n*=75; two-way ANOVA with *post-hoc* Bonferroni's test, *P*<0.0001). * *P*<0.05, **** P<0.0001. Error bars indicate s.e.m.

4.1.4 Cholesterol depletion attenuates tactile allodynia in mouse

To test the importance of cholesterol binding in tactile sensitivity, we made use of the tactile allodynia developed after nerve injury. Control C57BL/6N and *STOML3*$^{-/-}$ mice were subjected to CCI (chronic constriction injury) and developed reduced paw withdrawal threshold to von Frey filament stimulation. To avoid potential side effects of MβCD, low dose amount of MβCD (2mg/kg) was acutely injected into the hind paw on the injured side. Intriguingly, we observed that MβCD began to cause an attenuation of allodynia in control mice 2 hours post injection and reached the peak effect 4 hours post injection (Figure 25; one-way ANOVA with post-hoc Dunnett's Multipe Comparision Test, p<0.05). Our *in vitro* data showed voltage gated inward current density was reduced in nociceptor (Figure 9). To exclude the possibility that the attenuation of tactile allodynia was attributed to this, we have examined the effects of MβCD on acute pain behavior. Administration of MβCD exhibited no alteration on the paw withdrawal threshold, indicating the low dose MβCD is not capable of affecting nocifensive behavior (Figure 23). Remarkably, when we tested *STOML3*$^{-/-}$ mice, the analgesic effect of MβCD on tactile allodynia was completely absent (Figure 26; one-way ANOVA with post-hoc Dunnett's Multipe Comparision Test, p>0.05), strongly suggesting that lipid rafts could regulate tactile sensitivity and this regulation requires the involvement of STOML3, or in another word, cholesterol association is required for the proper function of STOML3 in touch sensitivity.

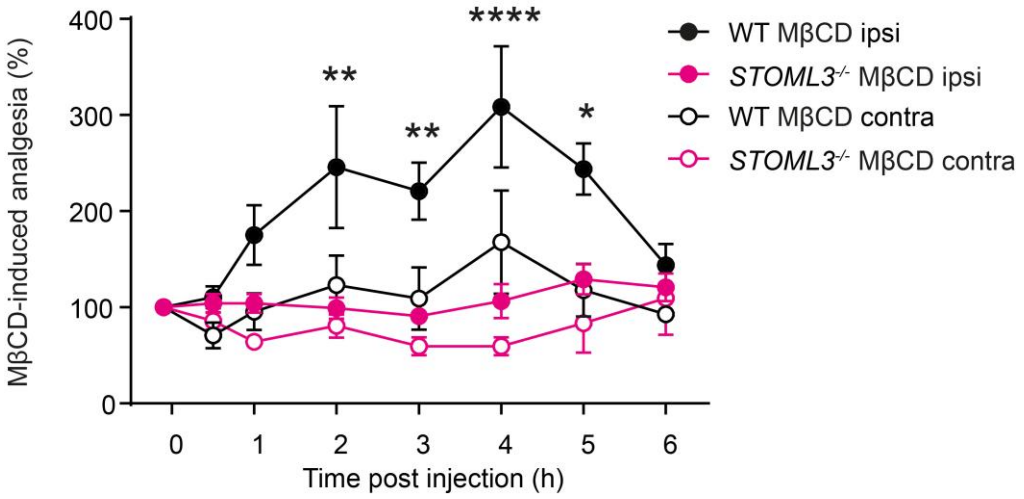

Figure 25. MβCD presents an analgesic effect on nerve injury induced tactile allodynia in C57BL/6N but not in *STOML3*$^{-/-}$ mice. MβCD (2mg/kg) was injected to the hind paw on the injured side of partially sciatic nerve-ligated *STOML3*$^{-/-}$ and control C57BL/6N mice, and mechanical sensitivity was examined in *STOML3* knockout and control WT mice at various time points after injection. Baseline thresholds (BL) were measured in injured mice before the drug injection. Normalized mechanical paw withdrawal threshold relative to baseline threshold were plotted over the time of post drug injection for *STOML3*$^{-/-}$ and control C57BL/6N mice. MβCD inhibited mechanical allodynia in C57BL/6N mice after 2 hours injection but not in *STOML3*$^{-/-}$ mice (n=6-12 mice/group, MβCD effect: one-way ANOVA with *post-hoc* Bonferroni's Multiple Comparison Test, C57BL/6N: ipsilateral, $P<0.05$; contralateral, $P>0.05$; *STOML3*$^{-/-}$: ipsilateral, $P>0.05$; contralateral, $P>0.05$; STOML3 influence: C57BL/6N versus *STOML3*$^{-/-}$, two-way repeated-measures ANOVA with *post-hoc* Bonferroni's test, $P<0.001$). * $P<0.05$, ** $P<0.01$, **** $P<0.0001$. Error bars indicate s.e.m.

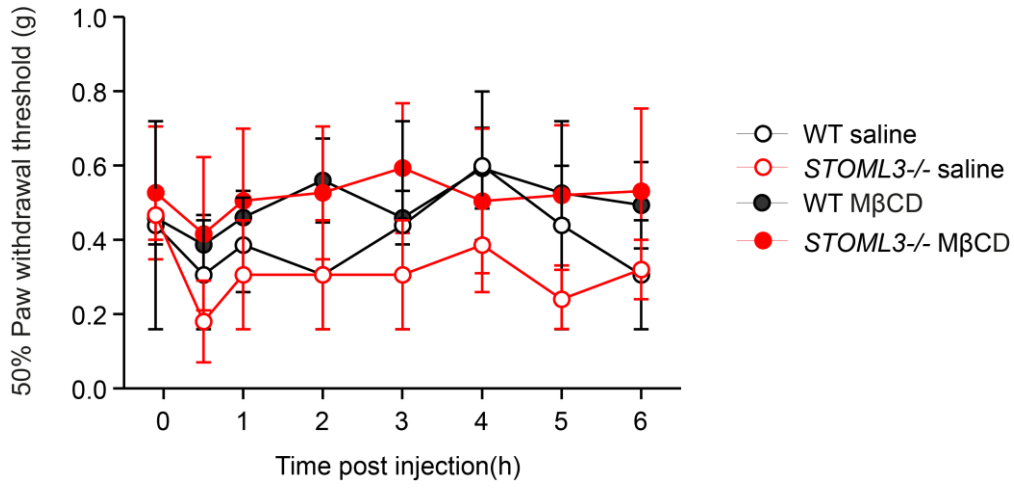

Figure 26. Effect of MβCD on acute nociceptive response to mechanical stimulus in either C57BL/6N or *STOML3*$^{-/-}$ mice. MβCD (2mg/kg) was injected to the hind paw on the one side of *STOML3*$^{-/-}$ and control C57BL/6N mice, and mechanical sensitivity was examined in *STOML3* knockout and control WT mice at various time points after injection. Mechanical paw withdrawal threshold was plotted over the time of post drug injection for *STOML3*$^{-/-}$ and control C57BL/6N mice. MβCD exhibited no effect on acute nociceptive response to mechanical stimulus in either C57BL/6N or *STOML3*$^{-/-}$ mice (n=6 mice/group, MβCD effect: one-way ANOVA with post-hoc Dunnett's Multiple Comparison Test, C57BL/6N**,** $p>0.05$; *STOML3*$^{-/-}$, $p>0.05$; STOML3 influence: C57BL/6N versus *STOML3*$^{-/-}$ mice, two-way ANOVA, $p>0.05$). Each data point is the mean ± s.e.m.

4.2 The role of cholesterol-rich lipid rafts in the regulation of ASICs activity by STOML3

The following chapter (4.2.1-4.2.5) are taken from "The regulation acid-sensing ion channels by STOML3 requires cholesterol-rich lipid rafts", Yanmei Qi, Jing Hu. Manuscript in preparation.

4.2.1 Effects of cholesterol depletion on proton gated currents in heterologous cells and sensory neurons

4.2.1.1 Depleting cholesterol enhances ASICs proton-gated activity in heterologous cells

To test if disrupting lipid rafts can affect ASICs proton-gated activity, we performed cholesterol depletion with Methyl-β-cyclodextrin (MβCD, 5mM, 1h, at 37°C) in CHO cells expressing ASIC1a, ASIC2a or ASIC3 alone. Cholesterol depletion with MβCD markedly increased the pH6-activated current of ASIC1a (Figure 27a, from 163±23pA/pF to 242±32pA/pF at -60mV, unpaired t-test $P<0.05$) and ASIC3 (Figure 29a, from 93±7pA/pF to 179±27pA/pF at -60mV, unpaired t-test $P<0.001$). The rate of ASIC3 desensitization was slowed after MβCD treatment (Figure 29b, τ: 300±12ms in control vs 396±24ms in MβCD group, unpaired t-test $P<0.01$), indicating the channel gating is modulated by lipid rafts. MβCD did not alter the decay kinetics of ASIC1a (Figure 27b, unpaired t-test P=0.86). In cells expressing ASIC2a, the proton-activated current was significantly increased by MβCD treatment at both stimuli of pH5 (Figure 28, from 44±5pA/pF to 156±25pA/pF at -60mV, unpaired t-test $P<0.01$) and pH4 (Figure 28; from 143±17pA/pF to 214±27pA/pF at -60mV, unpaired t-test $P<0.05$). Taken together, these data suggest lipid rafts modulate proton-gated ASICs activity in heterologous expression system.

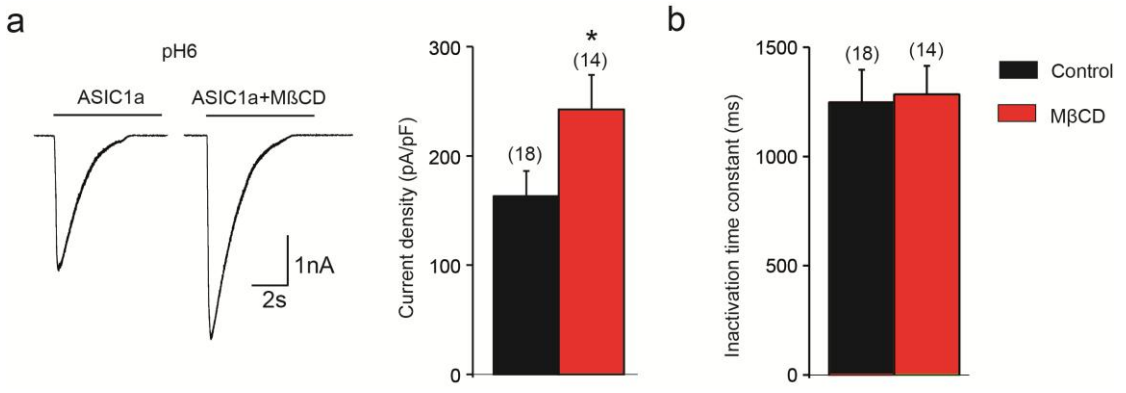

Figure 27. Cholesterol depletion with MβCD increases ASIC1a current. (a) Left: Representative proton-gated currents at pH6 in CHO cells expressing ASIC1a before and after MβCD treatment (5mM, 1h). Right: Mean peak current density at pH6 recorded from CHO cells transfected with ASIC2a before and after MβCD treatment. (b) The time constant of desensitization evoked by pH6 in CHO cells transfected with ASIC1a before and after MβCD treatment. The number of recorded cells is indicated in parentheses in each panel. Unpaired t-Test, **P*<0.05. Error bars indicate s.e.m.

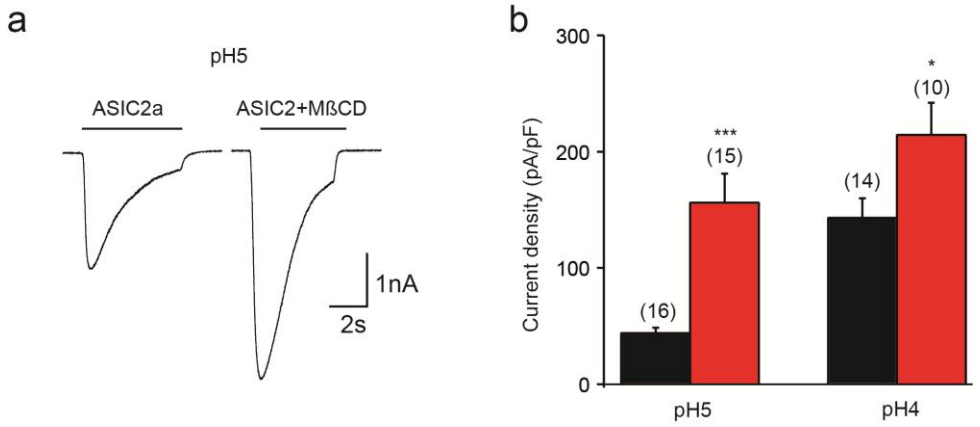

Figure 28. MβCD increases proton-activated current of ASIC2a. (a) Representative currents evoked by application of pH5 to CHO cells expressing ASIC2a before and after MβCD treatment. (b) Mean current density elicited by pH5 and pH4 in CHO cells transfected with ASIC2a before and after MβCD treatment. Data are expressed as mean±s.e.m, pA/pF, picoampere/picofarad. The number of recorded cells is noted, unpaired t-Test * *P*<0.05, *** *p*<0.001, compared with control without MβCD treatment.

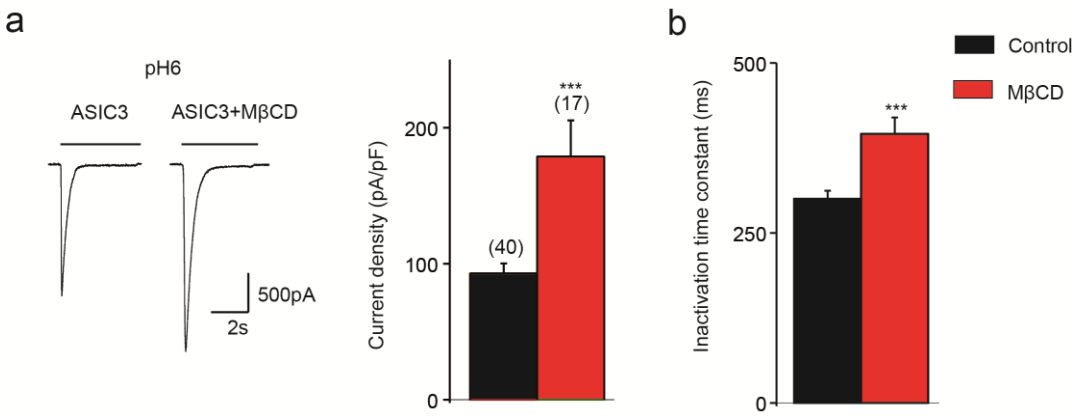

Figure 29. Cholesterol depletion increases proton gated ASIC3-medicated current. (a) left: Representative currents recorded at pH6 from CHO cells expressing ASIC3 alone before and after MβCD treatment. Right: Mean current density elicited by pH6 in CHO cells transfected with ASIC3 before and after MβCD treatment. The number of recorded cells is indicated in parentheses in each panel, data are expressed as mean±s.e.m, pA/pF, picoampere/picofarad. Note the significantly increased ASIC3 proton gated current after MβCD treatment (unpaired t-Test, *** p<0.001. (b) The time constant of desensitization evoked by pH6 in CHO cells transfected with ASIC3 before and after MβCD treatment. n=17-40, unpaired t-Test, *** p<0.001. Error bars indicate s.e.m.

4.2.1.2 Cholesterol depletion increases proton-gated ASICs-like transient currents in wild type sensory neurons

Next we test if cholesterol depletion affects proton gated currents in sensory neurons. To this end, cultured DRG sensory neurons from C57BL/6N mice were treated with or without MβCD (5mM, 1h). MβCD treatment resulted in a significant increase in the peak amplitude of a fast activating, rapidly inactivation ASIC-like transient currents (Figure 30; pH6: from 724±130pA at -60mV, n=13 to 2222±507pA, n=14; unpaired t-test * P<0.05), while the proton-activated sustained currents were slightly reduced.

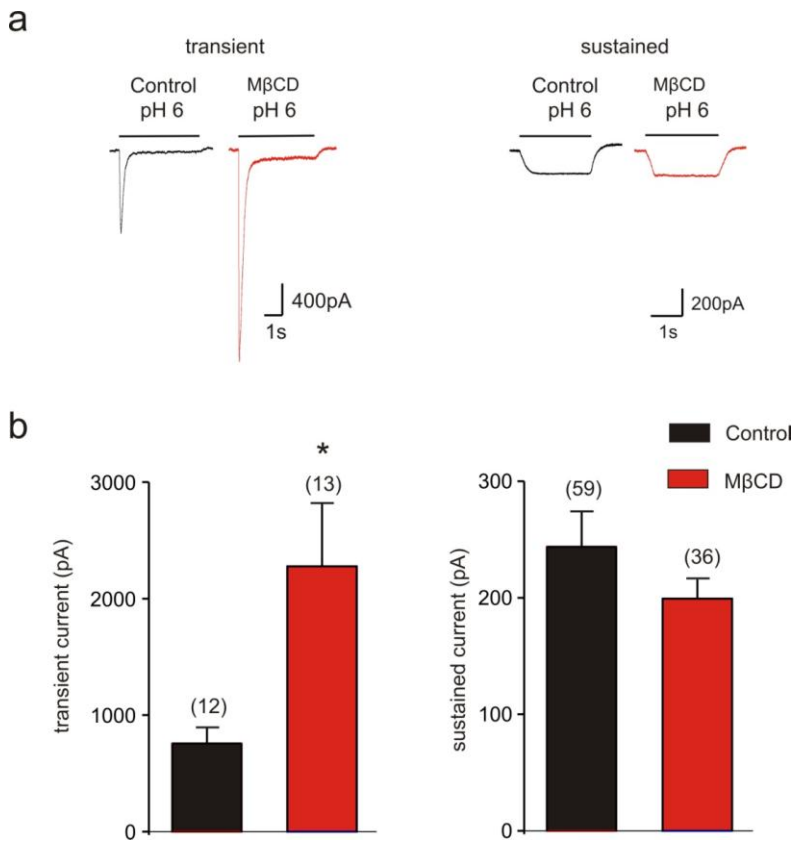

Figure 30. Cholesterol enriched lipid rafts regulate proton-gated currents in sensory neurons. (a) Representative traces of proton-gated transient and sustained currents recorded in control or MβCD treated neurons. (b) Quantitative comparison of the transient and sustained proton-gated currents recorded from control or MβCD treated neurons. Amplitude of ASIC-like transient but not sustained current at pH6 was significantly larger in MβCD treated neurons than in control neurons (unpaired t test, transient current: $p<0.05$; sustained current: $p>0.05$). The number of neurons recorded is indicated in parentheses in each panel. One asterisk, $p<0.05$; Error bars indicate s.e.m.

4.2.1.3 Cholesterol depletion does not change proton gated currents in *STOML3*$^{-/-}$ neurons

In the absent of STOML3, the proton-gated currents were also increased in sensory neurons [47]. Considering the similarity between cholesterol depletion and *STOML3* deficient, both affected acid evoked currents. We propose STOML3 and lipid rafts might regulate the activity of acid-sensing ion channels in the same pathway. To test this idea, we also treated *STOML3*$^{-/-}$ sensory neurons with MβCD (5mM, 1h). Intriguingly,

cholesterol depletion with MβCD did not alter the proton-gated transient current in *STOML3*$^{-/-}$ neurons (Figure 31, control: 1842±435pA at pH6, n=10 vs MβCD 2480±699pA, n=10; unpaired t-test *P*>0.05). Lack of an additive effect of MβCD on proton gated channel activity in *STOML3* deficient neurons suggest the regulation of acid-sensing ion channels by cholesterol enriched lipid rafts involves STOML3.

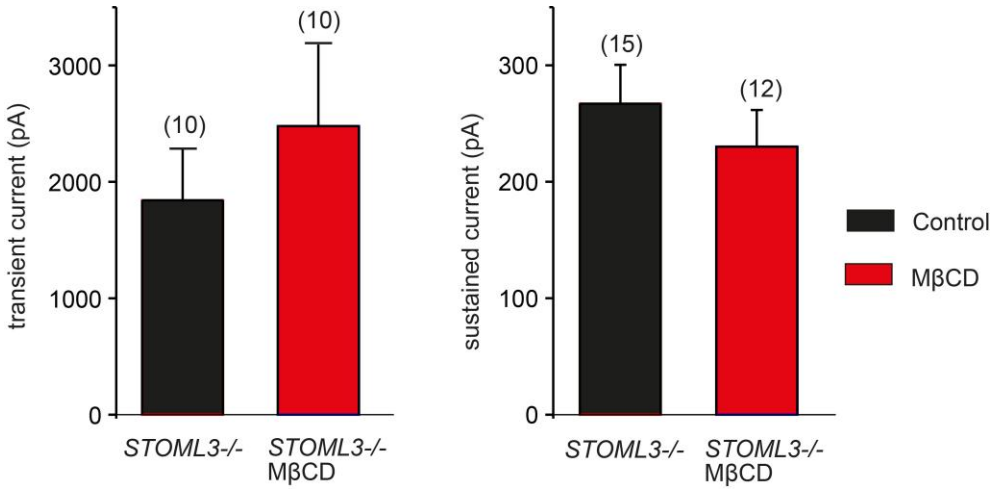

Figure 31. Cholesterol depletion does not alter proton-gated currents in *STOML3*$^{-/-}$ sensory neurons. Quantitative comparison of the transient (left) and sustained [126] proton-gated currents recorded from *STOML3*$^{-/-}$ neurons treated without or with MβCD. amplitude of ASIC-like transient current at pH6 was not altered by MβCD treatment (unpaired t test, transient current: *p*>0.05; sustained current: *p*>0.05).

4.2.2 Cholesterol depletion abolishes the repression of STOML3 on ASIC3 activity in heterologous cells

As shown previously [49], STOML3 inhibited ASIC3 pH-activated current in CHO cell line (Figure 32). To test if the inhibition of STOML3 on ASIC3 activity involves lipid rafts in heterogeneous expression cells, MβCD (5mM, 1h at 37°C) was again applied to disrupt cholesterol-rich lipid rafts in CHO cells expressing ASIC3 together with STOML3. We show MβCD pretreatment completely reversed the inhibition of STOML3 on ASIC3 activity (Figure 32; 68±8pA/pF in STOML3 vs 209±6pA/pF in STOML3+MβCD group at pH6, unpaired t-test P<0.001), suggesting the regulation of ASICs channel activity by STOML3 involves cholesterol enriched lipid rafts. Moreover, the ASIC3 pH-activated

current in group with the presence of STOML3 was not significantly different with that in group expressing ASIC3 alone after MβCD treatment (179±27pA/pF in ASIC3+MβCD group vs 223±7pA/pF in ASIC3+STOML3+MβCD group at pH6, unpaired t-test $p>0.05$), which accords well with previous report showing STOML3 does not alter ASICs surface protein expression [49], implying that STOML3 is not responsible for ASICs trafficking.

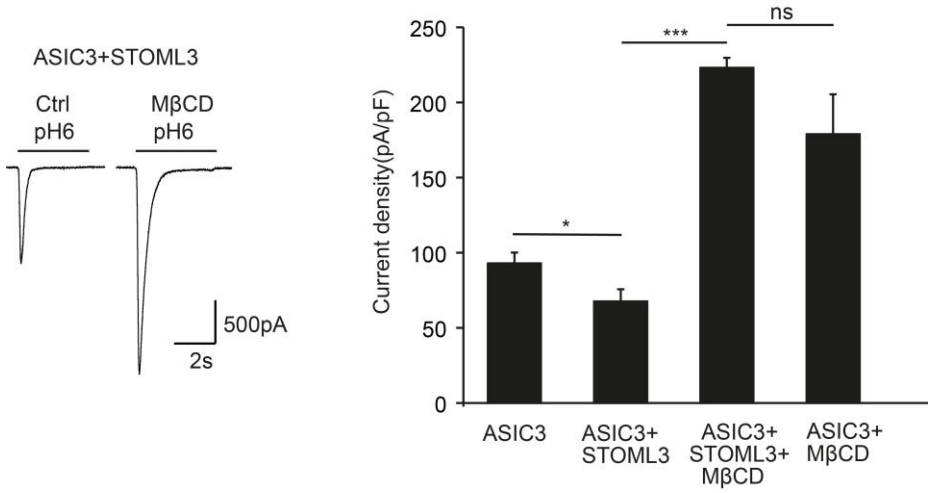

Figure 32. Cholesterol depletion abolishes the inhibition of STOML3 on ASIC3 acid evoked current. Left: Representative currents recorded at pH6 from CHO cells coexpressing ASIC3 and STOML3 before and after MβCD treatment. Right: Mean current density evoked by pH6 in CHO cells coexpressing ASIC3 either with empty vector eGFP or STOML3-eGFP before and after MβCD treatment. The number of recorded cells is indicated in parentheses in each panel. Unpaired t-Test, ASIC3 alone vs ASIC3+STOML3: * $P<0.05$; ASIC3+STOML3+MβCD vs ASIC3+STOML3 *** $p<0.001$; ASIC3+STOML3+MβCD vs ASIC3+MβCD $p>0.05$. Error bars indicate s.e.m.

4.2.3 Effects of STOML3 mutants on ASIC3 channel activity

The cholesterol binding property has been demonstrated to be essential for MEC-2 and podocin, two stomatin domain proteins, to regulate their associated ion channels[60]. To test the importance of cholesterol for STOML3 to regulate its associated ASIC channel, we sought to specifically disrupt the association of STOML3 with cholesterol. One conserved proline residue in the N-terminal hydrophobic domain and two conserved palmitoylation sites (cysteine residues) are known to be important for stomatin-domain family proteins to associate with cholesterol [60,127], we thus mutated the conserved proline

residue (STOML3^{P40S}) and two conserved cysteine residues (STOML3^{C46,80A}) in STOML3, and examined the effects of these two mutants on ASIC3 current. However, similar to STOML3 wild-type, both mutants inhibited ASIC3 current (Figure 33), and MβCD can completely abolish the inhibition of a STOML3 mutant deficient in cholesterol association (STOML3^{P40S}) to ASIC3 current (Figure 33; pH6: from 34±5pA/pF to 159±21pA/pF, unpaired t-test $p<0.0001$). Likewise, the proton activated current was comparable between group expressing ASIC3 with STOML3^{P40S} mutant and group expressing ASIC3 alone after MβCD treatment (Figure 33; ASIC3+STOML3-P40S+MβCD versus ASIC3+MβCD at pH6, unpaired t-test $p>0.05$), implying STOML3^{P40S} mutant also does not change the surface expression of ASIC3 protein. Altogether, we suggest cholesterol enriched membrane environment is important for the inhibition of ASIC3 channel activity by STOML3, including STOML3 mutant deficient in cholesterol association.

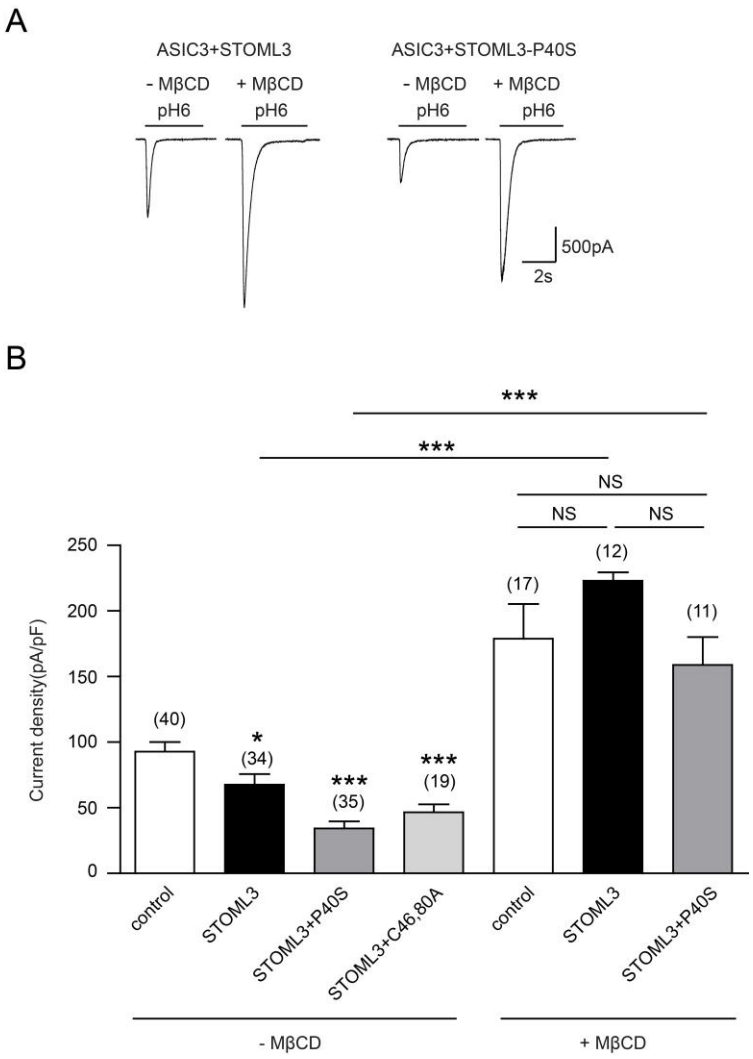

Figure 33. Effects of STOML3 mutants on ASIC3 proton-gated current. (a) Mean current density recorded at pH 6 from CHO cells expressing ASIC3 with STOML3-C46, 80A-EGFP or empty EGFP at 1:8 ratios (empty vector EGFP was used as a control to keep cDNA ratio constant). Note the significantly increased ASIC3 current when expressed with STOML3-C46, 80A mutant (Unpaired t-Test, *** p<0.001) (b) Mean current density recorded at pH 6 from CHO cells expressing ASIC3 with STOML3Δ40-80-EGFP or empty EGFP at 1:10 ratios. A separate group of cells expressing ASIC3 with STOML3Δ40-80-EGFP was studied after MβCD treatment (5mM, 1h). STOML3Δ40-80 mutant significantly reduced the ASIC3 proton-gated current (Unpaired t-Test, *** p<0.001). MβCD abolished the inhibition of STOML3Δ40-80 mutant on ASIC3 photon-gated current (Unpaired t-Test, *** p<0.001). The number of recorded cells is indicated in parentheses in each panel. Error bars indicate s.e.m.

4.2.4 Mutation of proline (P40) residue alters STOML3 protein N-glycolation in heterologous expression cells

Interestingly, three isoforms were detected with western blot for STOML3, including one dominant isoform of STOML3 with molecular mass around 32kD and two isoforms with higher molecular mass (~34 and 36kD, respectively). On the contrary, the two higher molecular isoforms were abundantly observed in STOML3^{P40} mutant (Figure 36). Previous *in vitro* study has shown stomatin protein is subjected to different level of N-glycolation modification, so that stomatin has many isoforms with different molecular mass [128]. We thus speculate that the observed isoforms with higher molecular mass in STOML3^{P40} mutant might be because of the protein N-glycosylation modification. STOML3 might have two potential consensus sites (N222 and N257) for N-glycolation (NXS/T, where X is any amino acid except for Proline). To test this, we introduced a mutation into STOML3^{P40} mutant at the position of N222 or N257. Western blotting show mutation of either N222 or N257 site abolished the antigen with the biggest molecular antigen (~36kDa) (Figure 36), suggesting mutation of this proline (P40) residue increases N-glycosylation of STOML3 *in vitro*.

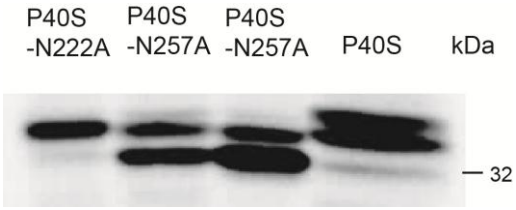

Figure 34. Mutation of proline (P40) residue enhances STOML3 protein N-glycolation in heterologous expression cells. CHO cells expressing Myc epitope-tagged STOML3-P40S, STOML3-P40S-N257A or STOML3-P40S-N222A mutant was lysated and detected by anti-Myc antibody. STOML3-P40S mutant protein had three isoforms, and mutation of the Asparagine residue at either N222 or N257 site abolished the antigen with the highest molecular mass (~36kDa). Experiment was performed twice with STOML3-P40S-N257A, and was performed once for STOML3-P40S and STOML3-P40S-N222A. Note that the molecular mass in kDa for the smallest isoform of STOML3-P40S mutant protein (~32kDa).

5. Discussion

5.1 STOML3 modulates sensory mechanotransduction through cholesterol enriched lipid rafts

Parts of the following discussion are adapted from:
"Membrane stiffening by STOML3 facilitates mechanosensation in sensory neurons", Yanmei Qi, Flavia Frattini, Laura Andolfi, Marco Lazzarino, Jing Hu. Nat. Commun. 6:8512 doi: 10.1038/ncomms9512 (2015).

5.1.1 Brief summary of our major findings

Cholesterol binding properties of MEC-2 are needed for both mechanosensitive channels activity *in vitro* and touch sensitivity in *C. elegans* [60]. But it remains elusive how STOML3, a mammalian MEC-2 orthologue, contributes to sensory mechanotransduction in mouse. Here in this study, we provide several lines of evidence to propose a novel mechanism by which STOML3 modulates sensory mechanostransuction: via associating with cholesterol-rich lipid raft, STOML3 controls the membrane mechanics, thus facilitates the force transfer and tunes the sensitivity of the mechanically gated channels, including Piezo channels. First, STOML3 was detected in cholesterol-rich lipid rafts. Depletion of cholesterol and deficiency of STOML3 in sensory neurons similarly and interdependently affect membrane mechanics and attenuate mechanosensitivity. Second, we demonstrate that an intact STOML3 is essential to maintain membrane mechanics to sensitize mechanically gated Piezo1 and Piezo2 channels in heterologous system. Importantly, such stiffened membrane can be softened by either depleting cholesterol or genetic disruption of cholesterol binding of STOML3. Thirdly, mutation of residue involved in cholesterol binding (STOML-P40S) failed to modulate the sensitivity of Piezo channels or restore the mechanosensitivity of *STOML3*$^{-/-}$ sensory neurons. Finally, using behavioural test, we show that cholesterol depletion could attenuate tactile allodynia and this effect involves STOML3. In summary, we for the first time have shown here, the cholesterol binding of STOML3 is essential for sensory

mechanotransduction *in vitro* and tactile sensitivity *in vivo*. By binding STOML3, the ordered cholesterol-rich lipid rafts could associate with mechanosensitive ion-channel complexes, for instance, the stretch activated SA channel complex, thus modulating its local membrane environment and facilitating force transfer. By recruiting cholesterol to the associated ion channels, STOML3 may alter the local membrane mechanics, influence the free energy of channels, and set the availability of mechanosensitive channels, such as the tether activated RA channel, thus determining its current amplitude when gated by force.

5.1.2 Cholesterol enriched lipid rafts regulate mechanosensitivity in sensory neurons

In this thesis, base on our *in vitro* data of the effects of reducing membrane cholesterol level with methyl-β-cyclodextrin on mechanically activated responses in DRG sensory neurons, we propose the importance of cholesterol enriched lipid rafts in sensory mechanotransduction. Cholesterol depletion caused to the suppression of SA-mechanosensitive currents and reduction of RA-mechanosensitive currents in sensory neurons. In line with these, the altered mechanical responses by cholesterol depletion are also observed in other mammalian cells, such as leukemia cells [129], osteoblastic cells [130], skeletal muscle [131] and myotubes [132]. In cochlear; there are increasing evidences indicating cholesterol enriched lipid rafts are important for sound processing. Depletion of membrane cholesterol changes calcium signaling in mature hair cells [133] and excitability during development [134], and affects electromechanics in outer hair cells that are responsible for hearing acuity [135]. Moreover, filipin staining has shown cholesterol is observed at the very tip of the sterocilia where transduction channel reside [136], implying cholesterol might be involved in force transfer. Collectively, these data provided by us and others suggest a possible unifying mechanism for cholesterol-enriched lipid rafts involved in regulation of cell mechanical response. Moreover, Anishkin and Kung have suggested in a recent review that all membrane force foci on animal cells are reinforced with cholesterol [137], indicating recruiting cholesterol to mechanotransduction supercomplex might facilitate the efficient force transfer.

5.1.3 Cholesterol enriched lipid rafts regulate tactile sensitivity in mice

Mechanotransduction in the sensory neurons allows animals to sense touch, dysfunction of mechanotransduction processing by lipid rafts disruption would be thus expected to affect animal' tactile sensitivity. Indeed, our behavioural data show acute intraplantar injection of cholesterol-chelating agent MβCD alleviated nerve injury-induced tactile allodynia, which is an abnormal painful sensation evoked by non-noxious mechanical stimuli such as light touch. This attenuation of tactile sensitivity after acute MβCD delivery may be attributed to alternation of mechanotransduction, or change of excitability at the peripheral terminal. Since cholesterol depletion slightly depolarized the resting membrane potential and increased the membrane excitability of sensory neurons *in vitro*, this *in vivo* analgesic effect of MβCD we observed here is not likely due to the change of neuron excitability. Our *in vitro* electrophysiological data revealed cholesterol depletion did not alter voltage gated inward and outward currents in mechanoreceptor, implying voltage gated sodium channels involved in AP firing may not be affected by rafts disruption in mechanoreceptor. In nociceptors, voltage gated currents were reduced after cholesterol depletion *in vitro*, implying MβCD might affect action potential firing in nociceptors [117]. However, intraplantar delivery of MβCD did not alter the acute pain behavior in wild-type mice, indicating that the attenuation of tactile allodynia after MβCD injection was not because of the change of voltage gated sodium channels in nociceptors. After excluding these possibilities, we thus suggest that the observed attenuation of tactile allodynia after MβCD delivery probably results from the reduction of mechanosensitivity in sensory afferent terminal. The reduced sensitivity of SA channel and reduction of RA current might contribute to the MβCD-mediated attenuation of neuopathic pain. In consistent with this, cholesterol-deprived worms are relatively touch-insensitive compared with normal animals [60], and subcutaneous delivery of cholesterol-modulator beta-cyclodextrin is capable of inducing severe hearing loss in mice [138].

5.1.4 Possible mechanisms by which cholesterol enriched lipid rafts regulate mechanosensitivity

5.1.4.1 Changing membrane physical properties affects mechanosensitivity

Altering physical properties of lipid bilayers are proposed to regulate the activity of mechanosensitive ion channels [18,96]. For examples, changing bilayer thickness has been reported to alter the stretch sensitivity of antibiotic gramicidin A channel, which is a popular biophysical model channel [120]. Changing local membrane curvature by external addition of amphipaths activates or closes stretch activated channels such as bacteria mechanosensitive channel MscL and mechano-gated K2P channels TREK-1 and TRAAK [18,19,139]. Changing the local pressure profile in lipid bilayer regulates the activity of bacteria mechanosensitive channel MscL [96]. These studies imply the importance of the membrane physical properties in mechanosensation.

Cholesterol is well known as an important component in lipid bilayer, presence of cholesterol in bilayer has been shown to increase the thickness and rigidity of lipid bilayer, suppress lipid lateral diffusion [96,140,141], and change the curvature and lateral pressure profile of lipid bilayer [18,96,142]. Depleting membrane cholesterol would be assumed to affect the physical properties of lipid bilayer. Indeed, depleting cholesterol with cyclodextrin reduces membrane stiffness measured by atomic force spectroscopy in DRG sensory neuron [123] and HEK293 cell lines (Figure 24a). Stiffened membrane by the presence of cholesterol might facilitate mechanical force transfer and thus enhance channel sensitivity.

Several other studies however show that depleting cholesterol results in an increase of membrane stiffness, which is in contrast to the known effect of cholesterol on stiffness of lipid bilayers. Byfield and colleagues show cholesterol depletion with cyclodextrin increases cell stiffness in Aortic endothelial cells by changing the organization of cytoskeleton [143,144]. Moreover, a proteomic study of rafts membrane reveals several cytoskeletal proteins are associated with rafts membrane fractions [145], suggesting cholesterol enriched lipid rafts probably couple the plasma membrane and submembrane cytoskeleton. In parallel, Sun *et. al* show cholesterol depletion increases the adhesion energy between the membrane and the cytoskeleton [146]. Thus, the observed increase of membrane stiffness after cholesterol depletion is probably due to the underlying cytoskeleton.

Recently, using *C. elegans* as a model, Petzold and colleagues have revealed that changing body stiffness affects touch sensitivity *in vivo* [147], and Krieg and colleagues have shown changing neurons cell mechanics by genetic manipulation of β-spectrin impaired touch sensation [20]. The alteration of membrane stiffness after cholesterol depletion might be one possible mechanism underlying the change of mechanosensitivity observed by us both *in vitro* and *in vivo*.

5.1.4.2 Changing local membrane environment by cholesterol depletion dramatically influences stretch activated ion channel

Two models of gating have been proposed for sensory mechanosensitive currents. The first one is stretch-activated gating model, in which tension or force changes within the lipid bilayer directly gate channel. The second model is called tether model, an extracellular structure is proposed to transfer forces from the surrounding matrix to the ion channel to promote opening in this model [5,14]. In sensory neurons, the two most common mechanosensitive current types, rapidly adapting (RA) and the slowly adapting (SA) mechanosensitive currents, represent the two distinct channel gating mechanisms: tether model and membrane stretch model respectively [14,42,43]. It has been proposed that altering the internal membrane force profile will not only affect the activity of stretch-activated channels, but would also affect the sensitivity of channels gated by force delivered through a tether protein [137]. Indeed, we did observe that changing membrane environment by cholesterol depletion had an influence on both RA and SA currents in sensory neurons (Figure 7, Figure 10 and Figure 11). However, as shown in Figure 7, cholesterol depletion dramatically affected SA current but not RA current in sensory neurons. This difference on RA and SA currents might result from the different gating mechanisms for SA and RA channels. RA-mechanosensitive currents but not SA currents requires a protein tether to transduce mechanical stimuli in mammalian sensory neuron [42,43]. The gating of SA channel, a stretch activated channel, may largely depend on membrane tension. Altering the local membrane environment would be expected to dramatically influence the stretch activated channel gated by force. In support of this,

suppression of stretch activated channels by changing membrane environment with cholesterol depletion has been observed in human leukemia cells [129].

Depleting membrane cholesterol reduced RA current amplitude and RA channel activity but did not affect the RA channel kinetics, suggesting the membrane environment does not have dramatic influences on RA channel sensitivity. This is similar to the effect of MEC-2 on sensory mechanotransduction channels MEC-4/MEC-10 in *c. elegans*, where the function is altered by increasing the number of channels in an active state rather than by dramatically affecting either single-channel properties of surface expression [35]. The reduced amplitude of RA current shown by us indicates the number of mechanosensitive channels in an active state might be altered by lipid rafts disruption. Our further detailed analysis of RA current revealed that disrupting cholesterol-enriched lipid rafts, thus changing the local membrane environment, had no effect on RA mechanosensitive channel kinetics, the abilities to respond to force with different intensities or velocities, ion selectivity and the ability to respond to repetitive stimulus, which support previous finding that RA channels require a protein tether to transfer the mechanical force other than being directly stretched by the internal force [42,43].

5.1.4.3 Regulation of mechanosensitivity by cholesterol enriched lipid rafts involves a stomatin like protein

The lipid rafts isolation experiment in heterologous cells showed STOML3, which has been reported to be an essential subunit for normal mechanosensitivity in mice, localized in cholesterol enriched lipid rafts. The presence of STOML3 in cholesterol-rich lipid rafts allows us to propose an assumption that STOML3 may be one possible target for cholesterol enriched lipid rafts to regulate mechanosensitivity in sensory neurons. Indeed, we provide evidences from *in vitro* to *in vivo* and suggest the regulation of mechanosensation by lipid rafts involves STOML3-cholesterol binding. *In vitro*, we show that cholesterol depletion with MßCD significantly reduced mechanosensitivity in sensory neurons from wild-type mice but did not induce a further reduction of mechanosensitivity in *STOML3*$^{-/-}$ neurons (Figure 13). *In vivo*, disruption of cholesterol enriched lipid rafts by intraplantar injection of MβCD alleviated mechanical allodynia

induced by neuropathic pain in wild-type but not in *STOML3*$^{-/-}$ mice (Figure 25). All together, we suggest the regulation of mechanosensitivity by cholesterol enriched lipid rafts involves a stomatin like protein..

Through STOML3-cholesterol association, the mechanosensitive ion channel complex might be recruited into cholesterol-rich microdomain or membrane surrounding the cholesterol-rich lipid rafts, where the force transfer to the channel would be facilitated. Moreover, Lapatsina and colleagues have Recently shown STOML3 is observed at Rab11-positive high mobile vesicle in DRG neuron, and this specialized STOML3 vesicle is speculated to be responsible for the trafficking of functional mechanotransduction complex into membrane of sensory neuron [49]. A large amount of studies have suggested lipid rafts server as a compartmentalized platform and regulate membrane trafficking [148], cellular exocytosis [149] and endocytosis cycle [150]. Thus another possibility for lipid rafts to modulate mechanosensitivity is that cholesterol enriched lipid rafts might facilitate the membrane targeting of STOML3 vesicle.

5.1.5 STOML3 regulates mechanosensitivity and membrane mechanical properties via associating with cholesterol enriched lipid rafts

5.1.5.1 STOML3 regulates sensory mechanotransdution through associating with cholesterol enriched lipid rafts

We have proposed that the regulation of mechanosensitivity by lipid rafts involves STOML3 cholesterol binding. In another word, STOML3 might regulate mechanosensitivity via binding cholesterol. An *in vitro* rescue experiment further revealed cholesterol binding activity is essential for STOML3 to regulate sensory mechanotransduction. Consistent with previous reports on other stomatin-domain containing proteins including stomatin, podocine and MEC-2 [60,128], mutation of one conserved proline residue (STOML3^{P40S}) also impaired the association of STOML3 with cholesterol enriched lipid rafts in heterologous expression system (Figure 19). Besides, mutation of this proline residue appears to affect the physiological association of STOML3 with cholesterol enriched lipid rafts given that the colocalization of STOML3

puncta with cholesterol along sensory neurite was impaired in STOML3^{P40S} mutant and reconstituting this STOML3^{P40S} mutant into *STOML3*-/- neurons failed to restore the mechanosensitive currents (Figure 20). Taken together, we propose STOML3 regulates mechanosensitivity via associating with cholesterol enriched lipid rafts. Similar findings have been observed on MEC-2, a close orthologue of STOML3 [35,60]. Thus, binding cholesterol may be a conserved mechanism for stomatin family proteins to regulate mechanotransduction. Regarding to how stomatin family proteins couple cholesterol to the processing of mechanotransduction, one possibility is that stomatin family proteins might recruit mechanotransduction apparatus into membrane rafts by associating with cholesterol, and thus facilitate the efficient force transfer [137]. Another possible mechanism is that stomatin family proteins are likely to change the local lipid environment of mechanotransducer by recruiting cholesterol, leading to the alteration of the membrane physical property surrounding the channel. In support of this, we indeed found disrupting STOML3-cholesterol association altered membrane physical properties (Figure 23 and Figure 24).

5.1.5.2 STOML3 regulates mechanically activated channels via cholesterol enriched lipid raft

Piezos proteins have been shown to be true mechanosensitive channel [21,45]. STOML3 is considered to be a modulator of piezo channel, presence of STOML3 substantially increases its sensitivity such that piezo channel is capable to detect molecular-scale stimuli [48]. We further suggest that STOML3 regulates piezo channels activity through cholesterol enriched lipid rafts given that the potentiation of piezo1 and Piezo2 currents by STOML3 was completely abolished by cholesterol depletion and a STOML3 mutant deficient in cholesterol binding failed to potentiate piezo currents in heterologous expression cells.

STOML3 has been shown to be able to interact with piezo channel in heterologous cells [48], STOML3 might recruit piezo channel into cholesterol enriched lipid rafts via direct interaction. It would be interesting to test whether piezos proteins localize in cholesterol enriched lipid rafts and STOML3 affects the rafts distribution of piezo proteins in the

future. Answering these questions would be useful for understanding better about the underlying mechanisms for mechanotransduction.

5.1.5.3 STOML3 regulates membrane mechanical properties via associating with cholesterol

Our data of cell stiffness, membrane viscosity and tension measured with atomic force spectroscopy in WT and *STOML3*$^{-/-}$ sensory neurons revealed that STOML3 is critical for maintaining membrane mechanics in sensory neurons. Similar as cholesterol-rich lipid rafts, STOML3 may influence sensory mechanotransduction via stiffening neuronal membrane and resulting in an efficient transfer of force to the mechanically gated ion channels. We further used heterologous expression system to show that STOML3 modulate membrane mechanics via associating with cholesterol. In heterologous expression system, cells expressing STOML3 mutant (P40S) deficient in cholesterol binding were significantly softer than cells with STOML3 wild-type, and the reduction of stiffness by STOML3-P40S mutant does not depend on the presence of mechanosensitive ion channel piezo1.

The next question would be how STOML3 alters membrane mechanics. One possible explanation is that STOML3 might change the local lipid environment of membrane via recruiting cholesterol. Future experiment would be needed to test if STOML3 could change the amount of membrane cholesterol or cholesterol-riched lipid rafts. The second possibility is that it is STOML3's intrincic property to modify membrane physical property. Stomatin like proteins are considered to assemble into a banana-shaped topology [128]. Like caveolin [151], STOML3 might insert into membranes in cholesterol-dependent manner. After inserting into membrane, STOML3 might modify the curvature of local membrane with its banana-shaped topology, which has been reported in BAR (Bin/Amphiphysin/Rvs) family domain [152]. The third one could be that the association of STOML3 with cholesterol might change the organization of cortical actin cytoskeleton localized underneath the membrane. Membrane-cytoskeleton interaction has been proposed to exist in membrane rafts structure [153]. STOML3 might interact with cortical actin and serve as one of scaffold proteins that connect cortical actin with membrane rafts

by binding to both cholesterol and cortical actin. It would be interesting to study if STOML3 could interact with cortical actin in the future.

5.2 The role of cholesterol-rich lipid rafts in the regulation of ASICs activity by STOML3

Parts of the following discussion are adapted from:
"The regulation acid-sensing ion channels by STOML3 requires cholesterol-rich lipid rafts", Yanmei Qi, Jing Hu. Manuscript in preparation.

5.2.1 Brief summary of our major findings

In this study, we demonstrate that cholesterol enriched lipid rafts suppress the activity of ASIC channel in both heterologous expression cells and mouse DRG neurons, and this effect involves STOML3 in primary sensory neuron. Using a heterologous expression system, we suggest cholesterol-rich membrane environment is important for STOML3 to modulate ASIC channel activity, and propose STOML3 is likely to inhibit the activity of ASIC channel within cholesterol-rich lipid rafts. The molecular mechanism we propose here for the regulation of acid-sensing ion channels might provide potential therapeutic targets for treatment against pain that accompanies to tissue ischemia such as inflammation

5.2.2 Cholesterol enriched lipid rafts modulate acid-sensing ion channels

Cholesterol enriched lipid rafts have been suggested to modulate the activity of many different types of ion channels, such as voltage-gated potassium channels and transient receptor potential (TRP) channels [105,109,154,155], but the role of lipid rafts in the regulation of ASIC channel function remains less understood. In this thesis, we found cholesterol depletion with MβCD potentiated proton-gated transient current in mouse sensory neurons. Consistent with this, the pH-gated current was indeed increased by MβCD in CHO cells expressing ASIC1a, ASIC2a or ASIC3, supporting ASIC1a/ASIC2a/ASIC3 heteromultimers underlie the transient current described in mouse DRG neurons [78,84,156]. We suggest cholesterol-rich lipid rafts suppress the activity of ASIC channels in sensory neurons. On the contrary, the proton-gated sustained current was slightly reduced by

cholesterol depletion in sensory neurons, which is likely due to the decreased surface expression of TRPV1 (vanilloid receptor subtype 1) that partially carries the sustained component of proton gated current and inhibition of TRPV1 channel activity by cholesterol depletion [157,158]. We suggest cholesterol enriched lipid rafts suppress the activity of the acid-sensing ion channels. The suppression of channel activity by cholesterol-enriched lipid rafts might include the decrease in the open probability, unitary conductance, and/or the number of active channels on the membrane [159].

5.2.3 The regulation of acid-sensing ion channels by cholesterol enriched lipid rafts involves stomatin like proteins in sensory neurons

With regards to the possible mechanisms for the cholesterol regulation of ion channels, one possibility is cholesterol might directly interact with the channel and regulates its function. For instance, TRPV1 channel has been suggested to have cholesterol binding sites and cholesterol binding prevents the channel from opening [20,157]. Another possibility is that cholesterol regulates channel indirectly through interaction with different signaling molecules that are segregated within the raft domains [155].

In terms of the first possible mechanisms for the cholesterol regulation of ion channels, we have no evidence to show if ASIC channel have cholesterol sensitive motif. However, in terms of the second one, STOML3 not only functionally interacts with ASICs [49], but also associates with cholesterol enriched lipid rafts (Figure 12), implying STOML3 might be one such rafts-associated molecular for the regulation of acid-sensing ion channels. We suggest the regulation of ASIC channel function by lipid rafts is likely to primarily involve STOML3, because depleting cholesterol did not induce a further increase of ASICs-like transient current in *STOML3*$^{-/-}$ sensory neurons. Stomatin is also expressed in DRG neurons [160] and associate with cholesterol rich lipid rafts *in vitro* [161], and thus might have a potential contribution to the regulation of ASIC3 current by lipid rafts in sensory neurons [53,92], however, stomatin appears to play a minor role in the regulation of ASIC channels by lipid rafts. Thus in sensory neurons, cholesterol rich lipid rafts are likely to regulate ASIC channel function through some raft-associated proteins, including STOML3.

In addition, changing membrane physical properties by altering lipid composition of bilayer has been established to affect the gating of many ion channels, such as voltage gated Na^+ channel [118], two-pore K+ channels [139] bacteria mechanosensitive ion channels [18]. Lipid rafts are characterized with deferential packing and dynamic clustering of lipids and proteins and are thereby suggested to have different biophysical properties in thickness, stiffness and lateral pressure profile of lipid bilayer, which might ultimately affect the structure and activity of surrounding ion channel [96,99,162,163]. We would consider the potential effect of membrane physical properties of STOML3-contained lipid rafts on ASIC channel structure and function in the future.

5.2.4 STOML3 modulates ASICs-mediated proton-gated current within cholesterol-enriched lipid rafts

MEC-2, a STOML3 orthologue in *C. elegans*, interacts and modulates mechanotransduction channel MEC-4/MEC-10 without affecting surface expression and single-channel properties [33,35]. STOML3 interacts and inhibits ASICs current but appears not to change trafficking, membrane expression and channel properties of ASIC subunits [49]. Likewise, stomatin interacts and modulates proton gated ASIC3-mediated current but without altering protein surface expression and channel properties [92]. These findings suggest stomatin-like family proteins probably modulate their associated channels by altering the amount of channels in an active state. For acid-sensing ion channels, cholesterol enriched lipid rafts appear to be an inactive environment in the plasma membrane. STOML3 probably recruits ASICs into cholesterol-enriched lipid rafts where the activity the ASICs is confined. Disrupting lipid rafts by cholesterol depletion would be expected to release STOML3-ASICs protein complex into surrounding non-rafts membrane and abolish the inhibition of ASICs current by STOML3. Indeed as we expected, the inhibition of STOML3 on ASIC3-mediated current was completely abolished by cholesterol depletion. We thereby suggest STOML3 might suppress ASICs-mediated proton-gated current within cholesterol-enriched lipid rafts.

5.2.5 Mutation of a proline residue in stomatin like proteins probably alters protein topology structure

One conserved proline residue in the hydrophobic region of stomatin has been reported to be crucial for the formation of hairpin-loop topology *in vitro*, mutation of this conserved proline residue might result in the change of stomatin topology from the hairpin-loop to the single-pass transmembrane form, which probably causes to the failure of this stomatin mutant to associate with cholesterol-enriched lipid rafts [128]. Similar phenomenon is also observed in caveoline-1, an important subunit to form cholesterol-enriched caveolae structure [164]. Aoki *et. al* show the conserved proline residue in the membrane-inserting segment of caveolin-1 is important for the membrane topology and rafts partition of the protein [164]. Mutation of this conserved proline residue (p40 in STOML3) probably causes to the change of STOML3 topology structure [128], which might result in more N-glycosylation modification in $STOML3^{P40}$ mutant protein and the deficiency of $STOML3^{P40}$ mutant to associate with cholesterol enriched lipid rafts .

6. References

1 Delmas, P., Hao, J. & Rodat-Despoix, L. Molecular mechanisms of mechanotransduction in mammalian sensory neurons. *Nature reviews. Neuroscience* **12**, 139-153, doi:10.1038/nrn2993 (2011).

2 Woo, S. H. *et al.* Piezo2 is required for Merkel-cell mechanotransduction. *Nature*, doi:10.1038/nature13251 (2014).

3 Lumpkin, E. A., Marshall, K. L. & Nelson, A. M. The cell biology of touch. *J Cell Biol* **191**, 237-248, doi:10.1083/jcb.201006074 (2010).

4 Chen, C. C. & Wong, C. W. Neurosensory mechanotransduction through acid-sensing ion channels. *Journal of cellular and molecular medicine* **17**, 337-349, doi:10.1111/jcmm.12025 (2013).

5 Lumpkin, E. A. & Caterina, M. J. Mechanisms of sensory transduction in the skin. *Nature* **445**, 858-865, doi:10.1038/nature05662 (2007).

6 Johnson, K. O. The roles and functions of cutaneous mechanoreceptors. *Current opinion in neurobiology* **11**, 455-461 (2001).

7 Lewin, G. R. & Moshourab, R. Mechanosensation and pain. *Journal of neurobiology* **61**, 30-44, doi:10.1002/neu.20078 (2004).

8 Drew, L. J., Wood, J. N. & Cesare, P. Distinct mechanosensitive properties of capsaicin-sensitive and -insensitive sensory neurons. *J Neurosci* **22**, RC228 (2002).

9 Hu, J. & Lewin, G. R. Mechanosensitive currents in the neurites of cultured mouse sensory neurones. *J Physiol* **577**, 815-828, doi:jphysiol.2006.117648 [pii]
10.1113/jphysiol.2006.117648 (2006).

10 Cho, H., Shin, J., Shin, C. Y., Lee, S. Y. & Oh, U. Mechanosensitive ion channels in cultured sensory neurons of neonatal rats. *J Neurosci* **22**, 1238-1247 (2002).

11 Drew, L. J. & Wood, J. N. FM1-43 is a permeant blocker of mechanosensitive ion channels in sensory neurons and inhibits behavioural responses to mechanical stimuli. *Molecular pain* **3**, 1, doi:10.1186/1744-8069-3-1 (2007).

12 Drew, L. J. *et al.* High-threshold mechanosensitive ion channels blocked by a novel conopeptide mediate pressure-evoked pain. *PloS one* **2**, e515, doi:10.1371/journal.pone.0000515 (2007).

13 Teng, J., Loukin, S., Anishkin, A. & Kung, C. The force-from-lipid (FFL) principle of mechanosensitivity, at large and in elements. *Pflugers Archiv : European journal of physiology* **467**, 27-37, doi:10.1007/s00424-014-1530-2 (2015).

14 Chalfie, M. Neurosensory mechanotransduction. *Nat Rev Mol Cell Biol* **10**, 44-52, doi:nrm2595 [pii]
10.1038/nrm2595 (2009).

15 Kung, C. A possible unifying principle for mechanosensation. *Nature* **436**, 647-654, doi:10.1038/nature03896 (2005).

16 Levina, N. *et al.* Protection of Escherichia coli cells against extreme turgor by activation of MscS and MscL mechanosensitive channels: identification of genes required for MscS activity. *EMBO J* **18**, 1730-1737, doi:10.1093/emboj/18.7.1730 (1999).

17 Sukharev, S. I., Blount, P., Martinac, B., Blattner, F. R. & Kung, C. A large-conductance mechanosensitive channel in E. coli encoded by mscL alone. *Nature* **368**, 265-268, doi:10.1038/368265a0 (1994).

18 Perozo, E., Kloda, A., Cortes, D. M. & Martinac, B. Physical principles underlying the transduction of bilayer deformation forces during mechanosensitive channel gating. *Nature structural biology* **9**, 696-703, doi:10.1038/nsb827 (2002).
19 Martinac, B., Adler, J. & Kung, C. Mechanosensitive ion channels of E. coli activated by amphipaths. *Nature* **348**, 261-263, doi:10.1038/348261a0 (1990).
20 Anishkin, A., Loukin, S. H., Teng, J. & Kung, C. Feeling the hidden mechanical forces in lipid bilayer is an original sense. *Proc Natl Acad Sci U S A* **111**, 7898-7905, doi:10.1073/pnas.1313364111 (2014).
21 Coste, B. *et al.* Piezo proteins are pore-forming subunits of mechanically activated channels. *Nature* **483**, 176-181, doi:10.1038/nature10812 (2012).
22 Vollrath, M. A., Kwan, K. Y. & Corey, D. P. The micromachinery of mechanotransduction in hair cells. *Annual review of neuroscience* **30**, 339-365, doi:10.1146/annurev.neuro.29.051605.112917 (2007).
23 Kazmierczak, P. & Muller, U. Sensing sound: molecules that orchestrate mechanotransduction by hair cells. *Trends in neurosciences* **35**, 220-229, doi:10.1016/j.tins.2011.10.007 (2012).
24 Alagramam, K. N. *et al.* Mutations in protocadherin 15 and cadherin 23 affect tip links and mechanotransduction in mammalian sensory hair cells. *PloS one* **6**, e19183, doi:10.1371/journal.pone.0019183 (2011).
25 Kazmierczak, P. *et al.* Cadherin 23 and protocadherin 15 interact to form tip-link filaments in sensory hair cells. *Nature* **449**, 87-91, doi:10.1038/nature06091 (2007).
26 Siemens, J. *et al.* The Usher syndrome proteins cadherin 23 and harmonin form a complex by means of PDZ-domain interactions. *Proc Natl Acad Sci U S A* **99**, 14946-14951, doi:10.1073/pnas.232579599 (2002).
27 Boeda, B. *et al.* Myosin VIIa, harmonin and cadherin 23, three Usher I gene products that cooperate to shape the sensory hair cell bundle. *EMBO J* **21**, 6689-6699 (2002).
28 Gillespie, P. G. & Muller, U. Mechanotransduction by hair cells: models, molecules, and mechanisms. *Cell* **139**, 33-44, doi:10.1016/j.cell.2009.09.010 (2009).
29 Bianchi, L. Mechanotransduction: touch and feel at the molecular level as modeled in Caenorhabditis elegans. *Molecular neurobiology* **36**, 254-271, doi:10.1007/s12035-007-8009-5 (2007).
30 O'Hagan, R., Chalfie, M. & Goodman, M. B. The MEC-4 DEG/ENaC channel of Caenorhabditis elegans touch receptor neurons transduces mechanical signals. *Nat Neurosci* **8**, 43-50, doi:nn1362 [pii]
10.1038/nn1362 (2005).
31 Suzuki, H. *et al.* In vivo imaging of C. elegans mechanosensory neurons demonstrates a specific role for the MEC-4 channel in the process of gentle touch sensation. *Neuron* **39**, 1005-1017, doi:S0896627303005397 [pii] (2003).
32 Chelur, D. S. *et al.* The mechanosensory protein MEC-6 is a subunit of the C. elegans touch-cell degenerin channel. *Nature* **420**, 669-673, doi:10.1038/nature01205
nature01205 [pii] (2002).
33 Goodman, M. B. *et al.* MEC-2 regulates C. elegans DEG/ENaC channels needed for mechanosensation. *Nature* **415**, 1039-1042, doi:10.1038/4151039a (2002).

34 Zhang, S. *et al.* MEC-2 is recruited to the putative mechanosensory complex in C. elegans touch receptor neurons through its stomatin-like domain. *Curr Biol* **14**, 1888-1896, doi:S0960982204008310 [pii]
10.1016/j.cub.2004.10.030 (2004).
35 Brown, A. L., Liao, Z. & Goodman, M. B. MEC-2 and MEC-6 in the Caenorhabditis elegans sensory mechanotransduction complex: auxiliary subunits that enable channel activity. *J Gen Physiol* **131**, 605-616, doi:jgp.200709910 [pii]
10.1085/jgp.200709910 (2008).
36 Du, H., Gu, G., William, C. M. & Chalfie, M. Extracellular proteins needed for C. elegans mechanosensation. *Neuron* **16**, 183-194, doi:S0896-6273(00)80035-5 [pii] (1996).
37 Emtage, L., Gu, G., Hartwieg, E. & Chalfie, M. Extracellular proteins organize the mechanosensory channel complex in C. elegans touch receptor neurons. *Neuron* **44**, 795-807, doi:S0896627304007251 [pii]
10.1016/j.neuron.2004.11.010 (2004).
38 Bounoutas, A., O'Hagan, R. & Chalfie, M. The multipurpose 15-protofilament microtubules in C. elegans have specific roles in mechanosensation. *Curr Biol* **19**, 1362-1367, doi:S0960-9822(09)01312-8 [pii]
10.1016/j.cub.2009.06.036 (2009).
39 Shida, T., Cueva, J. G., Xu, Z., Goodman, M. B. & Nachury, M. V. The major alpha-tubulin K40 acetyltransferase alphaTAT1 promotes rapid ciliogenesis and efficient mechanosensation. *Proc Natl Acad Sci U S A* **107**, 21517-21522, doi:10.1073/pnas.1013728107 (2010).
40 Akella, J. S. *et al.* MEC-17 is an alpha-tubulin acetyltransferase. *Nature* **467**, 218-222, doi:10.1038/nature09324 (2010).
41 O'Hagan, R. & Chalfie, M. Mechanosensation in Caenorhabditis elegans. *Int Rev Neurobiol* **69**, 169-203, doi:S0074-7742(05)69006-X [pii]
10.1016/S0074-7742(05)69006-X (2006).
42 Hu, J., Chiang, L. Y., Koch, M. & Lewin, G. R. Evidence for a protein tether involved in somatic touch. *EMBO J* **29**, 855-867, doi:emboj2009398 [pii]
10.1038/emboj.2009.398 (2010).
43 Chiang, L. Y. *et al.* Laminin-332 coordinates mechanotransduction and growth cone bifurcation in sensory neurons. *Nat Neurosci* **14**, 993-1000, doi:10.1038/nn.2873 (2011).
44 Kalebic, N. *et al.* Tubulin acetyltransferase alphaTAT1 destabilizes microtubules independently of its acetylation activity. *Molecular and cellular biology* **33**, 1114-1123, doi:10.1128/MCB.01044-12 (2013).
45 Coste, B. *et al.* Piezo1 and Piezo2 are essential components of distinct mechanically activated cation channels. *Science* **330**, 55-60, doi:10.1126/science.1193270 (2010).
46 Ranade, S. S. *et al.* Piezo2 is the major transducer of mechanical forces for touch sensation in mice. *Nature* **516**, 121-125, doi:10.1038/nature13980 (2014).
47 Wetzel, C. *et al.* A stomatin-domain protein essential for touch sensation in the mouse. *Nature* **445**, 206-209, doi:nature05394 [pii]
10.1038/nature05394 (2007).

48 Poole, K., Herget, R., Lapatsina, L., Ngo, H. D. & Lewin, G. R. Tuning Piezo ion channels to detect molecular-scale movements relevant for fine touch. *Nature communications* **5**, 3520, doi:10.1038/ncomms4520 (2014).
49 Lapatsina, L. *et al.* Regulation of ASIC channels by a stomatin/STOML3 complex located in a mobile vesicle pool in sensory neurons. *Open biology* **2**, 120096, doi:10.1098/rsob.120096 (2012).
50 Browman, D. T., Hoegg, M. B. & Robbins, S. M. The SPFH domain-containing proteins: more than lipid raft markers. *Trends in cell biology* **17**, 394-402, doi:10.1016/j.tcb.2007.06.005 (2007).
51 Snyers, L., Umlauf, E. & Prohaska, R. Oligomeric nature of the integral membrane protein stomatin. *J Biol Chem* **273**, 17221-17226 (1998).
52 Umlauf, E., Mairhofer, M. & Prohaska, R. Characterization of the stomatin domain involved in homo-oligomerization and lipid raft association. *J Biol Chem* **281**, 23349-23356, doi:M513720200 [pii]
10.1074/jbc.M513720200 (2006).
53 Brand, J. *et al.* A stomatin dimer modulates the activity of acid-sensing ion channels. *EMBO J* **31**, 3635-3646, doi:emboj2012203 [pii]
10.1038/emboj.2012.203 (2012).
54 Stewart, G. W. *et al.* Isolation of cDNA coding for an ubiquitous membrane protein deficient in high Na+, low K+ stomatocytic erythrocytes. *Blood* **79**, 1593-1601 (1992).
55 Stewart, G. W., Argent, A. C. & Dash, B. C. Stomatin: a putative cation transport regulator in the red cell membrane. *Biochimica et biophysica acta* **1225**, 15-25 (1993).
56 Martinez-Salgado, C. *et al.* Stomatin and sensory neuron mechanotransduction. *J Neurophysiol* **98**, 3802-3808, doi:00860.2007 [pii]
10.1152/jn.00860.2007 (2007).
57 Kobayakawa, K. *et al.* Stomatin-related olfactory protein, SRO, specifically expressed in the murine olfactory sensory neurons. *J Neurosci* **22**, 5931-5937 (2002).
58 Goldstein, B. J., Kulaga, H. M. & Reed, R. R. Cloning and characterization of SLP3: a novel member of the stomatin family expressed by olfactory receptor neurons. *J Assoc Res Otolaryngol* **4**, 74-82, doi:10.1007/s10162-002-2039-5 (2003).
59 Kim, S. E., Coste, B., Chadha, A., Cook, B. & Patapoutian, A. The role of Drosophila Piezo in mechanical nociception. *Nature* **483**, 209-212, doi:10.1038/nature10801 (2012).
60 Huber, T. B. *et al.* Podocin and MEC-2 bind cholesterol to regulate the activity of associated ion channels. *Proc Natl Acad Sci U S A* **103**, 17079-17086, doi:0607465103 [pii]
10.1073/pnas.0607465103 (2006).
61 Pavenstadt, H., Kriz, W. & Kretzler, M. Cell biology of the glomerular podocyte. *Physiol Rev* **83**, 253-307, doi:10.1152/physrev.00020.2002 (2003).
62 Saleem, M. A. *et al.* Co-localization of nephrin, podocin, and the actin cytoskeleton: evidence for a role in podocyte foot process formation. *Am J Pathol* **161**, 1459-1466 (2002).
63 Reiser, J. *et al.* TRPC6 is a glomerular slit diaphragm-associated channel required for normal renal function. *Nat Genet* **37**, 739-744, doi:ng1592 [pii]
10.1038/ng1592 (2005).

64 Tryggvason, K., Patrakka, J. & Wartiovaara, J. Hereditary proteinuria syndromes and mechanisms of proteinuria. *N Engl J Med* **354**, 1387-1401, doi:354/13/1387 [pii] 10.1056/NEJMra052131 (2006).
65 Huber, T. B., Schermer, B. & Benzing, T. Podocin organizes ion channel-lipid supercomplexes: implications for mechanosensation at the slit diaphragm. *Nephron Exp Nephrol* **106**, e27-31, doi:000101789 [pii] 10.1159/000101789 (2007).
66 Spassova, M. A., Hewavitharana, T., Xu, W., Soboloff, J. & Gill, D. L. A common mechanism underlies stretch activation and receptor activation of TRPC6 channels. *Proc Natl Acad Sci U S A* **103**, 16586-16591, doi:10.1073/pnas.0606894103 (2006).
67 Anderson, M., Kim, E. Y., Hagmann, H., Benzing, T. & Dryer, S. E. Opposing effects of podocin on the gating of podocyte TRPC6 channels evoked by membrane stretch or diacylglycerol. *American journal of physiology. Cell physiology* **305**, C276-289, doi:10.1152/ajpcell.00095.2013 (2013).
68 Kellenberger, S. & Schild, L. Epithelial sodium channel/degenerin family of ion channels: a variety of functions for a shared structure. *Physiol Rev* **82**, 735-767, doi:10.1152/physrev.00007.2002 (2002).
69 Waldmann, R., Champigny, G., Bassilana, F., Heurteaux, C. & Lazdunski, M. A proton-gated cation channel involved in acid-sensing. *Nature* **386**, 173-177, doi:10.1038/386173a0 (1997).
70 Garcia-Anoveros, J., Derfler, B., Neville-Golden, J., Hyman, B. T. & Corey, D. P. BNaC1 and BNaC2 constitute a new family of human neuronal sodium channels related to degenerins and epithelial sodium channels. *Proc Natl Acad Sci U S A* **94**, 1459-1464 (1997).
71 Chen, C. C., England, S., Akopian, A. N. & Wood, J. N. A sensory neuron-specific, proton-gated ion channel. *Proc Natl Acad Sci U S A* **95**, 10240-10245 (1998).
72 Price, M. P., Snyder, P. M. & Welsh, M. J. Cloning and expression of a novel human brain Na+ channel. *J Biol Chem* **271**, 7879-7882 (1996).
73 Lingueglia, E. *et al.* A modulatory subunit of acid sensing ion channels in brain and dorsal root ganglion cells. *J Biol Chem* **272**, 29778-29783 (1997).
74 Waldmann, R. *et al.* Molecular cloning of a non-inactivating proton-gated Na+ channel specific for sensory neurons. *J Biol Chem* **272**, 20975-20978 (1997).
75 Grunder, S., Geissler, H. S., Bassler, E. L. & Ruppersberg, J. P. A new member of acid-sensing ion channels from pituitary gland. *Neuroreport* **11**, 1607-1611 (2000).
76 Zhang, P. & Canessa, C. M. Single channel properties of rat acid-sensitive ion channel-1alpha, -2a, and -3 expressed in Xenopus oocytes. *J Gen Physiol* **120**, 553-566 (2002).
77 Hesselager, M., Timmermann, D. B. & Ahring, P. K. pH Dependency and desensitization kinetics of heterologously expressed combinations of acid-sensing ion channel subunits. *J Biol Chem* **279**, 11006-11015, doi:10.1074/jbc.M313507200 (2004).
78 Benson, C. J. *et al.* Heteromultimers of DEG/ENaC subunits form H+-gated channels in mouse sensory neurons. *Proc Natl Acad Sci U S A* **99**, 2338-2343, doi:10.1073/pnas.032678399 (2002).

79 Hattori, T. *et al.* ASIC2a and ASIC3 heteromultimerize to form pH-sensitive channels in mouse cardiac dorsal root ganglia neurons. *Circ Res* **105**, 279-286, doi:10.1161/CIRCRESAHA.109.202036 (2009).
80 Baron, A., Waldmann, R. & Lazdunski, M. ASIC-like, proton-activated currents in rat hippocampal neurons. *J Physiol* **539**, 485-494 (2002).
81 Wemmie, J. A., Taugher, R. J. & Kreple, C. J. Acid-sensing ion channels in pain and disease. *Nature reviews. Neuroscience* **14**, 461-471, doi:10.1038/nrn3529 (2013).
82 Wemmie, J. A. *et al.* The acid-activated ion channel ASIC contributes to synaptic plasticity, learning, and memory. *Neuron* **34**, 463-477 (2002).
83 Askwith, C. C., Wemmie, J. A., Price, M. P., Rokhlina, T. & Welsh, M. J. Acid-sensing ion channel 2 (ASIC2) modulates ASIC1 H+-activated currents in hippocampal neurons. *J Biol Chem* **279**, 18296-18305, doi:10.1074/jbc.M312145200 (2004).
84 Benson, C. J., Eckert, S. P. & McCleskey, E. W. Acid-evoked currents in cardiac sensory neurons: A possible mediator of myocardial ischemic sensation. *Circ Res* **84**, 921-928 (1999).
85 Price, M. P. *et al.* The mammalian sodium channel BNC1 is required for normal touch sensation. *Nature* **407**, 1007-1011, doi:10.1038/35039512 (2000).
86 Price, M. P. *et al.* The DRASIC cation channel contributes to the detection of cutaneous touch and acid stimuli in mice. *Neuron* **32**, 1071-1083, doi:S0896-6273(01)00547-5 [pii] (2001).
87 Sutherland, S. P., Benson, C. J., Adelman, J. P. & McCleskey, E. W. Acid-sensing ion channel 3 matches the acid-gated current in cardiac ischemia-sensing neurons. *Proc Natl Acad Sci U S A* **98**, 711-716, doi:10.1073/pnas.011404498
011404498 [pii] (2001).
88 Sluka, K. A. *et al.* Chronic hyperalgesia induced by repeated acid injections in muscle is abolished by the loss of ASIC3, but not ASIC1. *Pain* **106**, 229-239 (2003).
89 Moshourab, R. A., Wetzel, C., Martinez-Salgado, C. & Lewin, G. R. Stomatin-domain protein interactions with acid-sensing ion channels modulate nociceptor mechanosensitivity. *J Physiol* **591**, 5555-5574, doi:jphysiol.2013.261180 [pii]
10.1113/jphysiol.2013.261180 (2013).
90 Kang, S. *et al.* Simultaneous disruption of mouse ASIC1a, ASIC2 and ASIC3 genes enhances cutaneous mechanosensitivity. *PloS one* **7**, e35225, doi:10.1371/journal.pone.0035225 (2012).
91 Drew, L. J. *et al.* Acid-sensing ion channels ASIC2 and ASIC3 do not contribute to mechanically activated currents in mammalian sensory neurones. *J Physiol* **556**, 691-710, doi:10.1113/jphysiol.2003.058693 (2004).
92 Price, M. P., Thompson, R. J., Eshcol, J. O., Wemmie, J. A. & Benson, C. J. Stomatin modulates gating of acid-sensing ion channels. *J Biol Chem* **279**, 53886-53891, doi:M407708200 [pii]
10.1074/jbc.M407708200 (2004).
93 Brown, D. A. & London, E. Structure and function of sphingolipid- and cholesterol-rich membrane rafts. *J Biol Chem* **275**, 17221-17224, doi:10.1074/jbc.R000005200
R000005200 [pii] (2000).

94 Brown, D. A. & Rose, J. K. Sorting of GPI-anchored proteins to glycolipid-enriched membrane subdomains during transport to the apical cell surface. *Cell* **68**, 533-544, doi:0092-8674(92)90189-J [pii] (1992).
95 Ge, M. *et al.* Electron spin resonance characterization of liquid ordered phase of detergent-resistant membranes from RBL-2H3 cells. *Biophys J* **77**, 925-933, doi:S0006-3495(99)76943-2 [pii]
10.1016/S0006-3495(99)76943-2 (1999).
96 Niemela, P. S., Ollila, S., Hyvonen, M. T., Karttunen, M. & Vattulainen, I. Assessing the nature of lipid raft membranes. *PLoS computational biology* **3**, e34, doi:10.1371/journal.pcbi.0030034 (2007).
97 Filippov, A., Oradd, G. & Lindblom, G. Sphingomyelin structure influences the lateral diffusion and raft formation in lipid bilayers. *Biophys J* **90**, 2086-2092, doi:10.1529/biophysj.105.075150 (2006).
98 Sankaram, M. B. & Thompson, T. E. Modulation of phospholipid acyl chain order by cholesterol. A solid-state 2H nuclear magnetic resonance study. *Biochemistry* **29**, 10676-10684 (1990).
99 Gullingsrud, J. & Schulten, K. Lipid bilayer pressure profiles and mechanosensitive channel gating. *Biophys J* **86**, 3496-3509, doi:10.1529/biophysj.103.034322 (2004).
100 Brown, D. A. Lipid rafts, detergent-resistant membranes, and raft targeting signals. *Physiology (Bethesda)* **21**, 430-439, doi:21/6/430 [pii]
10.1152/physiol.00032.2006 (2006).
101 Simons, K. & Toomre, D. Lipid rafts and signal transduction. *Nat Rev Mol Cell Biol* **1**, 31-39, doi:10.1038/35036052
35036052 [pii] (2000).
102 Keller, P. & Simons, K. Cholesterol is required for surface transport of influenza virus hemagglutinin. *J Cell Biol* **140**, 1357-1367 (1998).
103 Harder, T. & Engelhardt, K. R. Membrane domains in lymphocytes - from lipid rafts to protein scaffolds. *Traffic* **5**, 265-275, doi:10.1111/j.1600-0854.2003.00163.x
TRA163 [pii] (2004).
104 Korade, Z. & Kenworthy, A. K. Lipid rafts, cholesterol, and the brain. *Neuropharmacology* **55**, 1265-1273, doi:S0028-3908(08)00064-6 [pii]
10.1016/j.neuropharm.2008.02.019 (2008).
105 Dart, C. Lipid microdomains and the regulation of ion channel function. *J Physiol* **588**, 3169-3178, doi:10.1113/jphysiol.2010.191585 (2010).
106 Mairhofer, M., Steiner, M., Salzer, U. & Prohaska, R. Stomatin-like protein-1 interacts with stomatin and is targeted to late endosomes. *J Biol Chem* **284**, 29218-29229, doi:10.1074/jbc.M109.014993 (2009).
107 Mairhofer, M., Steiner, M., Mosgoeller, W., Prohaska, R. & Salzer, U. Stomatin is a major lipid-raft component of platelet alpha granules. *Blood* **100**, 897-904 (2002).
108 Snyers, L., Umlauf, E. & Prohaska, R. Association of stomatin with lipid-protein complexes in the plasma membrane and the endocytic compartment. *Eur J Cell Biol* **78**, 802-812 (1999).
109 Morenilla-Palao, C., Pertusa, M., Meseguer, V., Cabedo, H. & Viana, F. Lipid raft segregation modulates TRPM8 channel activity. *J Biol Chem* **284**, 9215-9224, doi:M807228200 [pii]

10.1074/jbc.M807228200 (2009).
110 Eshcol, J. O. *et al.* Acid-sensing ion channel 3 (ASIC3) cell surface expression is modulated by PSD-95 within lipid rafts. *American journal of physiology. Cell physiology* **295**, C732-739, doi:00514.2007 [pii]
10.1152/ajpcell.00514.2007 (2008).
111 te Riet, J. *et al.* Interlaboratory round robin on cantilever calibration for AFM force spectroscopy. *Ultramicroscopy* **111**, 1659-1669, doi:10.1016/j.ultramic.2011.09.012 (2011).
112 Sneddon, I. N. The relation between load and penetration in the axisymmetric boussinesq problem for a punch of arbitrary profile. *International Journal of Engineering Science* **3**, 11 (1965).
113 Hochmuth, F. M., Shao, J. Y., Dai, J. & Sheetz, M. P. Deformation and flow of membrane into tethers extracted from neuronal growth cones. *Biophysical journal* **70**, 358-369 (1996).
114 Obata, K. *et al.* Contribution of injured and uninjured dorsal root ganglion neurons to pain behavior and the changes in gene expression following chronic constriction injury of the sciatic nerve in rats. *Pain* **101**, 65-77, doi:10.1016/s0304-3959(02)00296-8 (2003).
115 Christian, A. E., Haynes, M. P., Phillips, M. C. & Rothblat, G. H. Use of cyclodextrins for manipulating cellular cholesterol content. *Journal of lipid research* **38**, 2264-2272 (1997).
116 Zidovetzki, R. & Levitan, I. Use of cyclodextrins to manipulate plasma membrane cholesterol content: evidence, misconceptions and control strategies. *Biochimica et biophysica acta* **1768**, 1311-1324, doi:10.1016/j.bbamem.2007.03.026 (2007).
117 Pristera, A., Baker, M. D. & Okuse, K. Association between tetrodotoxin resistant channels and lipid rafts regulates sensory neuron excitability. *PloS one* **7**, e40079, doi:10.1371/journal.pone.0040079 (2012).
118 Lundbaek, J. A. *et al.* Regulation of sodium channel function by bilayer elasticity: the importance of hydrophobic coupling. Effects of Micelle-forming amphiphiles and cholesterol. *J Gen Physiol* **123**, 599-621, doi:10.1085/jgp.200308996
jgp.200308996 [pii] (2004).
119 Rugiero, F., Drew, L. J. & Wood, J. N. Kinetic properties of mechanically activated currents in spinal sensory neurons. *J Physiol* **588**, 301-314, doi:10.1113/jphysiol.2009.182360 (2010).
120 Martinac, B. & Hamill, O. P. Gramicidin A channels switch between stretch activation and stretch inactivation depending on bilayer thickness. *Proc Natl Acad Sci U S A* **99**, 4308-4312, doi:10.1073/pnas.072632899
072632899 [pii] (2002).
121 Hao, J. & Delmas, P. Multiple desensitization mechanisms of mechanotransducer channels shape firing of mechanosensory neurons. *J Neurosci* **30**, 13384-13395, doi:10.1523/JNEUROSCI.2926-10.2010 (2010).
122 Borbiro, I., Badheka, D. & Rohacs, T. Activation of TRPV1 channels inhibits mechanosensitive Piezo channel activity by depleting membrane phosphoinositides. *Sci. Signal.* **8**, ra15, doi:10.1126/scisignal.2005667 (2015).

123 Amin, L., Ercolini, E., Shahapure, R., Migliorini, E. & Torre, V. The role of membrane stiffness and actin turnover on the force exerted by DRG lamellipodia. *Biophys J* **102**, 2451-2460, doi:S0006-3495(12)00510-3 [pii]
10.1016/j.bpj.2012.04.036 (2012).
124 Kasas, S. *et al.* Superficial and deep changes of cellular mechanical properties following cytoskeleton disassembly. *Cell Motility and the Cytoskeleton* **62**, 124-132, doi:10.1002/cm.20086 (2005).
125 Sheetz, M. P. Cell control by membrane-cytoskeleton adhesion. *Nature Reviews Molecular Cell Biology* **2**, 392-396, doi:10.1038/35073095 (2001).
126 Glebov, O. O., Bright, N. A. & Nichols, B. J. Flotillin-1 defines a clathrin-independent endocytic pathway in mammalian cells. *Nature cell biology* **8**, 46-54, doi:10.1038/ncb1342 (2006).
127 Snyers, L., Umlauf, E. & Prohaska, R. Cysteine 29 is the major palmitoylation site on stomatin. *FEBS Lett* **449**, 101-104, doi:S0014-5793(99)00417-2 [pii] (1999).
128 Kadurin, I., Huber, S. & Grunder, S. A single conserved proline residue determines the membrane topology of stomatin. *Biochem J* **418**, 587-594, doi:BJ20081662 [pii]
10.1042/BJ20081662 (2009).
129 Morachevskaya, E., Sudarikova, A. & Negulyaev, Y. Mechanosensitive channel activity and F-actin organization in cholesterol-depleted human leukaemia cells. *Cell Biol Int* **31**, 374-381, doi:10.1016/j.cellbi.2007.01.024 (2007).
130 Xing, Y. *et al.* Effects of membrane cholesterol depletion and GPI-anchored protein reduction on osteoblastic mechanotransduction. *Journal of cellular physiology* **226**, 2350-2359, doi:10.1002/jcp.22579 (2011).
131 Vega-Moreno, J. *et al.* Cholesterol depletion uncouples beta-dystroglycans from discrete sarcolemmal domains, reducing the mechanical activity of skeletal muscle. *Cellular physiology and biochemistry : international journal of experimental cellular physiology, biochemistry, and pharmacology* **29**, 905-918, doi:10.1159/000186933 (2012).
132 Huang, H., Bae, C., Sachs, F. & Suchyna, T. M. Caveolae regulation of mechanosensitive channel function in myotubes. *PloS one* **8**, e72894, doi:10.1371/journal.pone.0072894
PONE-D-13-14361 [pii] (2013).
133 Purcell, E. K., Liu, L., Thomas, P. V. & Duncan, R. K. Cholesterol influences voltage-gated calcium channels and BK-type potassium channels in auditory hair cells. *PloS one* **6**, e26289, doi:10.1371/journal.pone.0026289 (2011).
134 Levic, S. & Yamoah, E. N. Plasticity in membrane cholesterol contributes toward electrical maturation of hearing. *J Biol Chem* **286**, 5768-5773, doi:10.1074/jbc.M110.186486 (2011).
135 Brownell, W. E., Jacob, S., Hakizimana, P., Ulfendahl, M. & Fridberger, A. Membrane cholesterol modulates cochlear electromechanics. *Pflugers Archiv : European journal of physiology* **461**, 677-686, doi:10.1007/s00424-011-0942-5 (2011).
136 Zhao, H., Williams, D. E., Shin, J. B., Brugger, B. & Gillespie, P. G. Large membrane domains in hair bundles specify spatially constricted radixin activation. *J Neurosci* **32**, 4600-4609, doi:32/13/4600 [pii]
10.1523/JNEUROSCI.6184-11.2012 (2012).

137 Anishkin, A. & Kung, C. Stiffened lipid platforms at molecular force foci. *Proc Natl Acad Sci U S A* **110**, 4886-4892, doi:10.1073/pnas.1302018110 (2013).
138 Crumling, M. A. *et al.* Hearing loss and hair cell death in mice given the cholesterol-chelating agent hydroxypropyl-beta-cyclodextrin. *PloS one* **7**, e53280, doi:10.1371/journal.pone.0053280 (2012).
139 Patel, A. J., Lazdunski, M. & Honore, E. Lipid and mechano-gated 2P domain K(+) channels. *Curr Opin Cell Biol* **13**, 422-428, doi:S0955-0674(00)00231-3 [pii] (2001).
140 Filippov, A., Oradd, G. & Lindblom, G. The effect of cholesterol on the lateral diffusion of phospholipids in oriented bilayers. *Biophys J* **84**, 3079-3086, doi:S0006-3495(03)70033-2 [pii]
10.1016/S0006-3495(03)70033-2 (2003).
141 McIntosh, T. J. The effect of cholesterol on the structure of phosphatidylcholine bilayers. *Biochimica et biophysica acta* **513**, 43-58 (1978).
142 Yesylevskyy, S. O., Demchenko, A. P., Kraszewski, S. & Ramseyer, C. Cholesterol induces uneven curvature of asymmetric lipid bilayers. *ScientificWorldJournal* **2013**, 965230, doi:10.1155/2013/965230 (2013).
143 Byfield, F. J., Aranda-Espinoza, H., Romanenko, V. G., Rothblat, G. H. & Levitan, I. Cholesterol depletion increases membrane stiffness of aortic endothelial cells. *Biophys J* **87**, 3336-3343, doi:10.1529/biophysj.104.040634
S0006-3495(04)73800-X [pii] (2004).
144 Byfield, F. J. *et al.* Evidence for the role of cell stiffness in modulation of volume-regulated anion channels. *Acta Physiol (Oxf)* **187**, 285-294, doi:APS1555 [pii]
10.1111/j.1748-1716.2006.01555.x (2006).
145 Nebl, T. *et al.* Proteomic analysis of a detergent-resistant membrane skeleton from neutrophil plasma membranes. *J Biol Chem* **277**, 43399-43409, doi:10.1074/jbc.M205386200
M205386200 [pii] (2002).
146 Sun, M. *et al.* The effect of cellular cholesterol on membrane-cytoskeleton adhesion. *Journal of cell science* **120**, 2223-2231, doi:jcs.001370 [pii]
10.1242/jcs.001370 (2007).
147 Petzold, B. C., Park, S. J., Mazzochette, E. A., Goodman, M. B. & Pruitt, B. L. MEMS-based force-clamp analysis of the role of body stiffness in C. elegans touch sensation. *Integrative biology : quantitative biosciences from nano to macro* **5**, 853-864, doi:10.1039/c3ib20293c (2013).
148 Hanzal-Bayer, M. F. & Hancock, J. F. Lipid rafts and membrane traffic. *FEBS Lett* **581**, 2098-2104, doi:10.1016/j.febslet.2007.03.019 (2007).
149 Salaun, C., James, D. J. & Chamberlain, L. H. Lipid rafts and the regulation of exocytosis. *Traffic* **5**, 255-264, doi:10.1111/j.1600-0854.2004.0162.x (2004).
150 Nichols, B. Caveosomes and endocytosis of lipid rafts. *Journal of cell science* **116**, 4707-4714, doi:10.1242/jcs.00840 (2003).
151 Li, S., Song, K. S. & Lisanti, M. P. Expression and characterization of recombinant caveolin. Purification by polyhistidine tagging and cholesterol-dependent incorporation into defined lipid membranes. *J Biol Chem* **271**, 568-573 (1996).
152 Frost, A. *et al.* Structural basis of membrane invagination by F-BAR domains. *Cell* **132**, 807-817, doi:10.1016/j.cell.2007.12.041 (2008).

153 Chichili, G. R. & Rodgers, W. Cytoskeleton-membrane interactions in membrane raft structure. *Cellular and molecular life sciences : CMLS* **66**, 2319-2328, doi:10.1007/s00018-009-0022-6 (2009).
154 Oldfield, S. *et al.* Receptor-mediated suppression of potassium currents requires colocalization within lipid rafts. *Mol Pharmacol* **76**, 1279-1289, doi:mol.109.058008 [pii] 10.1124/mol.109.058008 (2009).
155 Levitan, I., Fang, Y., Rosenhouse-Dantsker, A. & Romanenko, V. Cholesterol and ion channels. *Sub-cellular biochemistry* **51**, 509-549, doi:10.1007/978-90-481-8622-8_19 (2010).
156 Xie, J., Price, M. P., Berger, A. L. & Welsh, M. J. DRASIC contributes to pH-gated currents in large dorsal root ganglion sensory neurons by forming heteromultimeric channels. *J Neurophysiol* **87**, 2835-2843 (2002).
157 Jansson, E. T. *et al.* Effect of cholesterol depletion on the pore dilation of TRPV1. *Molecular pain* **9**, 1, doi:10.1186/1744-8069-9-1 (2013).
158 Liu, M., Huang, W., Wu, D. & Priestley, J. V. TRPV1, but not P2X, requires cholesterol for its function and membrane expression in rat nociceptors. *Eur J Neurosci* **24**, 1-6, doi:EJN4889 [pii]
10.1111/j.1460-9568.2006.04889.x (2006).
159 Levitan, I., Singh, D. K. & Rosenhouse-Dantsker, A. Cholesterol binding to ion channels. *Front Physiol* **5**, 65, doi:10.3389/fphys.2014.00065 (2014).
160 Mannsfeldt, A. G., Carroll, P., Stucky, C. L. & Lewin, G. R. Stomatin, a MEC-2 like protein, is expressed by mammalian sensory neurons. *Mol Cell Neurosci* **13**, 391-404, doi:10.1006/mcne.1999.0761
S1044-7431(99)90761-3 [pii] (1999).
161 Salzer, U. & Prohaska, R. Stomatin, flotillin-1, and flotillin-2 are major integral proteins of erythrocyte lipid rafts. *Blood* **97**, 1141-1143 (2001).
162 Tillman, T. S. & Cascio, M. Effects of membrane lipids on ion channel structure and function. *Cell Biochem Biophys* **38**, 161-190, doi:CBB:38:2:161 [pii]
10.1385/CBB:38:2:161 (2003).
163 Lingwood, D. & Simons, K. Lipid rafts as a membrane-organizing principle. *Science* **327**, 46-50, doi:10.1126/science.1174621 (2010).
164 Aoki, S., Thomas, A., Decaffmeyer, M., Brasseur, R. & Epand, R. M. The role of proline in the membrane re-entrant helix of caveolin-1. *J Biol Chem* **285**, 33371-33380, doi:M110.153569 [pii]
10.1074/jbc.M110.153569 (2010).

7. Acknowledgements

First of all, I would like express my gratitude to my thesis committee members, Dr. Jing Hu, Prof. Dr. Florian Lang and Prof. Dr. Simone Di Giovanni for their guidance and advice. I would like to express my special thanks to my supervisor Dr. Jing Hu, who provides supervision, guidance and constant support over the course of my doctoral work. I would also like to thank Prof. Dr. Gary Lewin for providing *STOML3* $^{-/-}$ mice, Prof. Dr. Ardem Patapoutian for providing piezo1 plasmid, Dr. Paul Heppenstall for providing piezo2 plasmid.

No project is completed without the assistance of others, special thanks to:
Dr. Laura Andolfi, for performing AFM measurement and analyzing related data
Flavia Fratini, for carrying out behavioral experiments
Dr. Tsung-Chieh Chen, Florian Mayer and Da Guo, for excellent technical support
Former technician Dr. Monika Papke, for excellent technical assistant
The Werner Reichardt Centre for Integrative Neuroscience (CIN) for supporting this work.

I take this opportunity to express my gratitude to all of members of CIN for help and support, especially to my colleagues Dr. Tsung-Chieh Chen, Florian Mayer, Da Guo and Flavia Fratini. I really had a great time with them during my study, and I would like to wish them all best of luck for the future.

I would like to express special gratitude to my family. Without their constant love, care, support and encouragement, I could not complete my study. I love each and every one of you and I am so grateful for all you have done. I would like to thank my friend Xiaoguang Tian for your continued support and encouragement, and thank you for being my best friend. I would also like to thank all my friends for their support.